REGULATION OF ENDOTHELIAL METABOLISM BY LAMINAR SHEAR STRESS AND FLOW-INDUCED TRANSCRIPTION FACTOR KLF2

Dissertation

zur Erlangung des Doktorgrades der Naturwissenschaften

vorgelegt beim Fachbereich Biowissenschaften (FB15) der

Johann Wolfgang Goethe Universität

in Frankfurt am Main

von Anuradha Doddaballapur

aus Davanagere, Indien

Frankfurt am Main 2015

(D30)

vom Fachbereich der Biowissenschaften (FB 15)

der Johann Wolfgang Goethe Universität als Dissertation angenommen.

Dekan: Prof. Dr. Meike Piepenbring

Gutachter: Prof. Dr. Stefanie Dimmeler

Prof. Dr. Amparo Acker Palmer

Datum der Disputation: 09.12.15

CONTENTS

1. INTRODUCTION

1.1 Mammalian circulatory system

In the human body, a vast specialized network of vessels facilitate transfer of oxygen, nutrients, carbon dioxide and signaling factors and allow waste removal from tissues. They are classified into the lymphatic system and the blood vessel network. The lymphatic system is essential for immune regulation, nutrient and waste circulation. It is an open circuit where capillaries collect lymph fluid from interstitial spaces and bring it back to the cardiovascular system via lymphatic vessels and nodes. The blood vessel or cardiovascular system includes blood, heart and blood vessels. It is a closed network transporting blood containing oxygen, immune cells and nutrients to tissues. Blood flow in the body is classified as pulmonary and systemic circulation. The pulmonary loop involves blood being carried from the heart to the lungs by pulmonary arteries where it is oxygenated and brought back to the heart through pulmonary veins. Systemic circulation encompasses the transport of oxygenated blood from the heart to all parts of the body by arteries and the collection of deoxygenated blood from tissues by veins back to the heart. Exchange of nutrients and oxygen to tissues occurs in the capillaries that form a connection between arteries and veins.

Vessels can be subdivided into arteries, arterioles, capillaries, veins and venules based on their size. The structure of veins, arteries and capillaries are adapted to the kind of hemodynamic forces and blood pressure they experience. Capillaries comprise mainly of an endothelial layer attached to a basement membrane and are partially covered by pericytes to maintain stability. Vessel walls of larger arteries and veins have three distinct layers, the tunica intima, tunica media and tunica externa connected by elastic laminae. The intima is the innermost layer of vessel wall which is in direct contact with blood flow. It is comprised of endothelial cells (ECs) lining the lumen, which are important for tissue growth and repair, to sense and transmit signals of blood flow and to maintain vascular tone, among many other functions. A sub-endothelial layer exists next to the intima in vessels having diameter larger than one millimeter. The intima is covered by the tunica media, which contains smooth muscle fibers sheathed by collagen and elastin fibrils. The media has elastic ability and exerts resistance to the blood pressure through which it mediates vasoconstriction and vasodilation processes. The outermost layer of tunica externa or adventitia comprises connective tissue with collagen fibers, fibroblasts, pericytes and extracellular matrix (ECM); and functions to anchor the vessel to surrounding tissue.

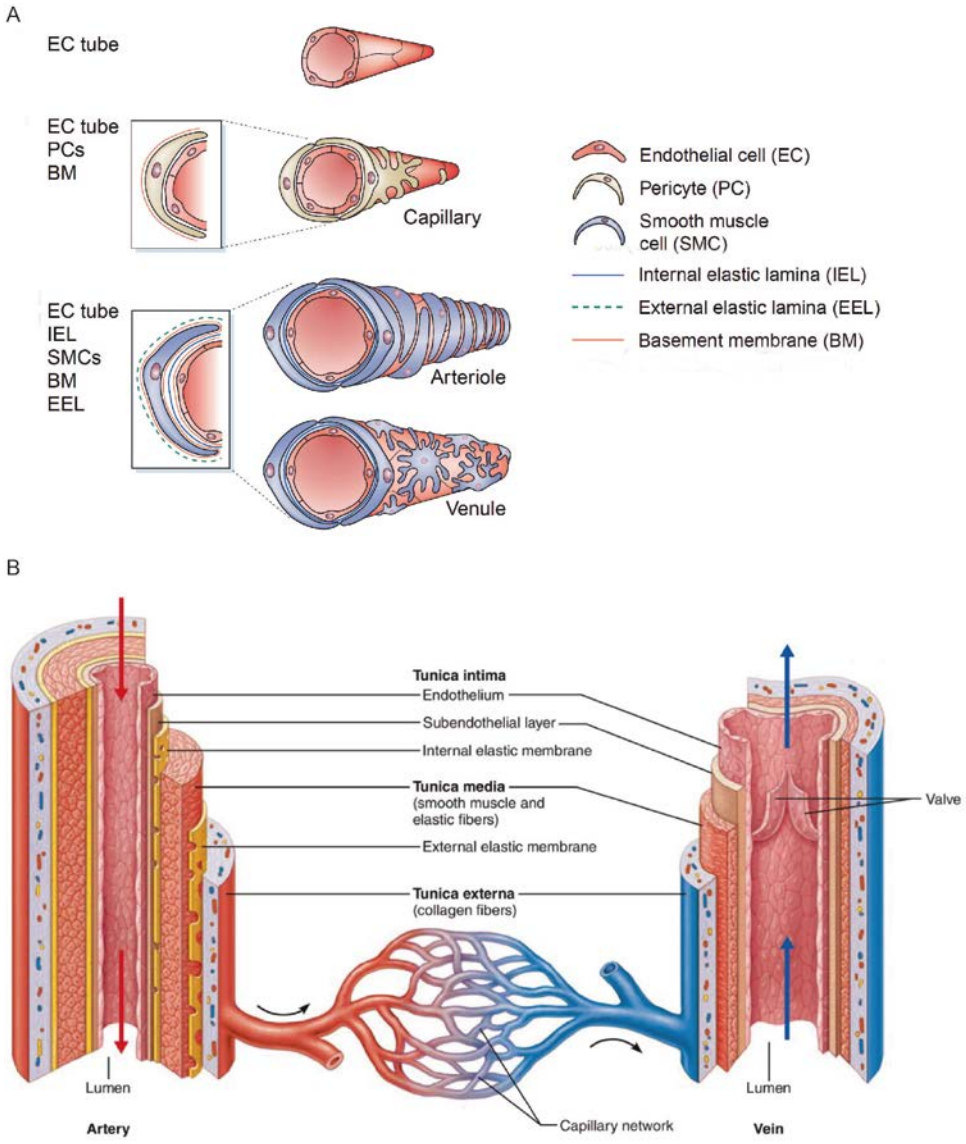

Figure I.1. Composition and structure of blood vessels.
A) Immature vessel consists of only the EC tube, whereas capillaries have EC tubes surrounded by a thin layer of basement membrane and few pericytes. Arterioles and venules have EC tubes lined with basement membrane, SMCs and elastin lamina. Arterioles have more compact circumferential coverage of SMCs (Adapted from Jain 2003)[1] B) Scheme showing various layers of larger vessel wall and differences in artery and vein structure. They both comprise of tunica intima, media and externa. The arteries have a thicker media layer in order to withstand higher blood pressure than that in veins. Veins have larger lumen than arteries and also have valves to regulate the direction of blood flow. Whereas, arteries have a thinner tunica externa compared to veins, the overall thickness of vessel wall is larger than veins. (Adapted from Human Anatomy and Physiology, 6th edition)

1.2 Mechanisms of vessel formation

Blood vessel formation occurs during development and postnatal, through three different processes vasculogenesis, angiogenesis and arteriogenesis. Vasculogenesis is an assembly process involving de-novo formation of vessels from precursor cells in early development stage. Mesoderm derived progenitor cells known as angioblasts arising from various

embryonic regions differentiate into endothelial cells and coalesce to form the first primitive vascular network[2,3]. Arteriogenesis refers to collateral vessel growth or enlargement of pre-existing arterioles in order to compensate for the interruption of blood flow at the occluded major supply vessel. In turn, new vessels allow blood supply to distal tissues preventing ischemia[4]. Angiogenesis is the process of vessel sprouting from pre-existent vessels, which majorly contributes to later stages of development and adult blood vessel formation. Expansion of primordial capillary plexus network can occur through sprouting angiogenesis characterized by sprouting and migration of preexisting vessels or by intussusceptive angiogenesis involving remodeling of preexisting vessels by internal splitting and transvascular growth[5].

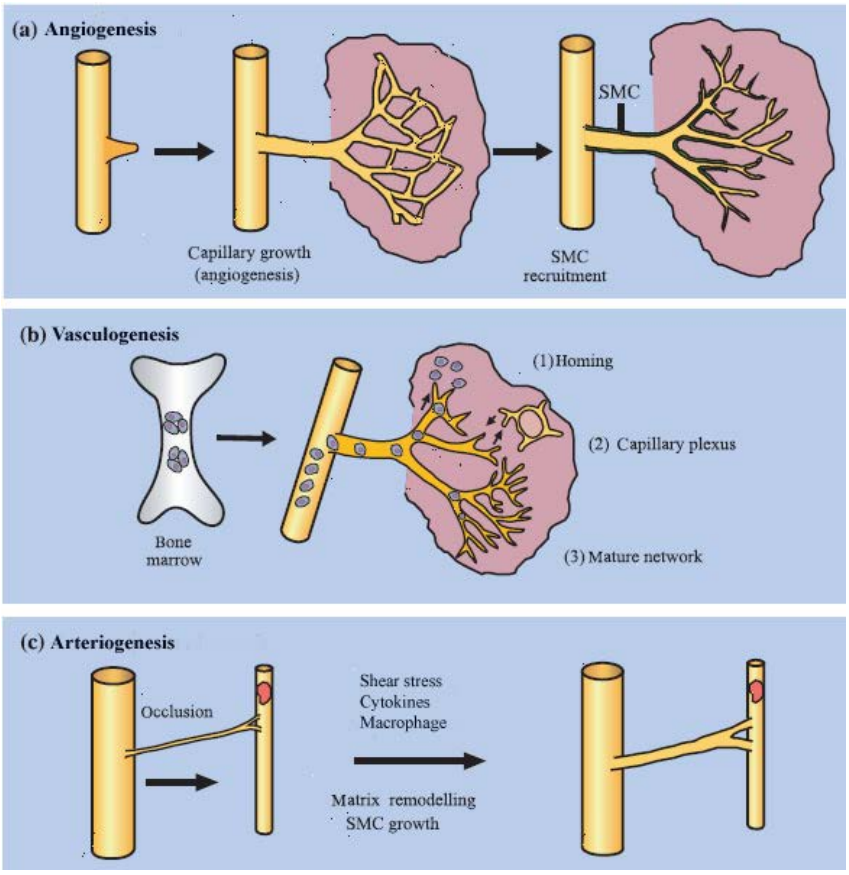

Figure I.2. Various mechanisms of blood vessel formation.

Vessel formation can be classified into three modes: angiogenesis, vasculogenesis and arteriogenesis. Angiogenesis involves proliferation and migration of ECs from pre-existing vessels into avascular regions. The vessels mature upon recruitment of mural cells. b) Vasculogenesis is the process of *de novo* formation of vessels from progenitor cells during development. In adult, precursor cells released from bone marrow integrate into pre-existing vessels and contribute to vessel growth c) Arteriogenesis describes the formation of collateral vessel growth in the event of vessel occlusion of a main vessel. SMC: smooth muscle cell. (Adapted from Carmeliet 2004)[3]

1.3 Process and regulation of angiogenesis

The vasculature in the healthy adult is largely quiescent, apart from the active female endometrial cycle and placental growth during pregnancy. However, ECs retain high plasticity and upon sensing directional cues such as vascular endothelial growth factor (VEGF) and hypoxia, quiescent vessels in adults are activated and angiogenesis occurs in physiological processes like development, wound healing or in pathophysiological conditions such as tumor growth and metastasis[6]. Impaired angiogenesis has also been implicated in several disease conditions such as ischemic retinopathies, stroke and metabolic disorders[7]. Fig I.3 illustrates a widely accepted model of angiogenic vessel sprouting[8].

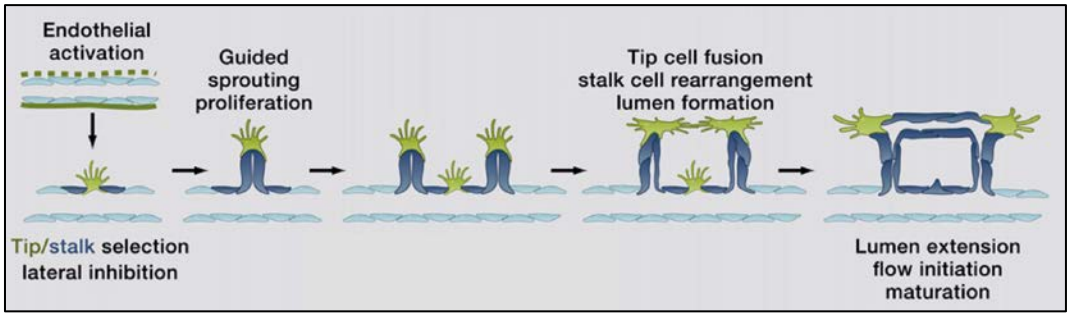

Figure I.3. Process of sprouting angiogenesis.
In response to pro-angiogenic signals, basement matrix is degraded by matrix metalloproteinase (MMPs) and mural cells are detached by Angiopoietin 2 (ANG2) released by ECs, thus allowing tip cells with high migration ability to navigate the vascular front by taking lead. Tip cells are followed by the trailing stalk cells, which elongate the sprout due to their high proliferative capacity. The tip cells from adjacent sprouts fuse and stalk cells undergo rearrangement to form a lumen. Next, blood flow and basement membrane are established, in addition to which, recruitment of mural cells to the newly formed EC tubule leads to maturation and remodeling of vessel. Tissue oxygenation upon blood perfusion reduces paracrine pro-angiogenic VEGF production, thus establishing a functional quiescent vessel. The cells lining the perfused quiescent vessel are also termed as "phalanx" cells[9]. (Adapted from Potente et al. 2011)[8]

Numerous molecular signals determine the initiation and dynamics of angiogenesis including the tip or stalk selection during the process. VEGF-A functions via signaling through its receptor; vascular endothelial growth factor receptor 2 (VEGFR2) and is implicated in angiogenesis in health and disease[3]. Loss of a single allele of VEGF in mice leads to impairment in blood vessel formation and embryonic lethality, while homozygous VEGF mouse embryos die at mid-gestation. Indeed, homozygous mice for either VEGF receptor VEGFR1 or VEGFR2 die in utero as well. These early studies highlighted the importance of VEGF as a key angiogenic regulator in a dose dependent manner during development[10,11]. The notch pathway is an evolutionarily conserved signaling pathway in vertebrates and invertebrates and plays an important role in controlling EC migration, lumen formation and

arteriovenous fate determination, among many other angiogenic functions[12]. Upon sensing a VEGF gradient and in response to hypoxia, tip cells bearing extended filopodia and VEGFR2, increase their expression of Notch ligand Delta-like 4 (DLL4) which leads to activation of Notch receptor in the neighboring stalk cell[13]. Moreover, VEGFR2 expression in stalk cells is down regulated thus making them less responsive to VEGF and actively suppressing the tip phenotype. Eventually, this leads to tip cells spearheading the front of the emerging vascular sprout[12].

Notch signaling controls the specification of tip and stalk cells by lateral inhibition[8]. High notch activity is seen in stalk cells as opposed to low notch activity in tip cells, conversely, tip cells show increased DLL4 expression. Two key studies in mice and zebrafish[14,15] demonstrate that in the absence of Notch signaling, ECs exhibit a predominant tip phenotype (hyper sprouting), while activation of Notch by its ligand (Jagged1, JAG1) and constitutively active notch intracellular domain (NICD) led to reduced number of tip cells and vascular branching.

Notch signaling, along with Wnt signaling regulates endothelial cell differentiation and patterning during development. ECs express various Wnt ligand and Frizzled receptors that are involved in canonical Wnt (β-catenin dependent) or non-canonical Wnt (β-catenin independent) pathway and mediate physiological and pathophysiological angiogenesis[16]. Notch-regulated ankyrin repeat protein (NRARP), that acts downstream of Notch signaling, activates Wnt in a lymphoid enhancer binding factor-1 (LEF1) dependent manner and collectively both pathways control stalk cell proliferation and vessel branching[17]. Interestingly, via a negative feedback loop that is prominent only in early development phase, β-catenin can activate Notch 1 and -4 by increasing expression of DLL4[18]. Overexpression of β-catenin can lead to vascular defects characterized by lack of venous specification and impaired remodeling[19], similar to phenotype observed under DLL4 overexpression[20]. Overall, the outcome of Notch signaling in ECs is to produce well perfused vessels and dismiss a hypoxic environment[8].

Ligands ANG-1-4 and receptors TIE-1 and TIE-2 constitute the ANG-TIE signaling system and play a significant role in vessel maturation and quiescence. ANG-1 expressed by mural cells activates the TIE-2 receptor on neighboring ECs, where ANG-1 promotes clustering of TIE-2 *in trans* at cell junctions[21] to stimulate a cascade of downstream pathways that contribute to EC quiescence. The association of ANG-1 to TIE-2 enhances mural cell

recruitment, tight endothelial junction formation and basement membrane deposition[22]. Furthermore, TIE-2/ANG-1 prevents VEGF-induced leakage in vessels by inhibiting endocytosis of vascular endothelial-cadherin (VE-cadherin) junction protein induced by VEGF[8]. ANG-2 has been described to work as an antagonist to TIE-2 receptor and destabilizes the vessel to promote sprouting. In response to angiogenic signals, ANG-2 stored in Weibel-Palade bodies is released from angiogenic tip cells and induces mural cell detachment and vascular permeability, thus functioning as a pro-angiogenic factor[22].

Endothelial cells possess oxygen sensors such as prolyl hydroxylase domain (PHD) proteins which hydroxylate hypoxia inducible factor (HIF) under normoxia, leading to degradation of HIFs by proteasome[23]. Under hypoxic conditions, PHDs are inactive and HIF1α is stabilized and translocated to the nucleus. HIF1 is implicated in EC metabolism and homeostasis[24], promotes transcription of hypoxia induced genes, the most crucial being VEGF[25] that initiate angiogenesis to increase oxygen levels in blood. PHD2 deficiency in ECs leads to tumor vessel normalization to reduce tumor invasiveness and induces EC quiescence[9]. HIF1α promotes vessel sprouting, loss of which leads to impaired vascularization after ischemia, and reduced angiogenesis in tumors and injured tissues[24]. Owing to this, HIF1α inhibitors are potential therapeutic agents to combat tumor angiogenesis. Moreover, inactivation of PHD2 leads to HIF2α mediated activation of sVEGFR1 and VE-cadherin resulting in better perfusion of vessels and hence contributes to vessel maintenance[8,24]. In summary, PHD oxygen sensors comprehensively help ECs to adapt vessel morphology in order to fulfil their oxygen transport function.

PDGF, TGF-β/Alk1, FGF, S1P/Edg1, Slit/Robo, Semaphorin/plexin, cell matrix and integrin signaling are some of the other pathways that have been previously described to be important for angiogenic regulation[12,26].

1.4 Laminar flow and atheroprotection

Blood vessels experience various kinds of hemodynamic forces exerted by the phasic blood flow during the cardiac cycle. As ECs form the inner lining of the vessel wall, they are constantly subjected to hemodynamic forces. The major mechanical forces exerted on the endothelial layer are shear stress (parallel to vessel wall), circumferential stretch (pressure leading to a cyclic stretch of the wall) and hydrostatic pressure (perpendicular to vessel wall)[27]. Shear stress is the force per unit area exerted by a tangential blood flow on the endothelial surface, which can determined using Poiseuille's law which states that shear stress

is proportional to blood viscosity and inversely proportional to third power of the internal radius of the vessel. Veins experience shear stress between 1-6 dyn/cm^2 and arteries anywhere between 10-70 dyn/cm^2 magnitudes[28].

1.4.1 Mechanosensing by the endothelium

ECs possess sensors that have the ability to sense and transduce the biomechanical stimulus to intracellular biochemical signals that mediate gene and protein regulation. The adaptive response of ECs is important in maintaining the vascular tone and homeostasis of the functional endothelium. Many components have been proposed to act as mechanosensors of shear stress such as primary cilia, caveolae, integrins, cell-cell junction proteins (VE-Cadherin, platelet endothelial cell adhesion molecule 1 (PECAM1), and VEGFR2), heterotrimeric G proteins, the apical glycocalyx, nucleus, actin cytoskeleton, ion channels and intermediate filaments[29,30]. Nonetheless, it is difficult to conclude which of these has the most prominent role and, perhaps an orchestrated action of many of the above mechanosensors contributes to translating the biomechanical input to intracellular responses in ECs.

Although the cytoskeleton of ECs is not considered as a primary mechanosensors per se, it plays a significant role in the response of ECs to shear stress. The cytoskeleton is crucial in maintaining cell tension at adhesion sites, cell junctions and at the nuclear membrane. It is also implicated in activation of mechanosensitive ion channels and in determining cell geometry[31]. Flow-mediated mechanotransduction involves all three main cytoskeleton proteins- actin microfilament, intermediate filaments and microtubules[31,32]. *In situ* studies report that upon sensing shear forces, ECs exhibit a striking change of morphology where they appear elongated and align themselves in the direction of blood flow. This has been attributed to the actin microfilament reorganization in ECs where shear induces a redistribution of F-actin from the cell periphery to central regions (peri-nuclear). Subsequent formation of central short stress fibers in the direction of flow leads to close association of these stress fibers to the abluminal surface of cells; eventually contributing to stronger substrate adhesion of ECs[33].

1.4.2 Endothelial cell response to shear stress

ECs sense and respond to shear stress exerted by different types of blood flow. Hemodynamic forces experienced by vessel wall are a large influence that determines which regions are prone to atherosclerotic lesion formation. ECs that are exposed to steady laminar blood flow

experience high shear stress and these parts of arteries are protected from atherosclerosis. At regions near bifurcation and bends in arteries, ECs are exposed to low shear stress and hence experience disturbed or turbulent flow. This disturbed flow comprises of non-uniform, irregular oscillations, flow separation and recirculation of blood; consequently predisposing these areas to atherosclerosis (Fig I.5). Shear stress in the magnitude of 4 dyn/cm^2 has been described as disturbed flow whereas steady laminar flow is usually >12 dyn/cm^2 as analyzed by fluid mechanical models[34].

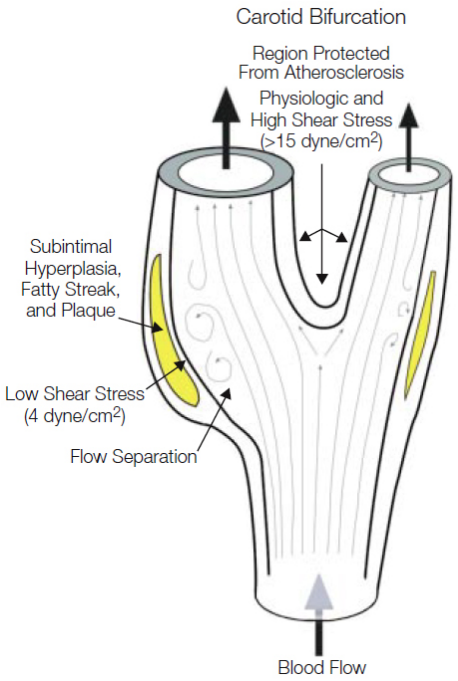

Figure I.5. Focal nature of atherosclerosis.
Schematic diagram of a carotid artery bifurcation illustrating regions protected from atherosclerosis (exposed to laminar flow and high shear stress) as opposed to those prone to plaque formation (yellow) that experience disturbed flow and low shear stress. (Adapted from Malek et al. 1999)[28]

Atherosclerosis is a chronic inflammatory disease which is a leading cause of death in the western world, associated with risk factors such as hypertension, diabetes, smoking, low density lipoprotein (LDL) cholesterol levels and genetic predisposition[35–37]. It is characterized by endothelial dysfunction and formation of atherosclerotic plaques in large and middle sized arteries exposed to low mean shear stress. The initiation and progression of atherosclerotic lesion formation is illustrated in figure I.6. As described earlier, hemodynamic forces are crucial for vessel remodeling and dictate which areas are predisposed or resistant to atherosclerosis. The outer edges of vessel bifurcations are most prone, where high risk coronary plaques develop upon experiencing consistent low shear stress over time, leading to increased lipid accumulation, matrix degradation, lumen narrowing and vessel remodeling.

All of these culminate in cardiovascular diseases such as myocardial infarction, stroke and heart failure.

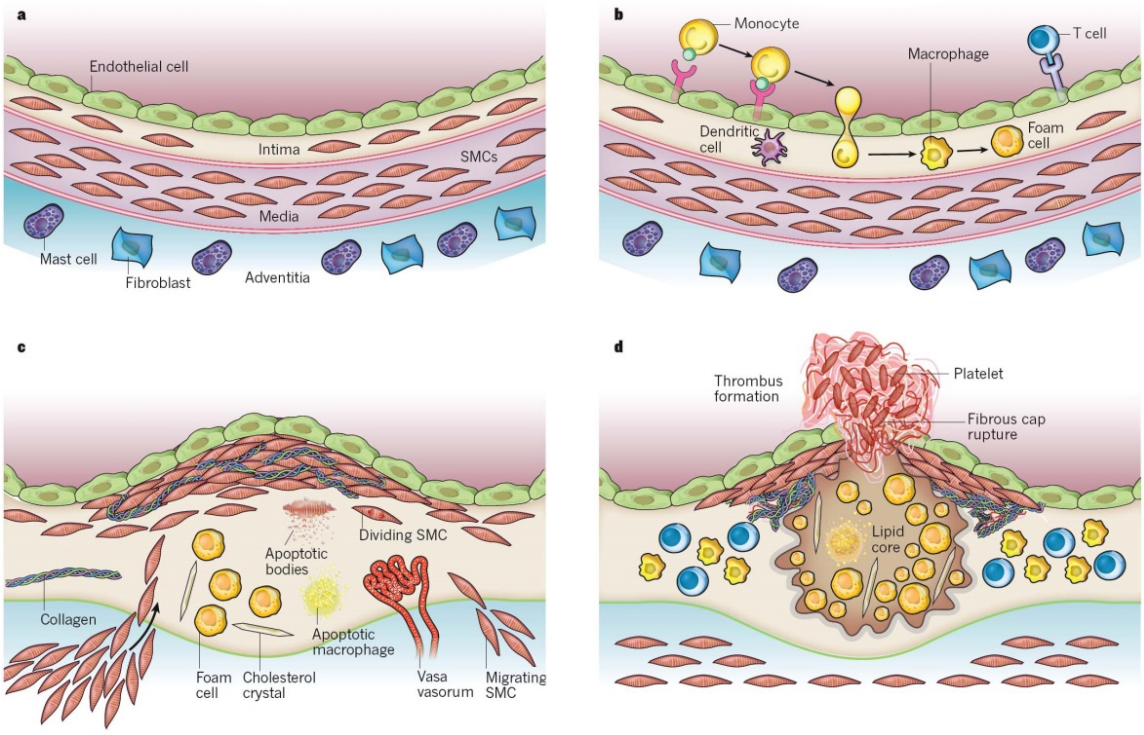

Figure I.6. Progression of atherosclerosis

a) Human arteries have three layers, the intima lined by an EC monolayer, the media and the adventitia. Human intima contains few resident vascular smooth muscle cells (VSMCs), the media contains VSMCs embedded in collagen, while the adventitia contains mast cells, fibroblasts and nerve endings. Plaque formation involves b) increased surface monocyte adhesion molecules like intracellular adhesion molecule 1 (ICAM1) and vascular cell adhesion molecule 1 (VCAM1) on ECs that activate endothelium causing monocytes and T-cells attachment, followed by infiltration of lipid and inflammatory cells into the intimal space. Monocytes differentiate into macrophages and take up lipids to form foam cells. c) VSMCs from the media migrate to intima and along with resident VSMCs in the intima they start to proliferate in response to mitogens such as platelet derived growth factor (PDGF). VSMCs additionally start synthesizing ECM proteins such as collagen and elastin which aids in the formation of a fibrous cap that later encloses the lipid core. d) On undergoing apoptosis, foam cells release lipids into the necrotic or lipid core that also contains cholesterol crystals in later stages. Furthermore, VSMCs are subjected to senescence by death receptor mediated signaling by macrophages and T-cells. Increased ECM activity along with VSMC senescence lead to fibrous cap plaque rupture followed by platelet interaction with lipid core components to form a thrombus. The thrombus extends into the blood lumen and can cause stenosis and ischemia, or can lead to embolism in other parts of arteries. (Adapted from Libby et al. 2011)[37]

1.4.3 Atheroprotection by laminar shear stress

In the recent years, multitudes of studies have confirmed laminar shear stress (LSS) to confer an atheroprotective and quiescent phenotype to the endothelium. LSS regulates many significant cell signaling pathways such as mitogen activated protein kinase (MAPK), mechanistic target of rapamycin (mTOR) and phosphoinositide 3-kinase (PI3K) through

which it exercises downstream protective effects against lesion formation[38]. These include anti-inflammatory, -proliferative, -coagulant, -oxidant and -apoptotic pathways as discussed below in detail.

Inflammation is a major contributor in the development of atherosclerosis. At the molecular level, pro-inflammatory stimuli tumor necrosis factor alpha (TNF-α) and disturbed flow instantaneously activate two key transcription factors, nuclear factor kappa B (NFκB, direct activation) and activator protein 1 (AP1) via c-Jun N-terminal kinase (JNK) and p38 MAPK pathways, an effect that is sustained for longer time periods. In contrast, although steady laminar flow may initially activate pro-inflammatory pathways as disturbed flow, upon longer exposure (in magnitudes of an hour or more) it induces an anti-inflammatory environment[32]. NFκB activation is crucial in leukocyte recruitment to endothelium and trans-endothelial migration of monocytes in lesion prone areas which is mediated by activation of monocyte adhesion molecules like VCAM1, ICAM1, E-selectin and chemokines like monocyte chemotactic protein 1 (MCP1) and interleukin 8 (IL-8). The transcription factor NFκB is sequestered in the cytoplasm through binding to its inhibitor IkB. Upon cytokine (TNF-α) activation, the IkB subunit is phosphorylated and degraded by ubiquitination thus dissociating from the NFκB dimer. The active NFκB translocates to the nucleus and binds to activate the target promoter of pro-inflammatory genes[39]. ECs exposed to disturbed flow have increased activity of NFκB[40] and this leads to subsequent increase in expression of surface adhesion molecules and chemokines.

LSS contributes to an anti-inflammatory effect by attenuating the TNF-α induced up regulation of pro inflammatory molecules E-selectin, VCAM1 and IL-8[41]. JNK and p38 MAPK activation is necessary for TNF-α induced expression of pro-inflammatory genes[42], and these two pathways function in concert with NFκB. JNK and p38 MAPK signaling increase MMP production, nicotinamide adenine dinucleotide phosphate (NAPDH) oxidase and pro-coagulation factors by ECs thus aggravating endothelial dysfunction and lesion formation[43]. LSS attenuates TNF-α induced JNK and p38 MAPK signaling[44,45] and also inhibits apoptosis signal regulating kinase 1 (ASK1), the upstream kinase of JNK[46]. Additionally, LSS activates mitogen activated protein phosphatase1 (MKP1) which is a negative regulator of JNK and p38 MAPKs[47].

LSS retards proliferation of ECs, where exposure for 6-12 hours of shear stress arrests transition of cells from G0/G1 to S phase, in addition to impeding DNA synthesis[48]. LSS

induces p21 gene, a cyclin inhibitor that leads to repression of cyclin dependent kinase 2 (cdk2) and cdk4 cyclins. Decrease in cdk activity prevents phosphorylation of retinoblastoma (Rb) protein and in turn leads to transcription factor E2F mediated cell cycle arrest[48]. Another proposed mechanism by which shear stress inhibits proliferation involves tumor suppressor p53. LSS activates JNK pathway that phosphorylates p53 in early time points of flow exposure. Active p53 induces growth arrest and DNA damage inducible 45 (GADD45) and p21 expression thus contributing to shear-mediated proliferation arrest in ECs[49].

Shear stress also mediates blood coagulation by inducing expression of thrombomodulin (TM) in ECs, a surface receptor that binds to thrombin and induces activation of protein C anticoagulant pathway[50]. LSS stimulates release of factors such as prostacyclin, nitric oxide (NO, anti-oxidant and vasodilator), calcium and tissue plasminogen activator (tPA), which collectively, promote an anti-thrombotic and anti-coagulant vascular endothelium[38]. Laminar flow plays an important role in regulating the vessel tone, by inducing expression of vasodilator endothelial nitric oxide synthase (eNOS)[51], and suppressing expression of vasoconstrictive genes such as endothelin[52], adrenomedullin[53] and angiotensin converting enzyme (ACE)[54].

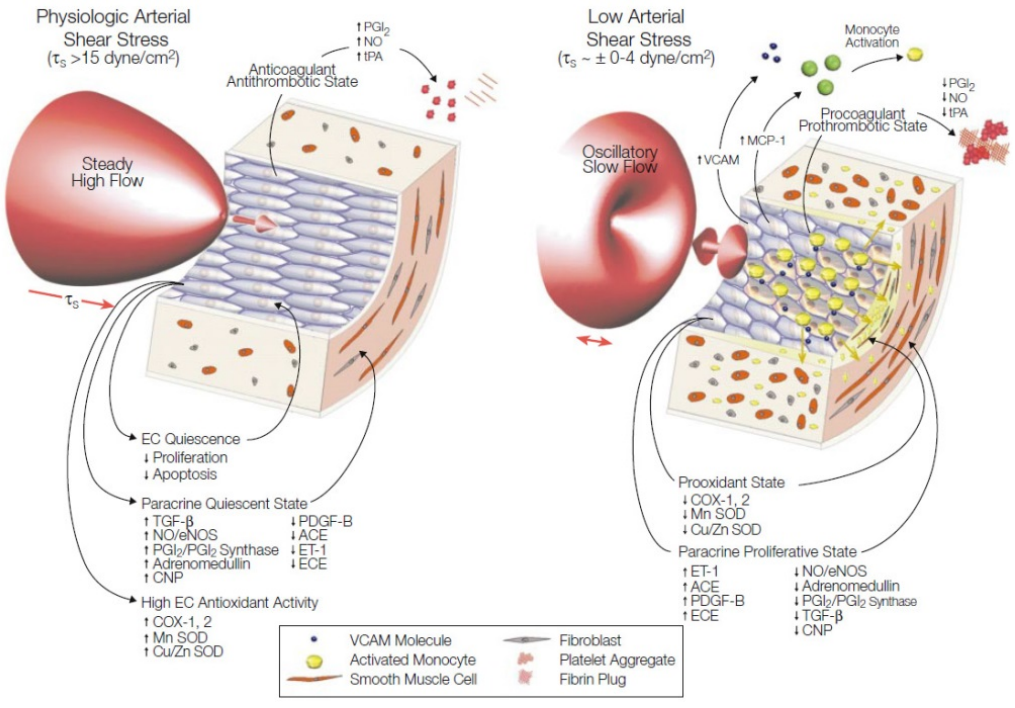

Figure I.7. Protective function of laminar shear stress exerted via multiple factors
Left panel illustrates the atheroprotective function of shear stress at 15 dyn/cm^2 exerted by steady laminar flow, where it induces an antithrombotic, antioxidant and pro-quiescence effect. The right panel describes the atherogenic phenotype of endothelium exposed to low shear stress < 4 dyn/cm^2 by disturbed flow at regions of

bifurcations. Low magnitude shear stress induced increased EC and SMC turn over, apoptosis and increased oxidant state. It also stimulates monocyte activation and increased platelet aggregation. (Adapted from Malek et al. 1999)[28]

Laminar flow initiates an anti-apoptotic, pro-survival environment for ECs by regulating various signal transduction pathways[43]. LSS protects ECs against apoptosis induced by growth factor deprivation, cytokine stimulation and oxidized LDL[55,56]. LSS inhibits apoptosis inducing oxidative stress generated from oxygen radicals (reactive oxygen species, ROS) by synergistically inducing copper/zinc superoxide dismutase (Cu/Zn SOD) expression (anti-oxidant) and eNOS gene expression and NO production[56]. Akt pathway plays a key role in mediating anti-apoptotic effects of LSS. Akt, a serine/threonine kinase, is upregulated upon flow[57] and it induces NO production that inhibits caspase-3 mediated apoptosis[43] and also inhibits bcl-2 associated death promotor (Bad) mediated apoptosis[58]. Another possible mechanism by which LSS inhibits TNFα induced apoptosis is by attenuating ASK1 and JNK activation that is required for caspase 3 function[43]. Interestingly, p21 also contributes to *in vitro* and *in vivo* shear dependent anti-apoptotic effects, where overexpression of p21 in mice post hind limb ischemia (HLI) led to reduced apoptosis and better vessel remodeling after ischemic damage[59].

1.4.4 Gene expression changes elicited by prolonged shear stress

Shear stress elicits time dependent response of many factors and pathways. In a matter of seconds of shear stress exposure, activation of potassium (K^+) channels, Src kinases, VEGFR2 and NO release is observed and in minutes, flow activates MAPK, Rho GTPases, integrins, NFκB, p21 activated kinase (PAK) and JNK pathways[30]. Longer exposure, hours or days, leads to activation of transcription factors such as early growth response protein 1 (EGR1), nuclear factor erythroid 2- related factor 2 (Nrf2), Krüppel like factor 2 (KLF2) and regulation of downstream gene expression patterns[30,60].

Gene expression studies of ECs exposed to atheroprone or atheroprotective shear stress wave forms, modeled on shear stress profiles in human carotid artery bifurcations, showed transcription factors Nrf2 and KLF2 to be highly induced by atheroprotective shear stress[61,62]. Nrf2 is thought to confer an anti-inflammatory and anti-oxidant feature[63], while KLF2 contributes to maintaining an anti-thrombotic and anti-inflammatory phenotype of the endothelium. Nrf2 is localized in the cytoplasm bound to kelch-like ECH-associated protein 1 (Keap1) under basal conditions, which leads to its proteasome degradation. Electrophiles that modify cysteine residues of Keap1 or oxidative stress conditions lead to dissociation of Nrf2

from its binding partner Keap1, resulting in Nrf2 localization to the nucleus and allowing downstream anti-oxidant responsive element (ARE) dependent gene expression[63,64]. Atheroprotective shear stress activates Nrf2 via the PI3K/Akt pathway and liberates Nrf2 from Keap1, consequently promoting Nrf2 nuclear localization and accumulation[61]. Nrf2 activates downstream anti-oxidant and phase II detoxification genes mainly heme oxygenase 1 (HO1), ferritin heavy polypeptide (FTH), glutamate cysteine ligase, modifier subunit (GCLM) and NAD(P)H dehydrogenase quinone 1 (NQO1), in turn regulating endothelial redox homeostasis, which was shown to be independent of KLF2 activity[61]. Many of these downstream genes have been implicated in atherosclerotic lesion formation (HO1)[65], coronary vasomotor function (GCLM)[66] and as a risk factor for myocardial infarction (GCLM)[67] which reinforces the important role of Nrf2 in atherogenesis and coronary artery disease. KLF2 is also known to improve nuclear localization of Nrf2 and the coordinated activation of both Nrf2 and KLF2 constitute 75% of shear stress induced vasoprotective gene expression in ECs[68]. Thus, shear stress tips the balance to an anticoagulant, anti-oxidant and anti-inflammatory environment via atheroprotective flow induced Nrf2 and KLF2 activation versus disturbed atheroprone flow promoting a pro-inflammatory milieu with increased oxidative stress involving NFκB and AP-1 pathway activation[27,69].

1.5 Krüppel like factor 2 (KLF2) and its role in vasculature

1.5.1 KLF transcription factor family

KLF family of DNA binding zinc finger transcription factors were first identified in Drosophila, where loss of the Krüppel protein in embryos led to impaired abdominal and thoracic segment development (crippling appearance) and fatality[70]. To date, seventeen mammalian KLFs have been identified (KLF1 to -17) and all of them recognize GC- and GT-rich sequences. Key features of this KLF zinc finger family is that they have three consecutive Cys2/His2 zinc finger motifs at the C-terminal end of the protein and they bind to specific DNA sequence motif “CACCC” or the GT box[71]. They also contain a consensus amino acid sequence [TGEKP(Y/F)X] between zinc finger motifs and are similar to the Sp1 family of zinc finger factors[71]. KLFs have been implicated in several cellular processes in various cell types explained elegantly by knockout studies[72]. Among them, KLF2, KLF4 and KLF6 have been described to be important in endothelial biology.

1.5.2 Phenotype of KLF2 knockout mice

KLF2 is developmentally regulated, where it is first noted at embryonic day E7, decreased at E11 and reactivated at E15 in wild type embryos[73]. It has been reported to be essential for normal lung development[74], blood vessel formation[75] and vascular tone maintenance[76]. Constitutive KLF2 knockout mice are lethal and embryos die between E12.5 and E14.5 due to intra-embryonic and intra-amniotic hemorrhage[77]. Embryos have impaired smooth muscle recruitment and tunica media formation[75,78], causing aneurysm of arteries and veins and resulting in vessel rupture and death. Additionally, a decrease in extracellular matrix deposition, reduced number of pericytes and EC necrosis was observed in embryos[78]. Endothelial specific KLF2 knockout mice die in utero due to embryonic heart failure caused by high cardiac output state which is attributed to abnormal peripheral vascular resistance or lack of vascular tone[76]. Interestingly, vasculogenesis and angiogenesis in both constitutive and EC-specific KLF2 knockout mice were unaffected; highlighting the role of KLF2 mainly in recruitment and migration of VSMCs and knockout of KLF2 in SMC *in vivo* had no apparent phenotype[76]. Hemizygous KLF2 knockout mice ($KLF2^{-/+}$) are viable and do not show any obvious phenotype possibly due to compensatory effect of KLF4. However, when crossed with apo lipoprotein deficient mice ($ApoE^{-/-}$), which are predisposed to the development of atherosclerosis, $KLF2^{-/+}$ mice show increased plaque burden and aggravated atherosclerosis development due to increased foam cell formation[79].

1.5.3 Mechanism of KLF2 activation by laminar flow

KLF2 expression levels are robustly upregulated in ECs by laminar shear stress *in vitro* and *in vivo*[80]. Endothelial KLF2 is induced by shear stress through binding of nuclear factors at an evolutionary conserved 62bp long shear stress response element in the promoter region (-157 to -95 nucleotides)[81]. More specifically a 30 base pair (bp) (-138 to -108 nucleotides) element with a tripartite AT rich palindromic motif elicits maximum shear response; however the full 62bp region is essential for the stable binding of the nuclear complex at the promoter. The mechanism for induction of KLF2 transcription on flow exposure has been elegantly described by Parmar and group to involve MAPKs, the MEK5/ERK5/MEF2 cascade[82].

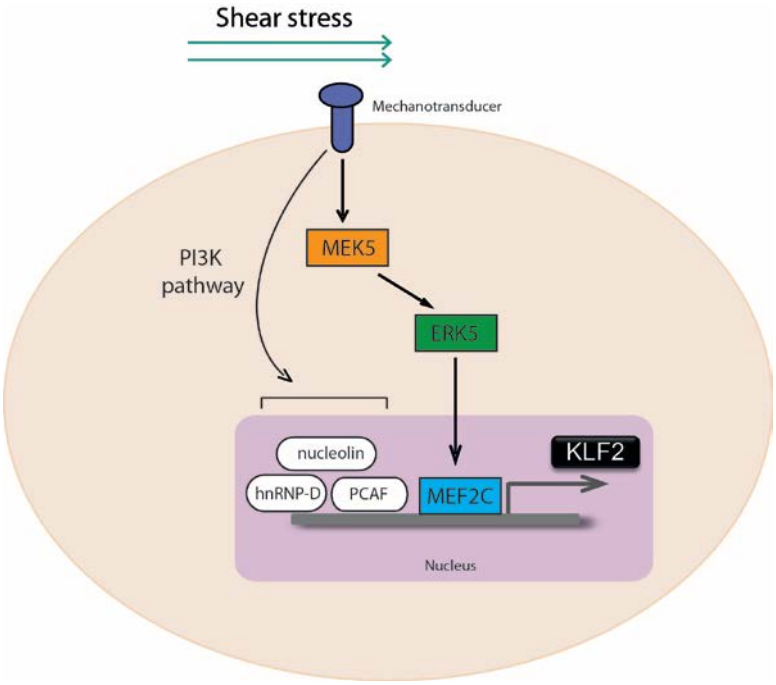

Figure I.8. Shear stress induces KLF2 transcription via MAPK pathway
Flow activates MAPK kinase 5 (MEK5), a kinase required for normal heart development and cell survival[83] and in turn MEK5 functions as an upstream activating kinase for extracellular signal regulated kinase 5 (ERK5). ERK5 is another important MAPKs essential for cardiovascular development and maintaining endothelial integrity[84,85]. Phosphorylation of ERK5 by MEK5 leads to downstream activation of myocyte enhancer binding factor 2 (MEF2), a transcription factor that has been implicated in vascular development[86] (MEF2C) and coronary artery disease[87] (MEF2A). MEF2C binds to the evolutionary conserved MEF2 binding site on the promotor of KLF2 and consequently leads to an increase in KLF2 transcription.

Other factors such as p300/CREB-binding protein associated factor (PCAF), heterogeneous nuclear ribonucleoprotein D (hnRNP-D) bind to this KLF2 promotor motif in response to shear stimuli to enhance MEF2C mediated transcriptional activation of KLF2 in a PI3K dependent/Akt independent manner[81]. Histone H3 and H4 are targets of PCAF acetylation[88] and acetylation of these two histones within the KLF2 promotor upon shear induced recruitment of the PCAF/hnRNP-D complex leads to chromatin remodeling and better access for RNA pol II to allow for transcription of KLF2[81]. Another protein, nucleolin has also been shown to bind to the KLF2 promotor and regulates KLF2 transcription in a flow specific PI3K dependent manner involving interaction with the p85 subunit of PI3K as well as hnRNP-D[89].

1.5.4 Functions of KLF2 in the vascular endothelium

KLF2 is atheroprotective and also induces EC quiescence, much similar to shear stress. *In situ* hybridization studies in human arteries showed a direct correlation between bifurcation regions experiencing low shear stress levels and decreased KLF2 levels in addition to neo

intima formation[62]. Indeed, shear stress increases expression of KLF2 *in vivo* and *in vitro* and KLF2 governs almost 70% of the gene sets regulated by shear stress[80] such as shear mediated-transcriptional activation of eNOS and TM gene expression[90]. KLF2 additionally suppresses thrombin adhesion to its receptor by down regulating expression of thrombin receptors coagulation factor 2 receptor (F2R) and proteinase activated receptor (PAR1)[91,92]. Shear stress induces resistance to oxidative stress and reduces adhesion of monocytes to ECs during atherosclerosis progression, in a KLF2 dependent manner[82].

KLF2 functions as an anti-inflammatory molecule by inhibiting NFκB transcriptional activity and inhibition of TNF-α and interleukin 1 beta (IL-1β) induced expression of adhesion molecules VCAM1 and E-selectin[51]. Additionally KLF2 prevents phosphorylation of c-Jun and nuclear localization of phosphorylated ATF2[93], both required for the formation of the pro-inflammatory AP1 complex[94]. On the contrary, TNF-α inhibits KLF2, by suppressing MEF2C via NFκB and histone deacetylase 4/5 (HDAC4/5) activity[95].

KLF2 is essential for actin shear fiber formation that mediates flow mediated EC elongation and alignment. KLF2 upon activation by shear stress promotes formation of short, thick actin filaments that prevents focal adhesion kinase (FAK) mediated activation of JNK. Consequently, KLF2 inhibits MAPK pathway, specifically pro-inflammatory JNK targets c-Jun and ATF2 in an actin dependent manner[96]. KLF2 inhibits EC migration, elegantly shown by wound healing assays, by inducing migration inhibitor semaphorin 3F (Sema3F)[91]. KLF2 is indeed anti-angiogenic and anti-proliferative, where it inhibits VEGF induced angiogenesis in a nude mouse ear model, by inhibiting VEGFR2 expression[97]. Hypoxia induced angiogenesis is inhibited by KLF2 through suppression of HIF1α expression and leads to its subsequent degradation[98]. Thus, by regulating multiple pathways, KLF2 drives ECs into a quiescent state.

1.5.5 Statins exert atheroprotective effects on endothelium via KLF2

Another key finding in the field of KLF2 protective function was the KLF2 mediated effects of statins on the vasculature. Statins are the most widely prescribed cardiovascular drugs to reduce mortality and morbidity related to cardiovascular diseases. They are essentially inhibitors of 3- hydroxy-3-methylglutaryl coenzyme A (HMG-CoA) reductase, a rate limiting enzyme in the cholesterol biosynthesis pathway and hence reduce plasma cholesterol levels[99]. Of the non-lipid lowering beneficial pleiotropic effect of multiple statins, induction of KLF2 expression via attenuation of Rho activity is one. Inhibition of cholesterol pathway by statins

leads to reduction in geranyl-geranyl-pyro phosphate (GGPP) that is required for Rho function[100,101]. Inhibition of Rho by statins thus leads to induction of KLF2 transcription[100] and also prevents NFκB pro-inflammatory activity[102], which would have additionally inhibited KLF2 function[95].

Stabilization of KLF2 steady state levels in ECs by shear stress has been described to be PI3K dependent[103]. Interestingly, this stabilization of KLF2 mRNA and subsequent protein induction is absent on statin treatment, owing to their inability to invoke induction of downstream eNOS and TM expression, especially during inflammatory insult by TNF-α[103]. In addition to the above explained effects in ECs, statins also induce KLF2 expression in lymphocytes[104] and macrophages[105], consequently eliciting an anti-inflammatory response in both cell types that play critical roles in atherogenesis.

1.6 Linking angiogenesis and endothelial metabolism

The crosstalk between angiogenesis and metabolism has only been recently explored. Angiogenic factors and vessels promote and repair metabolically active tissues such as liver, pancreas, adipose tissue. VEGF and VEGF-B, angiogenic factors also influence oxidative metabolism and fatty acid uptake by stimulating ECs to utilize oxygen and nutrients[24]. Conversely, many metabolic regulators seem to play a role in angiogenesis. Noteworthy is adenosine mono phosphate-activated protein kinase (AMPK), a metabolic sensor activated upon energy deprivation, which increases VEGF levels and promotes revascularization of ischemic tissue[106]. Peroxisome proliferator-activated receptor gamma, coactivator 1 alpha (PGC1α) and estrogen related receptor alpha (ERRα), both implicated in mitochondrial biogenesis and metabolism, play a role in exercise and VEGF induced angiogenesis since lack of these proteins in mice leads to impaired vascular density post exercise[107]. Sirtuin 1 (SIRT1), a NAD+ dependent deacetylase dictated by metabolic state of EC, is a pro-angiogenic factor that mediates angiogenesis via its downstream effectors Notch and forkhead box O (FOXO). FOXO, a transcription factor which is negatively regulated by PI3K/Akt signaling, inhibits angiogenesis in ECs[108]. Notch signaling, as described previously inhibits proliferation. Recent studies published during the course of this thesis study, have revealed the importance of various metabolic pathway regulations in endothelial cell functions and have given valuable insights into metabolism in actively proliferating and migrating EC subtypes, detailed below[109–111].

1.6.1 Glucose metabolism

Glycolysis is a key metabolic pathway regulating EC physiological functions. ECs have the capacity to switch from quiescence to actively angiogenic state upon stimulation by various factors. For ECs to migrate and proliferate, in addition to changes in genetic signals, a metabolic switch is necessary to adapt to the high energy demands of the sprouting process. Previous studies have shown that proliferating ECs predominantly are addicted to glycolysis and it serves as the major adenosine triphosphate (ATP) generating pathway contributing to almost 80% of cellular ATP[112,113]. Glucose is taken up by ECs through facilitated diffusion via GLUT transporters, mainly GLUT1. Once glucose enters the cells, it is metabolized to pyruvate by glycolysis yielding 2 moles of ATP per glucose molecule. Pyruvate is then converted to lactate (aerobic glycolysis) and exported out of the cell, instead of being oxidized using the available oxygen in the blood stream. Notably, <1% of pyruvate generated from glycolysis undergoes oxidation in the tricarboxylic acid (TCA) cycle, under glucose availability[111].

It is paradoxical for ECs to perform aerobic glycolysis instead of glucose oxidation, even in abundance of oxygen (O_2) in the environment (Warburg effect), a striking resemblance to highly proliferating tumor cells[114]. The reasons behind ECs to prefer aerobic glycolysis could likely be 1) lower oxygen consumption by ECs may contribute to better trans-endothelial transport and availability of O_2 to perivascular tissues 2) low mitochondrial content and oxidative metabolism means reduced oxidative phosphorylation (OXPHOS) generated ROS and oxidative stress[115,116] 3) rate of ATP production is as rapid or more than that in OXPHOS, when glucose in unlimited, which aids energy demanding processes like formation of lamellopodia and filopodia during migration 4) glycolysis shunts glucose into side branch pathways for biosynthesis of macro-molecules (cell mass) required for actively proliferating cells 5) for adaptation of ECs to hypoxic environment they grow into 6) lactate produced serves as a pro-angiogenic cue.

In proliferating ECs, an increased uptake of glucose and expression of GLUT1, lactate dehydrogenase A (LDHA) and 6-phosphofructose-2-kinase/fructose-2, 6-biphosphatase 3 (PFKFB3) among other glycolytic genes has been reported[117]. The rate limiting step of the pathway involves PFKFB3, an enzyme that catalyzes the conversion of fructose-1, 6-bisphosphate (F1,6BP) to fructose-2, 6-bisphosphate (F2,6BP) in the glycolytic pathway. F-2, 6-BP is an allosteric activator of phosphofructokinase 1 (PFK1) which is the most potent

stimulator of glycolysis. Increased expression of PFKFB3 in cancer cells is a hallmark feature, where PFKFB3 driven glycolysis is important for their rapid proliferation[118]. Genetic silencing of PFKFB3 and pharmacological inhibition of PFKFB3 by 3-(3-pyridinyl)-1-(4-pyridinyl)-2-propen-1-one (3-PO) in ECs reduces proliferation, migration and sprouting capacity *in vitro*. Loss of function studies *in vivo*, where EC-specific deletion of PFKFB3 led to hypo branching of retinal vasculature in mice and 3-PO treatment caused impaired vascular development in zebrafish embryos, underscore the role of glycolysis in EC angiogenesis[109,111].

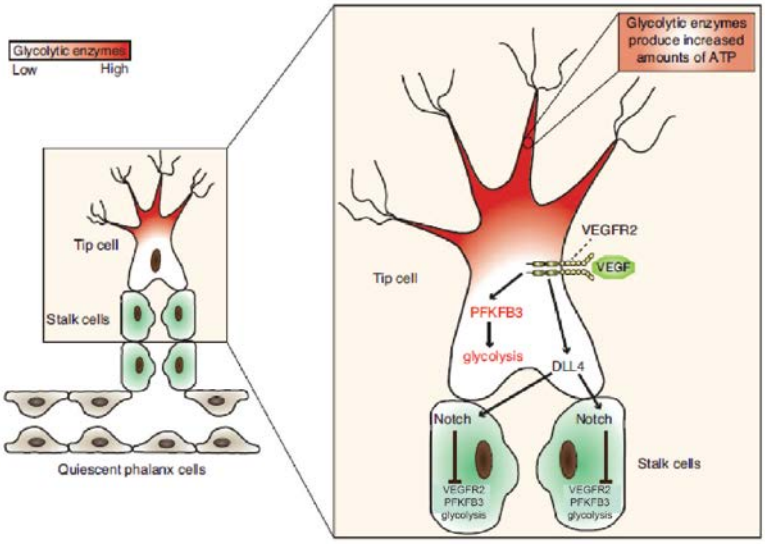

Figure I.9. Regulation of glycolysis in tip and stalk cells.
Binding of VEGF to VEGFR2 in tip cells (red) induces upregulation of DLL4, which activates Notch in the neighboring stalk cell (green). Notch inhibits VEGFR2 expression in stalk cells and prevents them from responding to VEGF or turning into a tip phenotype. Activation of VEGFR2 in tip cells also induces PFKFB3 expression and subsequent increase in glycolysis, which fuels rapid ATP production for migration during vessel sprouting. DLL4 dependent activation of Notch in stalk cells decreases PFKFB3 mediated glycolysis in stalk cells. (Adapted from Zecchin et al. 2015)[118]

PFKFB3 overexpression can overrule the pro-stalk activity of Notch signaling and promote stalk cells to adapt a more tip phenotype, highlighting that cellular metabolism in ECs (more specifically PFKFB3 driven glycolysis), without altering tip/stalk cell gene signatures, controls vessel sprouting in parallel with genetic signals[111]. Targeting EC glycolysis is a potential therapeutic option for impeding pathological endothelial angiogenesis.

1.6.2 Hexoamine and pentose phosphate pathways

The hexoamine biosynthesis pathway (HBP) is a side branch of glycolysis that involves conversion of glucose-6-phosphate (G6P) to UDP-N-acetyl-Glucosamine (UDPGlcNAc) which serves as a substrate for N-linked and O- linked glycosylation of proteins. The HBP is

dependent on glucose, acetyl-CoA, uridine and ATP availability for its functioning and is hence heralded as a nutrient sensing pathway in ECs[119]. HBP has been described to be essential for angiogenesis[120]. Furthermore, the functions of Notch and VEGFR2, key angiogenic factors, depend on their glycosylation status[121,122]. Another branch of glycolysis is the pentose phosphate pathway (PPP) which utilizes G6P or fructose-6-phosphate (F6P) to produce 5-carbon pentose sugars and NAPDH, which are required for biosynthesis of macromolecules and maintenance of redox homeostasis. Inhibition of glucose-6-phosphate dehydrogenase (G6PD) and transketolase, enzymes required for oxidative-PPP and non-oxidative PPP, reduces EC migration and viability and attenuates VEGF mediated angiogenesis[123,124].

1.6.3 Mitochondrial respiration

In ECs, mitochondria, as opposed to being the power house of the cell, functions mainly as a signaling organelle. Mitochondria are essential for generating pro-angiogenic ROS and NO which help in keeping basal mitochondrial respiration at low levels[119]. Mitochondria functions as an energy source only when glucose is limited, thus pushing ECs to switch from glycolytic to oxidative metabolism, known as the Crab-tree effect[125]. Mitochondria in ECs are functional but they contribute sparsely to total ATP production and hence activation or inhibition of mitochondrial respiration does not alter vessel sprouting and branching[111].

1.6.4 Fatty acid metabolism

Fatty acid uptake into cells is accomplished via fatty acid transporters, after which they are tagged with CoA moiety and transported into the mitochondria by carnitine palmitoyltransferase 1 (CPT1), a rate limiting enzyme in fatty acid oxidation (FAO). CPT1α loss leads to impaired EC permeability, indicating FAO regulates vessel stability[126]. In-vivo deletion of CPT1α in mice impaired angiogenesis, reduced proliferation but did not cause ATP or redox imbalance[110]. Schoors et al. recently described that FAO is important for the production of TCA intermediates used for biomass production and de novo nucleotide synthesis required for DNA replication[110]. During glucose deprivation, ECs have been shown to switch from glycolysis to fatty acid oxidation to generate and maintain ATP levels, in an AMPK dependent manner. VEGF stimulates expression of fatty acid uptake and trafficking protein fatty acid binding protein 4 (FABP4) that is implicated in EC proliferation and angiogenesis[127,128].

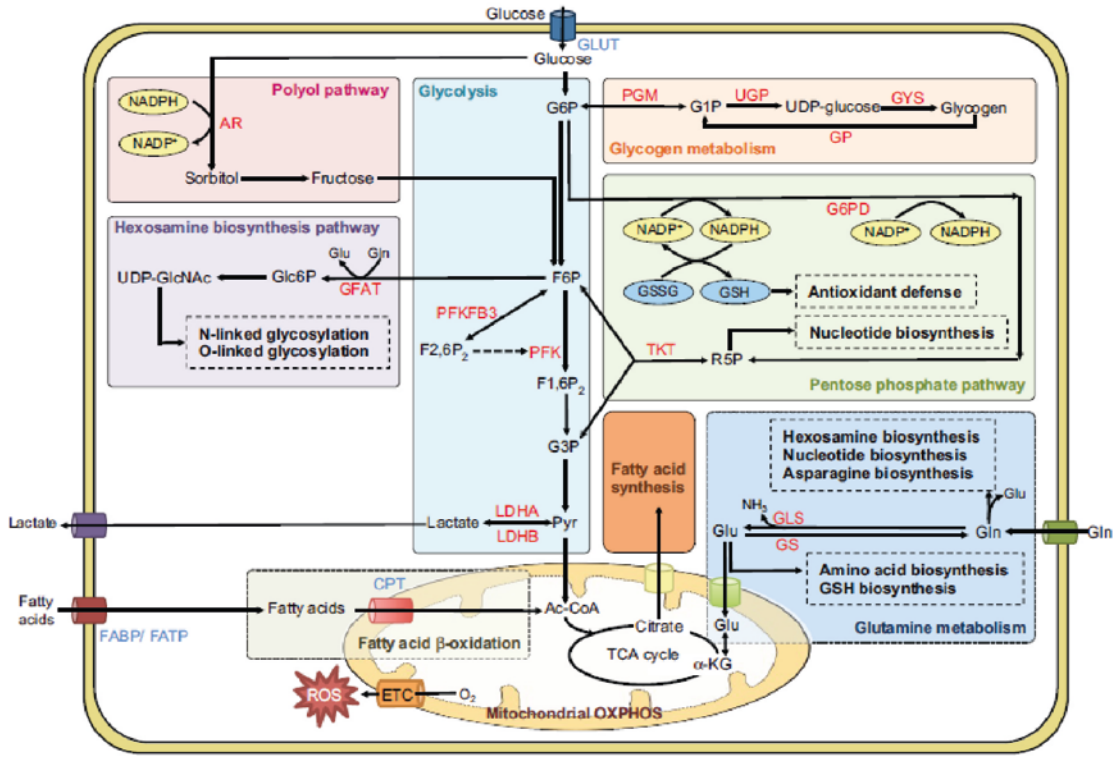

Figure I.10. Overview of endothelial metabolism

Scheme illustrating the principle metabolic pathways that influence EC metabolism. (Adapted from Stapor et al. 2014)[117].

1.6.5 Amino acid metabolism

Glutamine is the most abundant amino acid in the plasma and thus serves as an accessible fuel for ECs[129]. It is a conditionally essential amino acid that can be produced in ECs by glutamine synthetase using glutamate and ammonia as substrates or can be taken up by ECs via Na^+ dependent transporters[130]. Glutamine is further metabolized in ECs to yield predominantly glutamate and ammonia, apart from alanine, aspartate, asparagine, ornithine and carbon dioxide[129]. The first step of glutaminolysis is the conversion of glutamine to glutamate aided by enzyme glutaminase 1 and ECs show high activity of glutaminase 1 compared to other mammalian cell types[131,132]. This enzyme is crucial for EC function as pharmacological inhibition of glutaminase 1 leads to EC proliferation arrest and induction of premature senescence[133] thus stressing on glutamine metabolism as an important source of energy for ECs.

Glutamine metabolism is vital for ECs since it serves as a carbon and γ-nitrogen source for synthesis of purines and pyrimidine nucleotides essential during cell proliferation and for different biosynthetic processes. During glutaminolysis, carbons derived from glutamine are

supplied to the TCA cycle to compensate for the intermediates that are consumed for anabolic purposes (aneplerosis). Conversion of glutamate (derived from glutamine) to α-ketoglutarate occurs in the mitochondria and serves as a major source of energy to proliferating cells, especially in the context of tumor cells. Total oxidation of glutamine's carbon backbone eventually leads to multiple reactions involving conversion of α-ketoglutarate-malate-pyruvate and possible re-entry into TCA cycle as acetyl CoA[134]. Interestingly, glutamine being an oxidizable substrate, the contribution of glutamine oxidation to cellular ATP production and cell survival in ECs is significant only when glucose dependent ATP production is impaired due to oxidant injury[135].

1.6.6 Metabolic state of quiescent ECs

In a metabolic context, there is little known on the regulation of energy pathways of quiescent endothelial cells. Interestingly, despite having access to oxygen in blood, these rarely proliferating and migrating quiescent ECs have also been shown to rely on anaerobic glycolysis to derive energy for their baseline cellular functions[116]; however they have almost 40% reduction in glycolysis compared to actively proliferating cells[111]. Since proliferating ECs depend on glycolysis for dividing, reduction of glycolysis leads to proliferation arrest and a pro-quiescence milieu.

2. OBJECTIVE

Laminar flow and KLF2 have been described to promote EC quiescence and confer atheroprotection by mediating multiple signaling pathways. Until recently, the switching of ECs from an angiogenic state to quiescence was known to be governed mainly by growth factor and cell signaling pathways. Much work has been published in the last decades to uncover the metabolic pathways and mechanisms involved in angiogenic ECs and recent studies have described how metabolic pathways can greatly influence, even overrule growth factor and cell signaling pathways that control angiogenesis. However, little is known regarding the metabolic state of quiescent ECs which constitute most part of the vasculature. The objective of this thesis was to elucidate the following:

1) How do flow hemodynamics that promote endothelial quiescence affect metabolism of ECs? Does shear stress via KLF2 mediated effects alter metabolic pathways such as glycolysis (predominant energy producing pathway in ECs) or mitochondrial respiration? If so, what is the mechanism and does this contribute to the known anti-angiogenic effect of shear stress or KLF2?

2) Since shear stress and KLF2 are anti-inflammatory factors, does regulation of EC metabolism contribute to their anti-inflammatory, atheroprotective effects?

3. MATERIAL AND METHODS

3.1 Material

3.1.1 Consumables

Item	Manufacturer
1/4” ceramic spheres	MP Biomedicals (Illkirch, France)
96 well cell culture plates, U bottom	Greiner Bio-one GmbH (Frickenhausen, Germany)
96 well tissue culture plates, black	Corning (Big flats, NY, USA)
Cell culture dishes (6cm)	Greiner Bio-one GmbH (Frickenhausen, Germany)
Cell culture flasks (T25, T75, T150)	Greiner Bio-one GmbH (Frickenhausen, Germany)
Cell scraper	Greiner Bio-one GmbH (Frickenhausen, Germany)
Cell strainer (100µm)	BD Biosciences (Erembodegem, Belgium)
Color fixed pH indicator strips	Macherey-Nagel GmbH (Düren, Germany)
Combitips	Eppendorf (Hamburg, Germany)
Costar stripette serological pipettes	Corning (Big flats, NY, USA)
Filter Tips TipOne RPT (10, 20, 100, 200, 1000µl)	Starlab (Ahrensburg, Germany)
Hybond Nitrocellulose membrane	GE Healthcare (Little Chalfont, UK)
Immobilon-FL transfer membrane (PVDF)	Millipore (Billerica, MA, USA)
Lab-Tek II chamber glass slides (8 well)	Nalge Nunc Internationl (Naperville, IL, USA)
Microtubes 2ml, polypropylene	Sarsdtedt (Nümbrecht, Germany)
Multiwell cell culture plates (6, 12, 24 and 96 well)	Greiner Bio-one GmbH (Frickenhausen, Germany)
NucleoCasette	ChemoMetec A/S (Allerod, Denmark)
Nunc 96 microwell polystyrene plate, white	Thermo Scientific (Waltham, MA, USA)
Optical 96 well reaction plates	Applied Biosystems (Foster City, CA, USA)
Optical adhesive covers	Applied Biosystems (Foster City, CA, USA)
PCR tubes (0.5ml and 0.2ml)	Eppendorf (Hamburg, Germany)
Perfusion set (15cm, ID 1.6mm)	Ibidi (Martinsried, Germany)
Polypropylene falcon tubes (15ml and 50ml)	Greiner Bio-one GmbH (Frickenhausen, Germany)
Safe lock tubes (1.5 and 2ml)	Eppendorf (Hamburg, Germany)
Thincert transwell PET plates	Greiner Bio-one GmbH (Frickenhausen, Germany)
Ultra centrifugal filter devices 100K Amicon	Millipore (Billerica, MA, USA)
Whatman paper	Macherey-Nagel GmbH (Düren, Germany)
XF Seahorse 96 well tissue culture plates	Seahorse Bioscience (N.Billerica, MA, USA)
XF sensor cartridge	Seahorse Bioscience (N.Billerica, MA, USA)
µ slide y-shaped	Ibidi (Martinsried, Germany)
µ-slide I	Ibidi (Martinsried, Germany)
µ-slide I luer (0.4, 0.2, 0.1)	Ibidi (Martinsried, Germany)

3.1.2 Equipment

Instrument	Model/type	Manufacturer
8 channel multipipette		Eppendorf (Hamburg, Germany)
Adjustable volume pipettes		Eppendorf (Hamburg, Germany)
Cell counter	Nucleocounter	ChemoMetec A/S (Allerod, Denmark)
Centrifuge (falcons, plates)	Multifuge 3S-R	Heraeus Instruments (Osterode, Germany)
Centrifuge benchtop	Biofuge Primo R	Heraeus Instruments (Osterode, Germany)
CO_2 Incubator	Galaxy 170S	Eppendorf (Hamburg, Germany)
Confocal Microscope	LSM 780, Axio Observer	Zeiss (Jena, Germany)
Confocal Microscope	DMI6000B	Leica microsystems (Wetzlar, Germany)
Digital heat block	949307	VWR (Leuven, Belgium)
Extracellular flux analyzer	XFe96	Seahorse Bioscience (N.Billerica, MA, USA)
Extracellular flux analyzer and prep station	XF^e 96	Seahorse Bioscience (N.Billerica, MA, USA)
FACS	Canto II	BD Biosciences (Franklin lakes, NJ, USA)
Homogenizer	FastPrep24	MP Biomedicals (Solon, OH, USA)
Imaging system	FluorChem M system	Proteinsimple (Santa Clara, CA, USA)
Microplate multimode reader	GloMax®-Multi+with Instinct®	Promega (Madison, WI, USA)
Microplate reader	Synergy HT	Biotek (Winooski, VT, USA)
Microplate reader		TECAN (Männedorf, Switzerland)
Microscope	Axio Observer Z1	Zeiss (Jena, Germany)
Microscope	Axiovert 100	Zeiss (Jena, Germany)
Mini gel electrophoresis setup	Protean Tetra	Bio-Rad (Munich, Germany)
Mini Trans Blot Cell setup		Bio-Rad (Munich, Germany)
Multipipette	XStream	Eppendorf (Hamburg, Germany)
Neon transfection System	MPK5000	Invitrogen, Carlsbad CA, USA
Perfusion pump and fluidic unit	Version 1.1	Ibidi (Martinsried, Germany)
Perfusion unit	Perfusor fm	B.Braun (Melsungen, Germany)
Powersupply	Powerpac HC	BioRad (Munich, Germany)
Real time PCR system	StepOnePlus	Applied Biosystems (Foster city, CA, USA)
Safety cabinet	HeraSafe HS18	Heraeus (Hanau, Germany)
Shaking incubator	3003	GFL GmbH (Burgwedel, Germany)
Spectrophotometer	SmartSpec 3000	Bio-Rad (Munich, Germany)
Spectrophotometer	Nanodrop 2000	Thermo Scientific (Waltham, MA, USA)
Thermocycler	TProfessional basic	Biometra (Göttingen, Germany)
UV Trans illuminator	T2201	Sigma-Aldrich (St.Louis, MO, USA)
Vortexer	Vortex Genie 2	Scientific Industries (Bohemia, NY, USA)
Water bath	1008	GFL GmbH (Burgwedel, Germany)

3.1.3 Chemicals and reagents

Item name	Manufacturer
10X PCR buffer	Applied Biosystems (Foster City, CA, USA)
2,3-Butanedione monoxime (BDM)	Sigma-Aldrich (St.Louis, MO, USA)
2X Fast SYBR green mix	Applied Biosystems (Foster City, CA, USA)
3-(4, 5-Dimethylthiazol-2-yl)-2, 5-Diphenyltetrazolium Bromide (MTT)	Sigma-Aldrich (St.Louis, MO, USA)
37% Paraformaldehyde (PFA)	AppliChem (Darmstadt, Germany)
4', 6- diamidin-2-phenylindol (DAPI)	Roche (Indianapolis, USA)
7-AAD	BD Biosciences (San Diego, CA, USA)
Acetone	Sigma-Aldrich (St.Louis, MO, USA)
Acrylamide	AppliChem (Darmstadt, Germany)
Annexin V-V450	BD Biosciences (San Diego, CA, USA)
Ammonium per sulphate (APS)	Roth (Karlsruhe, Germany)
Binding buffer	BD Biosciences (San Diego, CA, USA)
Biotin isolectin B4	Vector laboratories (Burlingame, CA, USA)
Bovine Serum Albumin (BSA) Fraction V	PAA laboratories (Pasching, Austria)
Bradford reagent	Bio-Rad (Hercules, CA, USA)
Bromophenol blue	Merck (Darmstadt, Germany)
Calcium dichloride ($CaCl_2$)	Merck (Darmstadt, Germany)
CD31-APC	BD Biosciences (San Diego, CA, USA)
Chloroform	J T Baker (Phillipsburg, NJ, USA)
Collagenase Type II	Worthington Biochemical Corp. (New Jersey, USA)
Dimethyl sulfoxide (DMSO)	Sigma-Aldrich (St.Louis, MO, USA)
Dithiothretol (DTT)	AppliChem (Darmstadt, Germany)
DNAse, RNAse and protease-free water	5 Prime GmbH (Hamburg, Germany)
dNTP	Promega (Madison, WI, USA)
Ethanol absolute (EtOH)	Sigma-Aldrich (St.Louis, MO, USA)
Glycerin	AppliChem (Darmstadt, Germany)
Glycerol	AppliChem (Darmstadt, Germany)
Glycine	AppliChem (Darmstadt, Germany)
Goat antirabbit IgG secondary antibody AF-555	Molecular Probes (Eugene, OR, USA)
HCl	Sigma-Aldrich (St.Louis, MO, USA)
Immobilon western ECL reagent	Millipore (Billerica, MA, USA)
Isopropanol	Sigma-Aldrich (St.Louis, MO, USA)
JC-1	Molecular Probes (Eugene, OR, USA)
KH_2PO_4	Sigma-Aldrich (St.Louis, MO, USA)
$KHCO_3$	Sigma-Aldrich (St.Louis, MO, USA)
Magnesium dichloride ($MgCl_2$)	Sigma-Aldrich (St.Louis, MO, USA)

Magnesium dichloride ($MgCl_2$)	Applied Biosystems (Foster City, CA, USA)
Manganese dichloride ($MnCl_2$)	Sigma-Aldrich (St.Louis, MO, USA)
Methanol	Sigma-Aldrich (St.Louis, MO, USA)
Methyl cellulose	Sigma-Aldrich (St.Louis, MO, USA)
$MgSO_4.7H_2O$	Merck (Darmstadt, Germany)
Mitotracker deep red FM stain	Molecular Probes (Eugene, OR, USA)
Na_2HPO_4	Merck (Darmstadt, Germany)
$NaHCO_3$	AppliChem (Darmstadt, Germany)
Phalloidin AF-488	Molecular Probes (Eugene, OR, USA)
Phosphatase inhibitor	Roche (Indianapolis, USA)
Potassium chloride (KCl)	AppliChem (Darmstadt, Germany)
Protease inhibitor	Roche (Indianapolis, USA)
Protein block buffer, serum free	DAKO (Glostrup, Denmark)
Random primer	Thermo Scientific (Waltham, MA, USA)
RIPA buffer	Sigma-Aldrich (St.Louis, MO, USA)
SDS	Roth (Karlsruhe, Germany)
Sodium azide	Sigma-Aldrich (St.Louis, MO, USA)
Sodium chloride (NaCl)	J T Baker (Phillipsburg, NJ, USA)
Sodium hydroxide (NaOH)	Roth (Karlsruhe, Germany)
Staurosporine	Sigma-Aldrich (St.Louis, MO, USA)
Streptavidin AF-488	Molecular Probes (Eugene, OR, USA)
Sucofin skimmed milk powder	TSI GmBH (Zevern, Germany)
Tamoxifen base	Sigma-Aldrich (St.Louis, MO, USA)
Taurine	Sigma-Aldrich (St.Louis, MO, USA)
TEMED	AppliChem (Darmstadt, Germany)
Tris pure	AppliChem (Darmstadt, Germany)
Triton X-100	Sigma-Aldrich (St.Louis, MO, USA)
Tween 20	Sigma-Aldrich (St.Louis, MO, USA)
XF Calibrant solution	Seahorse Bioscience (N.Billerica, MA, USA)

3.1.4 Kits

Name	Manufacturer
Apo-ONE homogenous caspase 3/7 assay kit	Promega (Madison, WI, USA)
BrdU flow kit	BD Biosciences (San Diego, CA, USA)
Cell titer luminescent cell viability assay kit	Promega (Madison, WI, USA)
DNeasy blood and tissue DNA isolation kit	Qiagen (Hilden, Germany)
Dual luciferase reporter assay	Promega (Madison, WI, USA)
DuoSet IC Human Phospho AMPKα1 (T174) elisa kits	R&D Systems (Minneapolis, MN, USA)
EasyPrep Pro plasmid miniprep kit	Biozym Scientific (Oldendorf, Germany)

EnzyChrom NAD+/NADH assay kit	BioAssay Systems (Hayward, CA, USA)
Gateway LRII clonase kit	Invitrogen (San Diego, CA, USA)
Human Phospho-Kinase Array Kits (Proteome Profiler^{TM})	R&D Systems (Minneapolis, MN, USA)
miRNeasy RNA isolation kit	Qiagen (Hilden, Germany)
MitoPT TMRM assay kit	Immunochemistry Technologies
Neon transfection system 100µl kit	Invitrogen (Carlsbad CA, USA)
Plasmid maxi kit	Qiagen (Hilden, Germany)
QiaQuick Gel extraction kit	Qiagen (Hilden, Germany)
Senescence beta galactosidase staining kit	Cell Signaling (Danvers, MA, USA)
XF cell mito stress test kit	Seahorse Bioscience (N.Billerica, MA, USA)
XF Glycolysis stress test kit	Seahorse Bioscience (N.Billerica, MA, USA)

3.1.5 Bacteria

Name	Manufacturer
One Shot Stbl3chemically competent *E.Coli*	Invitrogen (San Diego, CA, USA)
One Shot Top10 competent cells	Life Technologies (Carlsbad, CA, USA)

3.1.6 Bacterial growth medium, agar plates

Name	Media formulation	Manufacturer
LB Agar capsules	1% Tryptone, 0.5% Yeast extract-B, 1% NaCl, 1.5% Agar-B	MP Biomedicals (Irvine, CA, USA)
LB medium capsules	1% Tryptone, 0.5% Yeast extract, 1% NaCl (pH 6.7)	MP Biomedicals (Irvine, CA, USA)
S.O.C medium	2% Tryptone, 0.5% Yeast extract, 10mM NaCl, 2.5mM KCl, 10mM $MgCl_2$, 10mM $MgSO_4$, 20mM glucose	Invitrogen (Carlsbad, CA, USA)

3.1.7 Plasmids

Plasmid name	Manufacturer
pGL4.10 [*luc2*]	Promega (Madison, WI, USA)
pGL4.74 [*Rluc*]	Promega (Madison, WI, USA)
pENTR221 (with PFKFB3 cDNA)	Source BioScience (Nottingham, UK)
pLenti4/V5 DEST	Invitrogen (San Diego, CA, USA)

3.1.8 Enzymes

Enzyme name	Manufacturer
Eco RV HF	New England Biolabs (Frankfurt am Main, Germany)

Hind III HF	New England Biolabs (Frankfurt am Main, Germany)
KpnI HF	New England Biolabs (Frankfurt am Main, Germany)
MuLV reverse transcriptase	Applied Biosystems (Foster City, CA, USA)
NcoI HF	New England Biolabs (Frankfurt am Main, Germany)
RNAse inhibitor	Applied Biosystems (Foster City, CA, USA)
T4 DNA ligase	Promega (Madison, WI, USA)

3.1.9 Cell culture solutions and supplements

Item name	Manufacturer
0.5% Trypsin EDTA	Life Technologies (Paisley, UK)
20kDa TMR Dextran	Sigma-Aldrich (St.Louis, MO, USA)
2-NBDG	Life Technologies (Carlsbad, CA, USA)
2-Deoxy-D-Glucose (2DG)	Seahorse Bioscience (N.Billerica, MA, USA)
3-PO	Millipore (Billerica, MA, USA)
Claycomb medium	Sigma-Aldrich (St.Louis, MO, USA)
DFO	Sigma-Aldrich (St.Louis, MO, USA)
DMEM/F-12	Invitrogen (San Diego, CA, USA)
Dulbecco's Phosphate Buffer Saline (PBS)	Life Technologies (Paisley, UK)
EGM single quots	Lonza (Verviers, Belgium)
Endothelial Basal Medium (EBM)	Lonza (Verviers, Belgium)
Fetal Bovine Serum	Invitrogen (San Diego, CA, USA)
Fetal Bovine Serum (F2442)	Sigma-Aldrich (St.Louis, MO, USA)
Fibronectin (F1141)	Sigma-Aldrich (St.Louis, MO, USA)
Fibronectin from human plasma (0.1% solution)	Sigma-Aldrich (St.Louis, MO, USA)
Gelatin from bovine skin	Sigma-Aldrich (St.Louis, MO, USA)
Genejuice Transfection reagent	Millipore (Billerica, MA, USA)
Glucose 40%	B.Braun (Melsungen, Germany)
Glutamax-I (100X)	Life Technologies (Paisley, UK)
Hanks BSS	PAA laboratories (Pasching, Austria)
HEPES, 1M	Invitrogen (San Diego, CA, USA)
L-Glutamine	Sigma-Aldrich (St.Louis, MO, USA)
Lipofectamine RNAimax	Life Technologies (Carlsbad, CA, USA)
L-NAME	Sigma-Aldrich (St.Louis, MO, USA)
M199 medium	Sigma-Aldrich (St.Louis, MO, USA)
Matrigel basement membrane matrix	BD Biosciences (San Diego, CA, USA)
Norepinephrine	Sigma-Aldrich (St.Louis, MO, USA)
OptiMEM	Invitrogen (San Diego, CA, USA)
Penicillin-Streptomycin	Sigma-Aldrich (St.Louis, MO, USA)
Penicillin-Streptomycin (500X)	Roche (Mannheim, Germany)

Phenol red	Sigma-Aldrich (St.Louis, MO, USA)
Rat tail collagen type I (aortic ring assay)	Millipore (Billerica, MA, USA)
Rat tail collagen type I (spheroid assay)	BD Biosciences (San Diego, CA, USA)
Sodium pyruvate	Life Technologies (Paisley, UK)
Tumor Necrosis factor alpha (TNF-α)	Peprotech (Rocky hill, NJ, USA)
Unbuffered DMEM base	Sigma-Aldrich (St.Louis, MO, USA)
Vascular Endothelial Growth Factor (VEGF)	Peprotech (Rocky hill, NJ, USA)

3.1.10 Primary cells and cell lines

Name	Species	Source	Manufacturer
HUVEC	*Homo sapiens*	Umbilical vein	Lonza (Verviers, Belgium)
HEK293FT	*Homo sapiens*	Kidney	Clontech (Mountain View, CA, USA)
HL-1	*Mus musculus*	Heart	Prof. W. Claycomb (New Orleans, LA, USA)

3.1.11 Animals

Name	Provided by
Cdh5-CreERT2 mice	Dr. Ralf Adams (Münster, Germany)
KLF2 flox/flox mice	Dr. Sebzda (Vanderbilt University, TN, USA)

3.2 Methods

3.2.1 Cell culture

3.2.1.1 Cell cultivation

Pooled Human Umbilical Vein Endothelial Cells (HUVEC) were purchased from Lonza and cultured in EBM (Lonza) supplemented with 10% FBS (Invitrogen) and bovine brain extract, hydrocortisone, epidermal growth factor, gentamycin sulphate, ascorbic acid and amphotericin-B (EGM-SingleQuots, Lonza). The supplemented media will be referred to as full EBM media in this thesis from here after.

Human Embryonic Kidney (HEK) 293FT cells were purchased from Clontech, cultured in DMEM containing L-glutamine (Invitrogen) supplemented with heat inactivated 10% FBS (Invitrogen) and 500U/ml of Pencillin and 0.1mg/ml Streptomycin (PenStrep, Roche).

HL-1 cardiomyocytes were obtained from Prof. William Claycomb's Lab (New Orleans, LA, USA) and were cultured in Claycomb medium (Sigma Aldrich) supplemented with 10% FBS (Sigma Aldrich), 100µg/ml Pencillin/Streptomycin (Sigma Aldrich), 0.1mM Nerepinephrine (Sigma Aldrich) and 2mM L-Glutamine (Sigma Aldrich). Cells were seeded in flasks or plates coated with fibronectin/gelatin solution (5µg/ml fibronectin in 0.02% gelatin; both purchased from Sigma Aldrich) for at least an hour at 37°C/5%CO_2.

All cell cultures were grown in incubators (Eppendorf) maintained at 37°C and 5% CO_2.

3.2.1.2 Cell seeding

Cells were washed once in PBS and detached by trypsin-EDTA (Life Technologies) incubation for 2 min at 37^0C/5% CO_2. Trypsin was neutralized by addition of growth medium and cell count was determined using NucleoCounter (ChemoMetec A/S), where 50µl cell suspension was mixed with equal amount of lysis buffer and neutralization buffer respectively. The solution was loaded on a cassette and cell number was analyzed by NucleoCounter and cells were seeded at required densities.

3.2.1.3 Ibidi shear stress setup

$1x10^5$ HUVECs were seeded in 100µl full EBM media on µ -Slides $I^{0.4}$ Luer (Ibidi) and after one hour, the reservoirs of slides were filled with media and cultured overnight. Next day, µ -Slides $I^{0.4}$ Luer were attached to the Ibidi perfusion pump according to manufacturer's instructions and cells were exposed to unidirectional laminar flow at a shear stress of 20 dynes/cm^2 for 72 hours controlled by the Ibidi perfusion pump. A constant shear rate of

15.2 ml/min was maintained. Cells seeded on µ-Slides I (Ibidi) served as static controls, for which 1ml media was replenished every day. After 72 hours of shear stress exposure, pump was stopped and cells were washed once with PBS and used for various assays.

$1x10^5$ HUVECs were seeded in µ-slides I (0.8, 0.4 and 0.2 Luer) which have the same growth area (2.5 cm^2) but varying channel volumes, thus exerting different shear stress rates in each slide. Cells were exposed to unidirectional laminar flow for 72 hours, and the following parameters were calculated as described below:

Flow rate (ϕ) for all slides, $\phi\left(\frac{ml}{min}\right) = \frac{2(ml)\times 60}{\text{time } (sec)}$; where time (*sec)* is the time taken for movement of 2ml media in the reservoirs.

Shear stress was calculated using the formula:

For µ-slides $I^{0.8}$, $\tau\left(\frac{dyn}{cm2}\right) = 0.347\ \phi\left(\frac{ml}{min}\right)$

For µ-slides $I^{0.4}$, $\tau\left(\frac{dyn}{cm2}\right) = 1.316\ \phi\left(\frac{ml}{min}\right)$

For µ-slides $I^{0.2}$, $\tau\left(\frac{dyn}{cm2}\right) = 5.129\ \phi\left(\frac{ml}{min}\right)$

Slide	Channel volume	Flow rate	Shear stress exerted
µ-slides $I^{0.8}$ luer	200µl	30 ml/min	≈10 dyn/cm^2
µ-slide $I^{0.4}$ luer	100µl	15 ml/min	≈20 dyn/cm^2
µ-slide $I^{0.2}$ luer	50µl	6 ml/min	≈30 dyn/cm^2

Table III.1. Flow rate and shear stress in µ-slides (0.8, 0.4 and 0.2 Luer)

After 72 hours of shear stress exposure, cells were washed once with PBS and RNA was isolated to perform real time qPCR.

24 hours after transduction with shCon or shKLF2 lentivirus, HUVECs were seeded in µ - Slides for shear stress experiment. Up regulation of KLF2 in shCon cells and abrogation of KLF2 in shKLF2 cells after shear stress exposure was confirmed by real time qPCR.

3.2.1.4 Cone and plate viscometer

$5x10^5$ HUVECs were seeded overnight in 6cm dishes and next day subjected to a uniform fluid shear stress in a cone plate viscometer as previously described[136]. The setup was used to

obtain more cell material to prepare protein lysates from static and shear exposed HUVECs. Briefly, rotors were placed in cell culture dishes and connected to a cooling unit and power supply such that a constant shear stress of 12 dyn/cm^2 was exerted on cells. At the end of 48 hours, media was aspirated and cells were washed with cold PBS and protein was isolated. HUVECs seeded in dishes that were maintained under static conditions served as controls.

3.2.2. Molecular biology

3.2.2.1 siRNA transfection

Short interfering RNA (siRNAs) against AMPKα1, HK2, PFK1 and PFKFB3 as well as negative control (siNeg) was purchased from Sigma Aldrich. Lipofectamine RNAiMax (Life Technologies) was used to transfect HUVECs and the following protocol was used for a 6cm dish: 3.5x10^5 HUVECs were seeded overnight in 6cm dishes, such that cells were 60-70% confluent next day for transfection. 250µl of OptiMEM mixed with 67nM siRNA was added to 250µl OptiMEM supplemented with 5µl RNAiMax Lipofectamine. The mixture was vortexed and allowed to stand at RT for 15 min for the transfection complex to form. Cells were washed once with OptiMEM media, supplemented with 2.5ml of OptiMEM and the 500µl of the transfection mix was added to cells. After 4 hours of incubation at 37^{0}C/5%CO2, cells were fed with full EBM medium and cultured for 24 hrs or 48 hrs. Universal negative control siRNA (Sigma) was used as control.

siRNA name	Sense sequence (5'-3')	Antisense sequence (5'-3')
siAMPKα1_1	CAAAUGCUUCCAUUUGUAA[dT][dT]	UUACAAAUGGAAGCAUUUG[dT][dT]
siAMPKα1_2	CCCAUAUUAUUUGCGUGUA[dT][dT]	UACACGCAAAUAAUAUGGG[dT][dT]
siHK2_1	GGCUUAUCCUGGUGAAGAU[dT][dT]	AUCUUCACCAGGAUAAGCC[dT][dT]
siHK2_2	CAAAGUCAUGCAUGAGACA[dT][dT]	UGUCUCAUGCAUGACUUUG[dT][dT]
siPFK1_1	GAUCAGAUCCCAAAGACCA[dT][dT]	UGGUCUUUGGGAUCUGAUC[dT][dT]
siPFK1_2	CAGUCAUCGCCUUGCUAGA[dT][dT]	UCUAGCAAGGCGAUGACUG[dT][dT]
siPFKFB3_1	CAAUGAGGAAGCCAUGAAA[dT][dT]	UUUCAUGGCUUCCUCAUUG[dT][dT]
siPFKFB3_2	CAGUACAGCUCCUACAACU[dT][dT]	AGUUGUAGGAGCUGUACUG[dT][dT]

Table III.2. Oligonucleotide sequences of siRNAs

Cells were harvested with qiazol for RNA isolation at 24 hours post transfection or lysed with RIPA buffer to isolate protein or 48 hours post transfection. For glucose uptake experiments, cells transfected with siRNAs were analyzed 48 hours after transfection. For seahorse flux analysis, cells were trypsinized 24 hours after siRNA transfection, counted and seeded on

seahorse cell culture plates (for 24 hours) and analyzed for metabolic parameters at 48 hours post transfection.

3.2.2.2 Cloning of expression vectors

Long term overexpression of KLF2[91] and shRNA mediated silencing of KLF2 was done as previously described[62]. Both overexpression (PGK-KLF2) and knockdown (shKLF2) vectors were a generous gift from Prof. Anton Horrevoets (Amsterdam) and were used to generate lentiviral particles. Briefly, the entire open reading frame of KLF2 was cloned into a pRRLcpptPGKmcspreSsin vector behind the human phophoglycerate kinase (PGK) promoter to obtain KLF2 overexpression vector. An identical vector without KLF2 cDNA was cloned which served as the mock control. To knockdown KLF2 expression, a short hairpin RNA against KLF2 mRNA was cloned into p156RRLsinPPT-CMV-GFP-PRE/NheI vector (shKLF2) behind the cytomegalovirus (CMV) promoter. shRNA sequence targeting Renilla luciferase in an identical vector was used as a control (shCon).

For cloning PFKFB3 overexpression plasmid, PFKFB3 cDNA (1563bp) was ordered from Source Bioscience in a pENTR221 plasmid. The linear cDNA (after EcoRV HF digestion) was shuttled into plenti4-V5 DEST vector (Invitrogen) by gateway cloning using Gateway LR clonase enzyme mix according to manufacturer's instructions (Invitrogen). The PFKFB3 lentivector plasmid was transformed into One Shot Stbl3 cells (Invitrogen) and the best clone was determined after restriction digestion with NcoI HF. The sequences were confirmed by sequencing. pLenti plasmid (pl4-V5-PFKFB3) was later used for lentivirus production and overexpression of PFKFB3 was confirmed by real time qPCR.

Plasmid DNA (pDNA) was isolated with either mini prep (Biozym Scientific) or maxi prep (Qiagen) plasmid purification kit depending on the volume of bacterial culture. Concentration of pDNA was determined using NanoDrop 2000 spectrophotometer (Thermo Scientific).

3.2.2.3 Lentivirus production and transduction

Lentiviral particles were generated as previously described[137]. Briefly, HEK293FT cells were co-transfected with lentivirus plasmid (mock, KLF2, PFKFB3, shCon, shKLF2), packaging plasmids pMD2.G and pCMVΔR8.91 using gene juice transfection reagent (Millipore). Early passage HEK293FT cells in T150 culture flasks were transfected at 70% confluence. 1.6ml of OptiMEM media was mixed with 40µl gene juice reagent, vortexed shortly and incubated for

10min at RT. 6µg of pCMVΔR8.91, 2µg of pMD2.G, 8µg of plentivector were mixed to a total volume of 100µl in OptiMEM. The DNA cocktail was mixed with the gene juice mixture and incubated for 20min at RT for the transfection complex to form. The transfection mix was added to HEK293FT cells (in 20ml culture medium) and incubated at 37^0C/5% CO_2. 24 hours after transfection, media was changed from flasks. Supernatant containing viral particles was collected at 48 hours and 72 hours post transfection, combined and subsequently concentrated in 100K cut off Amicon Ultra filter tubes (centrifugation at 2500rpm for 30min). Concentrated viral supernatant in the range of 20-70X concentration was stored at -80^0C.

HUVECs were either seeded in 6 well plates ($2.5x10^5$ in 2ml) or in T25 flasks ($3.5x10^5$ in 3ml) and 30-150µl of concentrated viral supernatant (based on concentration of virus) was added to cells. After 24 hours, media was aspirated and cells were washed 5 times with PBS and EBM full medium alternating before use for further experiments. Overexpression was confirmed by real time qPCR.

3.2.2.4 DNA isolation

Total DNA was isolated from cells using DNeasy Blood and Tissue kits (Qiagen) as per manufacturer's instruction. Briefly, cell pellets were resuspended in 200µl PBS and digested with 20µl proteinase K. To this mixture, 200µl lysis buffer, buffer AL was added, mixed thoroughly and incubated at 56^0C for 10min on a heat block. Next, samples were mixed with 200µl of 100% ethanol and added to DNeasy mini spin columns. Tubes were centrifuged at 6000g for 1min, and the silica columns were washed once with 500µl buffer AW1 and centrifuged. A second wash with 500µl buffer AW2 was performed and centrifuged at maximum speed (approx. 21,000g) for 3min to remove all traces of buffers. DNA was eluted by adding 30-50µl pure water directly to silica column membrane, incubated for 1 min at RT and centrifuged at 6000g for 1min at RT.

3.2.2.5 RNA isolation

Total RNA was isolated from cultured cells using miRNeasy kits (Qiagen) as per manufacturer's instructions. Briefly, cell pellets or cell layers were washed once with PBS and lysed with 700µl qiazol for 5min at RT. 140µl of chloroform was added to lysates, vortexed vigorously for 15sec and incubated for 3 min at RT. Next, samples were centrifuged at 12,000g for 15min at 4^0C. The upper aqueous phase containing RNA was transferred to a new Eppendorf tube and mixed with 1.5 volumes (approx. 525µl) of 100% ethanol and added

to spin columns. Tubes were centrifuged at 8000g for 15sec at RT to allow binding of RNA to silica columns and washed once with 700µl of RWT buffer and twice with 500ul RPE buffer (with centrifugation steps between washes). A final centrifugation at full speed (approx. 21,000g) for 1min at RT was performed to remove traces of buffers and ethanol. The bound RNA on the silica filter was eluted by adding 30-50µl of RNAse free water to the column and centrifuged at 8000g for 1min at RT.

RNA isolation from mouse hearts was performed after collecting hearts in 2ml microtubes (Sarstedt) containing qiazol and 1/4" ceramic spheres (MP Biomedical). The samples were homogenized in FastPrep24 homogenizer (MP Biomedical) in two 24 sec pulses at a speed of 4.0 m/s, until the organs were thoroughly disrupted, after which RNA isolation was carried out as described above.

3.2.2.6 Nucleic acid concentration determination

RNA or DNA concentration (in ng/µl) was determined using NanoDrop 2000 spectrophotometer by pipetting 1.5µl of nucleic acid on the optical pedestal. The spectrophotometer was blanked with RNAse/DNAse free pure water before measurements were done.

3.2.2.7 Reverse transcription of RNA

1µg RNA was reverse transcribed in a 20µl reaction to yield cDNA (50ng/µl) using the below protocol

1X Reverse transcription mix (final concentration)		Reverse transcription PCR reaction
(0.5µg) Random primer	1µl	10 min 20^0C
(0.5mM) dNTP	1µl	75 min 43^0C
(5mM) $MgCl_2$	4µl	5 min 99^0C
(1x) PCR buffer 10X	2µl	Hold ….. 4^0C
Water	0.5µl	
(20 units) RNAse Inhibitor	0.5µl	
(50 units) MuLV reverse transcriptase	1µl	
1µg RNA	10µl	
Total volume	20µl	

Table III.3 Reaction mix and PCR conditions for reverse transcription

The newly synthesized cDNA (50ng/µl) was diluted 1:5 with pure water to obtain a final concentration of 10ng/µl cDNA which was subsequently used for real time quantitative PCR.

3.2.2.8 Real time quantitative PCR

Real time qPCR was carried out in a StepOnePlus machine (Applied Biosystems). Oligonucleotide primer sequences were designed using NCBI-primer BLAST and purchased from Sigma Aldrich. Primer sequences used are listed in Table III.4 and PCR reaction mix and parameters are shown in Table III.5. Analysis was carried out in duplicates and relative gene expression was calculated using $2^{\wedge(-\Delta Ct)}$, where $\Delta Ct = Ct_{gene} - Ct_{endogenous\ control}$. RPLP0 or GAPDH were used as endogenous controls.

Target gene	Species	Forward and reverse primers
KLF2	Human	CGGCAAGACCTACACCAAGAG CTGTGTGCGTGCGCAGAT
RPLP0	Human	TCGACAATGGCAGCATCTAC ATCCGTCTCCACAGACAAGG
GAPDH	Human	ATGGAAATCCCATCACCATCTT CGCCCCACTTGATTTTGG
HK2	Human	GCTTGGAGCCACCACTCACCC AGCCAGGAACTCTCCGTGTTCTGT
PFKFB3	Human	GGAGGCTGTGAAGCAGTACA CAGCTAAGGCACATTGCTTC
PFK1	Human	ACTTGGAAGAGATCGCCACA CCCAGGTAGGCCTCGAATC
AMPKα1	Human	AGGCTCCACGAAGGAGCTGGAT ATGGACCACCATATGCCTGTGACAA
mt.ND1	Human	CCCTAAAACCCGCCACATCT GAGCGATGGTGAGAGCTAAGGT
p21	Human	CAGCATGACAGATTTCTACC CAGGGTATGTACATGAGGAG
VCAM1	Human	TGAAGGATGCGGGAGTATATGA TTAAGGAGGATGCAAAATAGAGCA
ICAM1	Human	AGCCCAAGTTGTTGGGCATA TACACCTTCCGGTTGTTCCC
E-selectin	Human	GAAGTTCTGGCTGAACACTGG CTCAAACACAAACCACACTGG
KLF2	Mouse	GGCGCATCTGCGTACACA GCATCCTTCCCAGTTGCAAT
RPLP0	Mouse	GCGTCCTGGCATTGTCTGT GAAGGCCTTGACCTTTTCAGTAAG

Table III.4. Oligonucleotide primer sequences used for real time qPCR

SYBR green real time qPCR mix (1X)		qPCR reaction		
2X Fast SYBR green master mix	10µl	20 sec	95^0C	
Forward primer (10µM)	1µl			
Reverse primer (10µM)	1µl	3 sec	95^0C	] 40 cycles
Water	5µl	30 sec	60^0C	
cDNA (10ng/µl)	3µl			
		15 sec	95^0C	] Melting curve
		60 sec	60^0C	
Total volume	20µl	15 sec	95^0C	

Table III.5. SYBR green reaction mix and PCR conditions for real time qPCR

3.2.2.9 Mitochondrial DNA content measurement

30ng DNA was analyzed by real time qPCR using primers designed to amplify mitochondrial DNA within mtND1 gene (mitochondrial encoded) and RPLP0 gene (nuclear encoded). The ratio of the DNA levels of mtND1 and RPLP0 was used to express mitochondrial DNA content.

3.2.2.10 RNA sequencing

For RNA sequencing, 0.5µg total RNA isolated from static and shear stress exposed HUVECs (20 dyn/cm^2 for 72 hours) were used. Sequencing libraries were prepared as described previously[138]. This was done in collaboration with the lab of Dr. Wei Chen (MDC, Berlin). Briefly, RNA was fragmented and primed for cDNA synthesis and libraries were constructed using Illumina TruSeq RNA Sample Preparation kit, according to manufacturer's instructions. Libraries were pooled and sequenced on Illumina HiSeq 2000 flow-cell. The deep sequencing data was mapped against the reference genome GRCH37 by applying tophat2. Afterwards, the transcript abundance was calculated by Cufflinks v2.2 based on the Ensemble annotation. Analysis was done in collaboration with the group of Dr. Shizuka Uchida (Institute of Cardiovascular Regeneration, Frankfurt). The sequence data have been deposited in the NCBI GEO database under accession number GSE54384.

3.2.2.11. Cloning of luciferase reporter constructs

Using ECR browser DCODE[139], a 757bp evolutionary conserved region (chr10: 6244721-6245477) in PFKFB3 promoter was identified. Putative KLF/Sp1 binding sites in this region was predicted by rVISTA web browser[140]. A 312bp conserved region bearing the KLF/Sp1 binding site was chosen to sub clone into luciferase reporter constructs. The 312bp fragment, flanked by Kpn1 and HindIII restriction sites, was synthesized and ordered from Eurofins mwg operon company in a pEX-A2 vector. Additionally, a mutated version of KLF2 binding

site, mutated from ggCCCGCCcc to ggAATTAAcc was ordered in pEX-A2 vector. After restriction digestion of pEX-A2 plasmids bearing wild type (WT) and mutated binding sites with KpnI and HindIII, the digest was separated by electrophoresis and the 312bp fragment was extracted from gel using QiaQuick gel extraction kit (Qiagen) according to manufacturer's protocol. The 312bp WT promoter or mutant promoter fragments were next ligated in front of the luciferase gene in the pGL4.10 [*luc2*] luciferase reporter plasmid using T4 DNA ligase according to manufacturer's protocol (Promega). The luciferase plasmids were transformed into One Shot Top 10 cells (Life Technologies) and pDNA was isolated. Successful clones were determined by restriction digestion followed by hot shot sequencing performed at Sequence Laboratories Göttingen (SeqLab).

3.2.3 Immunological methods

3.2.3.1 Protein isolation

Cell pellets or adherent cells were washed with ice-cold PBS twice and lysed in RIPA buffer (Sigma) supplemented with protease and phosphatase inhibitors (Roche) using cell scrapers for 20min on ice. The samples were centrifuged at 15,000g for 15min at 4^0C and the resulting supernatant was transferred to a new tube and concentration was determined by Bradford method. Protein lysates were used for immunoblot analysis immediately or stored at -80^0C.

3.2.3.2 Bradford assay

Protein concentration was determined by mixing 200µl of Bradford reagent with 800µl water and 1µl of protein sample in a cuvette and incubated for 5min at room temperature. All samples and blank control (no protein sample) were assayed in duplicates and their absorbance at 595nm was measured in the SmartSpec 3000 spectrophotometer (Bio-Rad). Using the absorbance values, final protein concentration was calculated against a standard curve with BSA stock solution (10 mg/ml) serial dilution.

3.2.3.3 Immunoblotting (Western blot)

30-50µg of protein was mixed with 4x loading buffer and heated at 95^0C for 10min to denature proteins. Samples were cooled on ice briefly, loaded onto SDS-PAGE gels and separated by electrophoresis in running buffer in a Mini Protean II Tetra electrophoresis system (Bio-Rad) at 80V and further at 120V once the samples moved into the resolving gel. Gels were prepared as shown in Table III.6.

	Stacking gel	Resolving gel		
Reagent	5%	8%	10%	12%
Water	2.7ml	5.35ml	4.6ml	3.85ml
30% Acrylamide	850µl	3ml	3.75ml	4.5ml
Stacking/resolving buffer	1.3ml	2.8ml	2.8ml	2.8ml
10% APS	125µl	225µl	225µl	225µl
TEMED	12.5µl	9µl	9µl	9µl

Table III.6. SDS gel constitution

Separated proteins from the SDS-gel was blotted onto a nitrocellulose or PVDF membrane in wet blotting buffer in a Mini Trans Blot Cell (Bio-Rad) for 90min at 80V at 4^0C. Prior to protein transfer by blotting, PVDF membrane was activated in methanol for 1min and washed in water for 2-3 min. After protein transfer, membranes were blocked in 5% non-fat dry milk (in TBS with 0.1% Tween 20 (TBS-T)) for 1hr at room temperature on a shaking platform followed by three washes of 15min each with TBS-T to reduce background noise and unspecific antibody binding. Primary antibody as shown in Table III.7 was incubated with membrane overnight at 4^0C on a shaking platform. Next day, membranes were washed three times with TBS-T for 15min to remove unspecific bound antibody. Membranes were next probed with horse radish peroxidase conjugated secondary antibody dependent on the source of primary antibody (mouse or rabbit) as described in Table III.8 for 1hr at room temperature under agitation.

Primary antibody	Dilution	Manufacturer
Rabbit anti-KLF2	1:500 in 5% milk	A. Horrevoets lab, Amsterdam
Rabbit monoclonal anti-HK2	1:1000 in 5% BSA	Cell signaling
Rabbit polyclonal anti-PFKP	1:1000 in 5% BSA	Cell signaling
Rabbit monoclonal anti-PFKFB3 (D7H4Q)	1:1000 in 5% milk	Cell signaling
Mouse monoclonal anti-AMPKα (F6)	1:1000 in 5% BSA	Cell Signaling
Mouse monoclonal anti-Tubulin α Ab2	1:2000 in 5% milk	Neomarker, Thermo Scientific
Rabbit polyclonal anti-Tubulin α	1:2000 in 5% milk	Neomarker, Thermo Scientific

Table III.7: Primary antibodies used for immunoblotting

Secondary antibody	Dilution	Manufacturer
Anti-rabbit IgG, HRP-linked $F(ab')_2$ (from donkey)	1:5000 in 5% milk	GE Healthcare
Anti-mouse IgG, HRP-linked $F(ab')_2$ (from sheep)	1:5000 in 5% milk	GE Healthcare

Table III.8: Secondary antibodies used for immunoblotting

After 3 washes with TBS-T for 15min, membranes were treated with enhanced chemiluminescence reagent (ECL, Millipore) for 2min and exposed in FluorChem M system (Proteinsimple). Using NIH ImageJ digital image analysis software (FIJI), the intensity of the protein signal was quantified densitometrically from chemi luminescent images and normalized to the signal of Tubulin-α, which served as a loading control.

4x loading buffer	Stacking buffer	Resolving buffer	Running buffer	Wet blot buffer
250mM Tris/HCl pH8.0 8%SDS 40% Glycerin 0.04% Bromophenolblue 200mM DTT	0.5M Tris/HCl pH6.8 0.4% SDS	1.5M Tris/HCl pH8.8 0.4% SDS	25mM Tris base 96mM Glycine 1% SDS	48mM Tris base 278mM Glycine 0.1% SDS

Table III.9: Immunoblot buffer compositions

3.2.3.4 Phospho kinase proteome profiling

$5x10^6$ mock and KLF2 transduced cells were processed using Human Phospho-Kinase Array Kits (Proteome Profiler™ R&D Systems, Minneapolis, MN) according to manufacturer's instructions. Briefly, nitrocellulose membranes (part A and part B) with capture and control antibodies were blocked for 1hr at RT in kit array buffer 1. Cells were lysed with kit lysis buffer 6 for 30 min at RT and centrifuged at 14,000g for 5 min. Supernatant lysate was transferred to new tubes and protein concentration was determined by Bradford method. Equal amount of protein lysates from mock and KLF2 transduced cells were diluted to a final volume of 2ml with array buffer 1. Blocked membranes were incubated with 1ml of cell lysate each overnight at 4^0C on a rocking platform. 20µl detection antibody cocktails (A and B) were diluted in 1ml assay buffer 2/3 and added to their respective membranes (A and B) and incubated for 2 hours at RT. Next, membranes were incubated with streptavidin-HRP in 1ml of assay buffer 2/3 for 30 min at RT. Between all incubation steps, membranes were washed thrice, 10 min each, with wash buffer. 1ml chemi reagent mix was overlayed on membranes for 1min and exposed in FluorChem M system (Proteinsimple). The phosphorylation level of proteins was analyzed by quantification of chemi luminescent signals on membrane panels by NIH ImageJ digital image analysis software with a Dot Blot Analyzer macro plugin. Spots on the membrane were compared with the co-ordinates in a transparency overlay to co-ordinate target proteins and their phosphorylation sites to the orientation of signal spots on the membranes. The signal values were subtracted from negative control values (PBS) and further normalized to whole membrane signal intensity.

3.2.3.5 AMPKα1 phosphorylation measurement

Mock and KLF2 transduced cells were analyzed for levels of AMPKα1 phosphorylation using DuoSet IC Human Phospho AMPKα1 (T174) elisa kits (R&D Systems) according to manufacturer's instruction. Briefly, ELISA plate was incubated with capture antibody overnight at 4^{o}C and next day blocked with blocking buffer for 2 hours at RT. $2x10^{7}$ mock and KLF2- transduced cells were lysed for 15min on ice in lysis buffer and centrifuged at 2000g for 5min. Protein concentration of supernatant was measured by Bradford assay and 10µg of protein was incubated in ELISA plate for 2 hours at RT. Samples were next treated with detection antibody for 2 hours at RT, followed by streptavidin-HRP antibody incubation for 20 min at RT in the dark. Substrate solution was added to each well and after 20min incubation at RT in the dark, reaction was stopped by addition of stop solution. Between every step, the plate was washed thrice with wash buffer. Optical density (absorbance) of samples was measured at 450nm using a GloMax®-Multi+ Microplate Multimode Reader with Instinct® (Promega) and wavelength correction was set to 560nm. Sample values were subtracted from diluent only (blank) control and final concentration was determined from a phospho AMPKα1 (T174) standard curve performed along with the samples.

3.2.3.6 Immunofluorescence staining

3.2.3.6.1 PFKFB3 staining

8 chamber glass slides (Labtek) were coated with 10µg/ml fibronectin (Sigma) for 1hr at 37^{0}C/5% CO_2. $1x10^{4}$ mock and KLF2 transduced cells were seeded overnight in each chamber. Next day, cells were rinsed with PBS and fixed in 4% PFA for 10min at RT. Further, cells were permeabilized with 0.1% TritonX in PBS for 10min at RT and blocked with 10% goat serum in 2% BSA (blocking buffer) for 30min at RT to reduce unspecific antibody binding. Rabbit PFKFB3 (Cell signaling) at 1:100 dilution in blocking buffer was incubated with cells overnight at 4^{0}C. After washing unbound antibody, cells were incubated with AF-555 conjugated antirabbit secondary antibody (6 µg/ml in PBS, Invitrogen) for 1hr at RT. Actin filaments were visualized upon AF-488 conjugated phalloidin (2.5 U/ml in PBS, Invitrogen) staining for 2 hr at RT and cell nuclei were visualized upon DAPI staining (1µg/ml in PBS, Roche) for 10min at RT. Confocal images were captured using the LSM 780, Axio Observer microscope (Carl Zeiss) with Plan Apochromat 63x/1.40 Oil objective. Secondary antibody only control was used to optimize microscope settings.

3.2.3.6.2 Mitotracker staining

$1.5x10^4$ mock and KLF2 transduced cells were seeded overnight on 10µg/ml fibronectin (Sigma) coated (1hr at 37^0C) 8 chamber glass slides. Cells were washed once with PBS and incubated with 150nM of carbocyanine conjugated Mito tracker Deep red FM stain (Molecular probes) in culture medium for 30min at 37^0C. After washing thrice, cells were fixed in acetone:methanol (1:1) mixture for 1 min. Cells were washed thrice and stained with DAPI (1µg/ml, Roche) for 10min at RT to visualize cell nuclei. Images were captured on Axio Observer Z1 microscope (Plan Apochromat 63x/1.40 Oil objective).

3.2.4. In-vitro methods

3.2.4.1 Glucose uptake analysis by flow cytometry

HUVECs were seeded at a density of $2x10^5$ cells per well in a 6 well plate overnight. Next day, cells were washed once with PBS and incubated with 100µM of 2-(N-(7-Nitrobenz-2-oxa-1,3-diazol-4-yl)Amino)-2-Deoxyglucose (2-NBDG, Life Technologies) for 1hour at 37°C in culture medium. For static and shear exposed cells, the incubation time was reduced to 30 min, so that the shear effect was not reduced due to longer incubation time after stopping the flow. Cells were trypsinized, neutralized with media and washed once with PBS by centrifuging at 300g for 5min at RT. Cell pellets were resuspended in 300µl PBS and 2-NBDG fluorescence was measured in the FITC channel (FL-1) using a FACS Canto II device (BD Biosciences). Mean fluorescence intensity of 2-NBDG was used to represent glucose uptake in cells. Unstained control was used to optimize FACS settings.

3.2.4.2 Glucose uptake analysis by microscopy

$1x10^5$ HUVECs were seeded overnight on µ-slide Y shaped (Ibidi) and exposed to laminar flow at a shear stress of 20 dynes/cm^2 for 72 hours controlled by an Ibidi perfusion system. Slides were washed once with PBS and incubated with 1mM of 2-NBDG (Life Technologies) in culture medium for 30 min at 37°C and confocal micrographs were imaged on LSM 780, Axio Observer (Carl Zeiss) with Plan-Apochromat 25x/0.8 Imm objective. 10 images each were captured from straight channel high shear region and branched low shear regions (see fig III.1), and analyzed for 2-NBDG mean fluorescence (FITC green) and cell alignment to direction of flow using NIH ImageJ digital image analysis software. Pearson's correlation analysis was performed for signal intensity of 2NBDG to cell alignment angles.

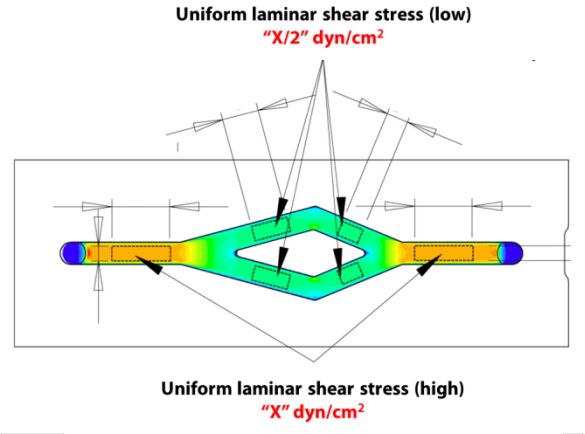

Figure III.1. Graphical representation of flow conditions in a µ-slide Y shaped slide.
(Adapted from www.ibidi.com)

3.2.4.3 Glucose trans well assay

24 well ThinCert trans well PET inserts (1.0µM pore size, Greiner bio-one) were coated with 250µl fibronectin (10µg/ml, Sigma) for 2 hours at 37^0C while placed in 24 well plates containing 950µl PBS in each well. $7.5x10^4$ mock or KLF2 transduced cells were seeded in 250µl media on fibronectin coated inserts placed into 24 well plates containing 950µl media. Next day, inserts were washed on both top and bottom surfaces twice in Hank's BSS and placed in 24 well plates containing 950µl HBSS and incubated for 1 hour at 37°C in HBSS (250µl) containing 100µM 2-NBDG (Life Technologies) and 10µM 20kDa -Dextran (TMR-Dextran, Sigma), which served as an internal control. Hank's BSS in the 24 well plates (beneath the cell monolayer) was transferred to 96 well black plates and TMR-dextran fluorescence (Ex 525nm and Em 580-640nm) followed by 2-NBDG fluorescence (Ex 490nm and Em 510-570nm) was measured in duplicates using a GloMax®-Multi+ Microplate Multimode Reader with Instinct®. Values from HBSS only control was subtracted from all sample values and a ratio of 2-NBDG to TMR-Dextran fluorescence was calculated to represent glucose transported through monolayer of cells.

3.2.4.4 Measurement of cellular metabolism

XF^e 96 extracellular flux analyzer (Seahorse Bioscience) was used to determine glycolytic function (extra cellular acidification rate, ECAR) and mitochondrial respiration (oxygen consumption rate, OCR) in cells. A day prior to the assay, cells were seeded in 200µl media as follows: for HUVECs, Seahorse XF96 polystyrene tissue culture plates (Seahorse Bioscience) were coated with fibronectin (25µg/ml, Sigma) for at least an hour at 37^0C/5% CO_2 and HUVECs were seeded overnight at $6x10^4$ cells per well density in full EBM

medium. siRNA transfected cells in 6cm dishes were seeded in seahorse culture plates 24 hours after transfection. HEK293FT cells were seeded overnight at a density of $6x10^4$ cells per well in supplemented DMEM. For HL-1 cells, seahorse culture plates were coated with fibronectin/gelatin for 1 hour and cells were seeded overnight at $4x10^4$ per well density in supplemented clay comb medium. Cell-free wells with media were used as background controls. Assay cartridges were hydrated by pipetting 200µl calibration solution in each well of a 96 well plate and allowing probes to be hydrated in this plate overnight in a XF prep station non CO_2 incubator at 37^0C.

24 hours after cell seeding, the cell plate was washed twice in either glycolytic function assay medium or mitochondrial respiration assay medium (Table III.10) based on measurement performed.

Glycolytic function assay media	Mitochondrial respiration assay media
Unbuffered DMEM (DMEM base+143mM NaCl+3mg/l phenol red) Glutamax, 2mM Adjust pH to 7.35 at 37C	Unbuffered DMEM (DMEM base+143mM NaCl+3mg/l phenol red) Glutamax, 2mM Glucose, 10mM Sodium pyruvate, 1mM Adjust pH to 7.35 at 37C

Table III.10. Composition of seahorse flux analysis assay media

Cells were fed with 175µl of respective assay medium and incubated for 1 hour in a XF prep station non-CO_2 incubator at 37°C before measurement in XF^e 96 extracellular flux analyzer. Both ECAR and OCR were measured over a 2 hour time period, divided into 4 stages. Each stage (30min) consisted of five measurement cycles (4 min periods with a mixing of 2 min). As shown in figure III.2, stage 1 consisted of basal measurements in assay medium, followed by port injections (25µl each) at the beginning of every stage before making measurements.

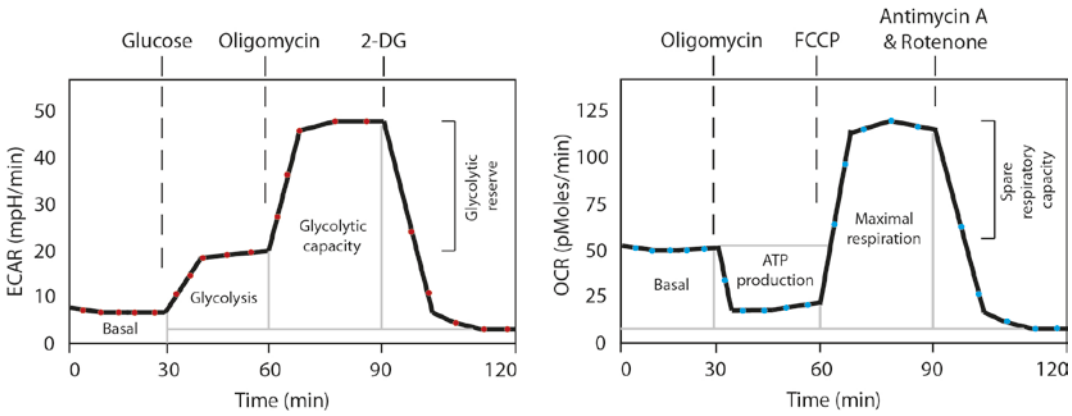

Figure III.2. Depiction of stages in metabolic measurements by Seahorse flux analyzer. (Adapted from www.seahorsebio.com)

Table III.11 lists inhibitors or activators (XF cell mito stress or glycolysis stress test kits, Seahorse Bioscience) injected by ports during glycolytic function and mitochondrial respiration measurements. For every cell line, cell number and concentration of reagents were first titrated to determine optimal conditions. Injection dilutions were calculated based on total volume of media residing in wells prior to latest injection.

Port injection for glycolytic function	HUVEC	HEK293FT	HL-1
Glucose	10mM	10mM	10mM
Oligomycin	3µM	3µM	1µM
2-DG	100mM	100mM	100mM
Port injection for mitochondrial respiration	**HUVEC**	**HEK293FT**	**HL-1**
Oligomycin	3µM	3µM	1µM
FCCP	1µM	1µM	0.3µM
Antimycin A & Rotenone	1.5µM & 3µM	1.5µM & 3µM	1µM & 0.5µM

Table III.11. Concentration of port injection reagents for different cell types

At the end of measurements, cell plate was analyzed for DNA content to determine cell number. Cells were washed once with PBS and fixed in 4% PFA for 20min at RT. After another wash with PBS, cells were incubated in DAPI (0.2 µg/ml in PBS) for 15 min in dark at RT. Cellular DNA content was measured on a microplate reader (TECAN) using excitation at 360nm and emission at 460nm for DAPI fluorescence (RFU). Background fluorescence from media only control wells was subtracted from sample wells and final data was represented as OCR or ECAR levels normalized to cell number. Different parameters of glycolytic function and mitochondrial respiration (as shown in figure III.2) were calculated from ECAR and OCR values obtained after normalization. All measurements were averaged from triplicate wells.

For specific experiments, HUVECs were treated with the following reagents in full EBM media in seahorse cell plates, after which cells were washed and fed with assay medium. Nω-nitro-L-arginine-methyl ester hydrochloride (L-NAME, Sigma), an inhibitor of nitric oxide was added at a concentration of 1mM for 4 hours. Hypoxia mimicking agent, desferrioxamine (DFO, Sigma, 100µM), vascular endothelial growth factor (VEGF, Peprotech, 50ng/ml) and tumor necrosis factor alpha (TNF-α, Peprotech, 10ng/ml) were incubated with HUVECs for 24 hours before seahorse flux analysis.

3.2.4.5 Mitochondrial activity measurement

Adherent HUVECs ($3x10^5$ seeded overnight in 6 well plates) were incubated with 0.5mg/ml of 3-(4, 5-Dimethylthiazol-2-yl)-2, 5-Diphenyltetrazolium Bromide (MTT, Sigma) in EBM culture medium for 4 hours at 37°C. Next, cells were washed once with PBS and lysed with lysis buffer (40nM HCl in isopropanol) for 30 min at room temperature. Lysate was centrifuged at 500g for 3 min at RT. The absorbance of the cleared lysate was measured at 550nm. All measurements were assayed in duplicates.

3.2.4.6 NAD^+ assay

EnzyChrom NAD^+/NADH assay kit (BioAssay Systems) was used to determine NAD^+ concentration in mock and KLF2 transduced HUVECs. Cells were trypsinized and washed once with PBS, followed by resuspension of $1x10^5$ cells in 100µl NAD extraction buffer. Extracts were incubated for 5 min at 60^0C and neutralized with 100µl NADH extraction buffer and 20µl assay buffer. Mixture was vortexed and centrifuged at 14,000rpm for 5 min. Next, 40µl of supernatant was transferred to 96 well plates for the assay. Reaction mixture containing 60µl assay buffer, 1µl each of enzyme A and enzyme B, 14µl lactate and 14µl MTT was freshly made. 80µl of this working reaction mixture was added to 40µl of sample or standard well. Plate was gently mixed and optical density at time 0 (OD_0) and after 15 min incubation at RT was measured (OD_{15}) in microplate reader (Synergy HT, Biotek). A standard curve was determined using a serial dilution of 10µM NAD standard as per manufacturer's instruction. ΔOD values (OD_{15}-OD_0) were used against the standard curve to calculate NAD^+ concentration in samples. Samples were assayed in triplicates and values were normalized to a blank control (no cells).

3.2.4.7 ATP assay

Cell titer Glo luminescent cell viability assay kit (Promega) was used to quantify ATP levels in cells. After trypsinization, HUVECs were neutralized with media and $3x10^4$ cells were counted and resuspended in 100µl culture media. The cell suspension was transferred to 96 well white plates and incubated with an equal volume i.e. 100µl Cell-Titer-Glo Reagent (Promega) for 10min at room temperature. Luminescence signal was measured with FlourChem M system (Proteinsimple) initially for some experiments but later on adapted to be analyzed with GloMax®-Multi+ Microplate Multimode Reader with Instinct® (Promega). Signal intensity from all wells were normalized to background media control and all conditions were assayed in triplicates.

3.2.4.8 Mitochondrial membrane potential measurement

Mitochondrial membrane potential in HUVECs was assessed using two different assays. First, we analyzed mitochondrial membrane potential dependent accumulation of 5,5′,6,6′-tetrachloro-1,1′,3,3′-tetraethylbenzimidazolocarbo-cyanine iodide (JC1, Molecular Probes) dye in cells, where a shift from JC1 aggregates (red channel PE) to JC1 monomer (green channel FITC) formation is measured. PE/FITC fluorescence intensity ratio is an indirect measurement of mitochondrial membrane potential per unit mass in cells. $3x10^5$ mock or KLF2 transduced HUVECs were seeded overnight and next day treated with 1µg/ml JC1 for 30 min in culture media at 37^0C. Cells were detached by trypsin treatment, neutralized with PBS containing 10% FCS and washed once with PBS by centrifuging at 300g for 5min at RT. Pellets were resuspended in 300µl PBS and analyzed using FACS Canto II device (Benton Dickson).

A second assay with MitoPT® tetramethylrhodamine, methyl ester (TMRM) Assay Kit (Immunochemistry Technologies) was performed to measure mitochondrial membrane potential. $3x10^5$ mock or KLF2 transduced HUVECs seeded overnight, or shear stress exposed (72 hours at 20 dyn/cm^2) and static control HUVECs in µ-slides were harvested by trypsin treatment, neutralized with media and incubated with 100nM TMRM in media for 20 min at 37°C. After washing cells once with PBS by centrifuging at 300g for 5min, pellets were resuspended in 300µl PBS and the orange red fluorescence (FL2) in cells was analyzed using FACS Canto II device.

3.2.4.9 Proliferation assay

Cell proliferation in mock and KLF2 transduced cells was analyzed using the BrdU Flow Kit (BD Pharmingen). 10mM BrdU was added to cells in culture medium and incubated for 45 min to allow incorporation of BrdU in the nucleus of dividing cells. Cells were harvested by trypsinization, neutralized with media and washed once with PBS by centrifugation at 2000rpm for 5min at RT. Fixing and permeabilization was achieved by incubating cells in 100µl Cytofix/Cytoperm buffer (30min at RT), followed by 100µl Cytoperm Plus buffer (10min on ice) and again in 100µl Cytofix/Cytoperm buffer (5min on ice). At the end of each incubation step, cells were washed with 1ml Perm wash buffer by centrifuging at 4000rpm for 3 min at RT. Next, cells were digested with 100µl DNAse (300 µg/ml) for 1hr at 37^0C. After a wash step, cells were resuspended in 50µl Perm wash buffer and stained with 2.5µl of anti-BrdU-V450 for 20min at RT, washed once and stained with 10µl of 7-AAD for 10min at RT. Finally, cells were resuspended in 300µl PBS and analyzed using FACS Canto II device. Cells that were not treated with BrdU served as controls for FACS laser settings.

3.2.4.10 Caspase 3/7 activity assay

Apo-ONE Homogeneous Caspase-3/7 assay kit (Promega) was used to analyze caspase dependent apoptosis in mock and KLF2 transduced HUVECs. Caspase 3/7 substrate rhodamine 110, bis-(N-CBZL-aspartyl-L-glutamyl-L-valyl-L-aspartic acid amide) [Z-DEVD-R110] is pro-fluorescent and upon cleavage and removal of DEVD peptides by caspase 3/7 enzyme from cells, rhodamine 110 leaving group turns fluorescent on excitation, this signal generated is proportional to the activity of caspase 3/7 in the sample. $1x10^4$ cells were seeded overnight in 96 well plates and next day 100µl of Apo-ONE Caspase-3/7 reagent mix (100X caspase substrate Z-DEVD-R110 diluted in kit assay lysis buffer) was added to each well with existing 100µl growth medium and mixed gently. After incubation of 1hr at 37^0C, fluorescence was measured from samples at an excitation of 490nm and emission of 510-570nm using GloMax®-Multi+ Microplate Multimode Reader with Instinct® (Promega). Mock transduced cells treated with 200nM of staurosporine for 4 hours at 37^0C were used as a positive control and all values were normalized to fluorescence read out of media only (no cells) control.

3.2.4.11 Annexin V staining

Mock and KLF2 transduced cells were quantified for apoptotic cell death by flow cytometry analysis. $2x10^5$ cells were seeded overnight, next day they were trypsinized and collected in

their initial culture medium, followed by centrifugation at 300g for 5 min at 4^0C. Cell pellets were washed once with PBS and once with binding buffer (BD biosciences). Next, cells were resuspended in 50µl binding buffer, 5µl Annexin V V450 (BD Biosciences) and 5µl 7-AAD (BD Biosciences) and incubated for 15 min at room temperature in the dark. After a final wash with binding buffer, cells were resuspended in 200µl binding buffer and analyzed by flow cytometry on FACS Canto II for apoptotic cells. Single stain controls where cells were stained only with Annexin V-V 450 or 7-AAD were used to configure the FACS laser settings.

3.2.4.12 Senescence staining

$3x10^5$ mock and KLF2 transduced cells were seeded overnight in 6 well culture plates. Senescence β-galactosidase staining kit (Cell signaling) was used to quantify senescent cells, where cells were first washed once with PBS and fixed for 15min at RT in fixative (20% formaldehyde, 2% glutaraldehyde in PBS). After washing cells, acidic β-gal staining mixture containing X-gal was prepared and added to cells as per manufacturer's instruction and incubated at 37^0C in a dry incubator (no CO_2) for 24 hours. Staining solution was removed and cells were overlayed with 70% glycerol before imaging on a bright field microscope (Axiovert 100, Zeiss) with 10x objective. 5 image fields were analyzed per condition; development of blue color in cells served as an indicator of senescence. Number of positive β-gal stained (blue) cells was counted using digital image analysis software (AxioVision Rel. 4.8, Carl Zeiss) and represented as percentage of positive cells among total number of cells in microscopic field.

3.2.4.13. Dual luciferase reporter assay

Transfection of luciferase reporter plasmids (bearing WT or mutated binding sites in PFKFB3 promoter) in HUVECs was achieved by electroporation using the Neon transfection kit system (Invitrogen) according to manufacturer's instructions. $1x10^5$ mock and KLF2 transduced cells were co-transfected with 0.5µg of firefly luciferase plasmid (pGL 4.10 [*luc2*] bearing WT or mutant fragment) and 0.5µg of Renilla luciferase plasmid pGL4.74 [*hRluc*] (Promega) at 1150 V for 30ms in 2 pulses. Suspension was seeded in 24 well culture plate in EBM medium with 10% FCS, but without supplements and antibiotics and assayed after 24 hours. Renilla luciferase plasmid served as a control for transfection efficiency. Additionally, mock and KLF2 cells not transfected with any plasmids were used as controls.

Luciferase promoter reporter experiments were performed as described[141]. Briefly, 24 hours after electroporation with luciferase plasmids, cells were assayed using the dual luciferase reporter assay kit (Promega) for activity of firefly luciferase and Renilla luciferase. Plasmid transfected cells in 24 well plates were washed once with PBS and lysed with 100µl of 1X PLB lysis buffer for 15min on a shaker. Cell supernatant was collected after centrifuging lysate at 16,000g for 2min at 4C. 20µl cell supernatant was transferred to a white 96 well plate and assay was performed in the GloMax®-Multi+ Microplate Multimode Reader with Instinct® (Promega). Firefly luciferase activity was first measured after an injection of luciferase substrate to each well. After a second injection of Stop and Glow reagent, Renilla luciferase activity was measured by the machine. Each sample was assayed in triplicate and background activity was subtracted from respective untransfected controls (mock or KLF2). A ratio of firefly to renilla luciferase activity was calculated.

3.2.4.14 Tube formation assay

Precooled 12 well culture plates were coated evenly with 200µl of Matrigel basement membrane matrix (BD Biosciences) and incubated for 1hour at 37^0C for the matrix to solidify. Next, the matrix was equilibrated with 500µl of supplemented EBM media for 1hour at 37^0C in the incubator. HUVECs (overexpressing KLF2 alone, PFKFB3 alone, both KLF2 and PFKFB3 or mock) were seeded at a density of $1x10^5$ in a total volume of 1.5ml per well on the matrix and analyzed after 24 hours for their network forming capacity. 5 random fields for every condition were imaged by Axio Observer Z1 microscope (5X magnification, bright field) and cumulative tube length was quantified using digital image analysis software (AxioVision Rel. 4.8, Carl Zeiss).

3.2.4.15 Spheroid based angiogenic assay

Endothelial cell spheroids were generated as previously described[142]. HUVECs overexpressing KLF2 alone, PFKFB3 alone, both KLF2 and PFKFB3 or mock were used for the assay. Methocoel was prepared by autoclaving 6g of methyl cellulose, which was later mixed with 250ml full EBM medium at 60^0C for 40min. Additional 250ml of full EBM medium was added and stirred overnight at 4^0C. The solution was centrifuged for 2 hours at 2000rpm at RT and the soluble fraction (methocoel) was separated and stored at 4^0C. $4.8x10^4$ HUVECs per condition were counted and resuspended in a 12ml mixture of full EBM-methocoel mix (80% media + 20% methocoel). 100µl of mixture (400 cells) was seeded in a 96 well U bottomed culture plate using a multi pipette and incubated for 24 hours

at 37^0C/5% CO_2 to allow formation of spheroid aggregates. Next day, spheroids were collected in a 50ml falcon, centrifuged at 200g for 3 min at RT and pellet was resuspended in 500µl of 80% methocoel + 20% FBS mixture. 500µl of collagen solution was mixed with each spheroid/methoceol solution, incubated for 3 min at RT and seeded in a 24 well plate. The plate was placed in an incubator for 30min to allow polymerization and then fed with 100µl full EBM media. After 24 hour incubation to allow capillary sprouting at 37^0C/5% CO_2, media was removed from wells and spheroids were fixed with 10% formaldehyde for 30min at RT. Angiogenic capacity was assessed by quantifying cumulative length of sprouts from 10 spheroids for every condition which was imaged by Axio Observer Z1 microscope (10X magnification, bright filed). Quantification was carried out by manual counting using digital image analysis software (AxioVision Rel. 4.8, Carl Zeiss).

Collagen solution (5ml, prepared on ice)
10X M199 media……..…….500µl
HEPES (1M)…...……...…90µl
Rat-tail collagen Type I…… …....4ml
(3.66 mg/ml, BD biosciences)
400-800µl of 0.2M NaOH, until solution turns light red

Table III.12. Composition of collagen solution used for spheroid assay

3.2.5 Bioinformatics

3.2.5.1 *In silico* promoter analysis

ECR browser DCODE platform[139] (http://ecrbrowser.dcode.org) was used to identify evolutionary conserved regions in PFKFB3 promoter conserved between humans and other species. Putative transcription factor KLF/SP1 binding sites in the conserved region were predicted using rVISTA 2.0 web browser[140] (http://rvista.dcode.org).

3.2.6 Mice experiments

All mice experiments were carried out in accordance with the principles of laboratory animal care as well as according to the German national laws. The studies have been approved by the local ethical committee (Regierungspräsidium Darmstadt, Hessen). Cdh5-CreERT2 mice[143] and KLF2 flox/flox[76] were described previously and kindly provided by Dr. Adams (Münster, Germany) and Dr. Sebzda (Vanderbilt University, TN), respectively. The two lines were mated to generate inducible endothelial specific KLF2 knockout mice and were fed on normal chow diet. Animals were administered with seven injections of 2 mg tamoxifen base (Sigma)

each intraperitoneally over a time period of 10 days to achieve deletion of KLF2 and sacrificed on day 11 or day 12.

3.2.6.1 *Ex vivo* glucose up-take in mice hearts

Hearts from WT ($KLF2^{fl/fl}$) and KLF2 EC-KO (Cdh5-CreERT2;$KLF2^{fl/fl}$) mice were harvested and retrograde perfusion by Langendorff method was setup as previously described[144]. Briefly, aorta of hearts was cannulated on a perfusion system (120 ml/hr, Braun), perfused for initial 3 minutes with perfusion buffer containing 50µM 2-NBDG. Next, hearts were digested by perfusion with digestion buffer containing collagenase type II (Worthington) and 50µM 2-NBDG for 8 minutes. The resultant swollen and pale heart tissue was finely minced using scalpel and scissors for 1 min and collagenase II reaction was stopped by adding 2ml stop buffer. The cell suspension was passed through a 100µm cell strainer and centrifuged at 300rpm for 3 min to remove cardiomyocytes. The supernatant containing ECs and cardiac fibroblasts was next incubated with 200µM 2-NBDG (Life Technologies) and 5µl CD31-APC antibody (BD Pharmingen) for 30 min in dark at 37°C. Next, the digest was washed once with PBS by centrifuging at 300g for 5min and analyzed using FACS Canto II device. Viable cells were first gated for CD31 negative and CD31 positive (ECs) population which was further analyzed for their glucose uptake by quantifying 2-NBDG fluorescence. Unstained WT samples as well as compensation bead (BD Pharmingen) controls were used for FACS setup.

Stock perfusion buffer	Perfusion buffer	Digestion buffer	Stop buffer
113mM NaCl	0.98X Stock perfusion buffer	1X Perfusion buffer	1X Perfusion buffer
4.7mM KCl	10mM BDM	1.14 mg/ml Collagenase II	10% FBS
0.6mM KH_2PO_4	5.5mM Glucose	30 µM $CaCl_2$	12.5 µM $CaCl_2$
0.6mM Na_2HPO_4			
1.2mM $MgSO_4.7H_2O$			
12mM $NaHCO_3$			
10mM $KHCO_3$			
10mM HEPES buffer			
30mM Taurine			

Table III.13. Buffers used for Langendorff retrograde perfusion

3.2.6.2 Aortic Ring Outgrowth Assay

Aorta were isolated from WT ($KLF2^{fl/fl}$) and EC-KO (Cdh5-CreERT2;$KLF2^{fl/fl}$) mice and cultured as previously described[145]. Briefly, adventitial tissue was carefully removed and aorta

was cut into 1 mm long tissue segments and placed in cold HBSS/$MgCl_2$. Aortic tissue was next embedded in rat tail collagen type I gel (Millipore) prepared in M199 medium (Sigma) with a final concentration of collagen at 1mg/ml. pH of gel was adjusted with 5N NaOH to obtain basic pH (solution turns light red). 50µl of collagen gel was added to wells in a 96 well plate and aortic rings were placed in them using forceps before polymerization, with the luminal axis of aorta parallel to the bottom of the well. Plate was placed undisturbed at RT for 15min and further incubated at 37^0C/5% CO_2 for 1hr. Embedded aortas were cultured in 150µl of DMEM/F-12 medium (Life technologies) containing 2.5% FBS and 1X PenStrep (Roche). PFKFB3 inhibitor 3-PO (Millipore) solubilized in DMSO was added to media at a concentration of 50µM or DMSO was used as a control. Endothelial sprouts were allowed to develop for 7 days, and samples were replenished with 150µl fresh medium every 2 days. Samples were washed once with 100µl PBS and fixed with 4% PFA for 30min at RT. Permeabilization was performed by incubation of samples with PBS+0.25% Triton X-100 buffer for 15min which was followed by 30min blocking with protein blocking buffer (DAKO). The aortic tissue was next stained with biotin Isolectin B4 (Vector laboratories) overnight at 4^0C at a 1:100 dilution in PBLEC buffer (1mM $MgCl_2$, 1mM $CaCl_2$, 0.1mM $MnCl_2$, 1% Triton X-100). After washing three times for 15 min each in PBS-T (PBS+0.1%Triton X-100) to remove unbound isolectin B4, aortas were incubated with streptavidin AlexaFluor 488 (Molecular Probes) at 1:500 dilution in a 1:1 solution of PBS and buffer A (0.5% Triton X-100, 3% FBS, 0.02% sodium azide) for 3 hr at RT in the dark. After 3 washes of 15min each with PBS-T, photomicrographs of sprouts from aortic rings were captured as stitched mosaics with Axio Observer.Z1 microscope (Zeiss) with a 5X objective. Cumulative outgrowth length from 3 rings per condition was quantified using NIH Image J digital image analysis software. Representative images were captured as a Z-stack with the Leica DMI6000B microscope (Leica microsystems) with HCX PL FLUOTAR 5x/0.15 DRY objective.

3.2.7 Statistical analysis

Data in graphs are expressed as mean ± S.E.M. GraphPad Prism 5 software was used to assess statistical significance by student t-test or Mann-Whitney U test when comparing two groups. For multiple comparisons, analysis of variance (ANOVA) was performed followed by Bonferroni's correction or Kruskal-Wallis test with Dunns correction posthoc tests. Statistical significance was defined as follows: *$p<0.05$, **$p<0.01$, ***$p<0.001$.

4. RESULTS

4.1 Shear stress and KLF2 reduce glycolytic metabolism of endothelial cells

4.1.1 Laminar flow exposure induces changes in morphology and KLF2 up regulation in ECs

In order to assess the effect of laminar shear stress in endothelial cells, HUVECs were exposed to laminar shear stress of 20 dyn/cm^2 for 72 hours; HUVECs under static conditions were used as controls. Shear stress exposed cells show an elongated morphology where they align in the direction of flow (Fig IV.1A). This alignment has been attributed to actin cytoskeleton reorganization along with RhoA activation and FAK phosphorylation by shear stimulation[31,33,146]. One of the key transcription factors that are upregulated in HUVECs upon flow exposure is krüppel like factor 2 (KLF2)[80]. We confirmed an increase in KLF2 expression at mRNA level by real time qPCR analysis (Fig IV.1B). HUVECs were exposed to shear stress of a maximum 12 dyn/cm^2 for 48 hours in a cone plate viscometer setup or kept under static conditions, to obtain protein lysates. A distinctive increase in KLF2 protein levels (Fig IV.1C) was observed in shear stress exposed ECs by immunoblotting.

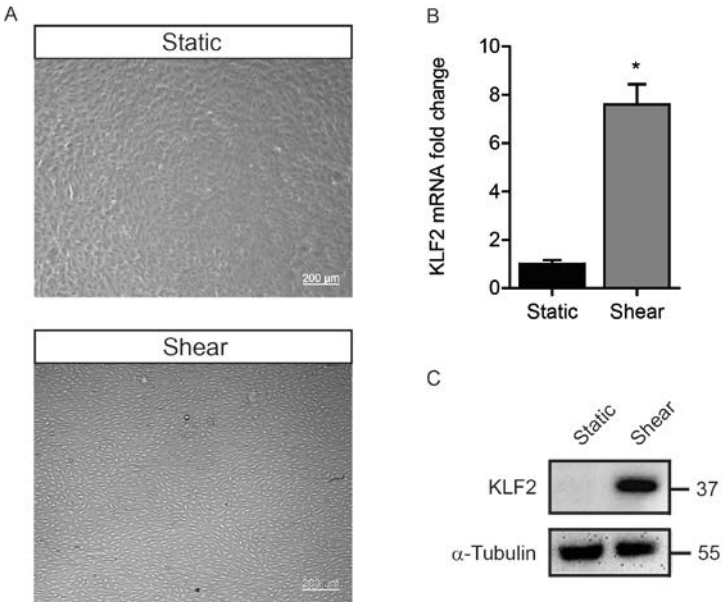

Figure IV.1. Laminar shear stress induces KLF2 expression in ECs

(A) Representative images of HUVECs cultured under static conditions or exposed to laminar shear stress of 20 dyn/cm^2 for 72 hours. Scale bar: 200µm. (B) Total cell mRNA was isolated and relative mRNA expression levels

of KLF2, normalized to RPLP0 mRNA in static or shear exposed HUVECs (20 dyn/cm^2 for 72 hours) was analyzed by real time qPCR. (n=3) (C) Static control and shear exposed HUVECs (12 dyn/cm^2 for 48 hours) were lysed and KLF2 protein level was determined by immunoblot analysis. α-Tubulin protein levels served as loading control, representative blot image is shown here. Data are represented as mean ± S.E.M; *p<0.05.

4.1.2 Shear stress reduces endothelial glucose uptake

Angiogenic endothelial cells are known to be highly dependent on glycolysis as energy source for proliferative and migratory functions of stalk and tip cell phenotype respectively[111]. However, little is known regarding the energy pathways and dependency in quiescent endothelial cells. Shear stress in known to induce a quiescent phenotype to ECs and in order to determine pathways involved in metabolism of quiescent ECs we first looked at glycolysis and assessed glucose uptake in shear exposed and static control ECs. Upon flow cytometry analysis of uptake of fluorescently labeled glucose analog, 2-N-7-Nitrobenz-2-oxa-1,3-diazol-4-yl-Amino-2-Deoxyglucose (2-NBDG), we could show that HUVECs exposed to shear stress (20 dyn/cm^2) for 72 hours take up reduced amounts of 2-NBDG (Fig IV.2A). In addition, we confirmed that the uptake of glucose is inversely correlated with the alignment of HUVECs to the direction of flow by fluorescent microscopy analysis, thus underlining the effect of shear stress on glucose uptake (Fig IV.2B).

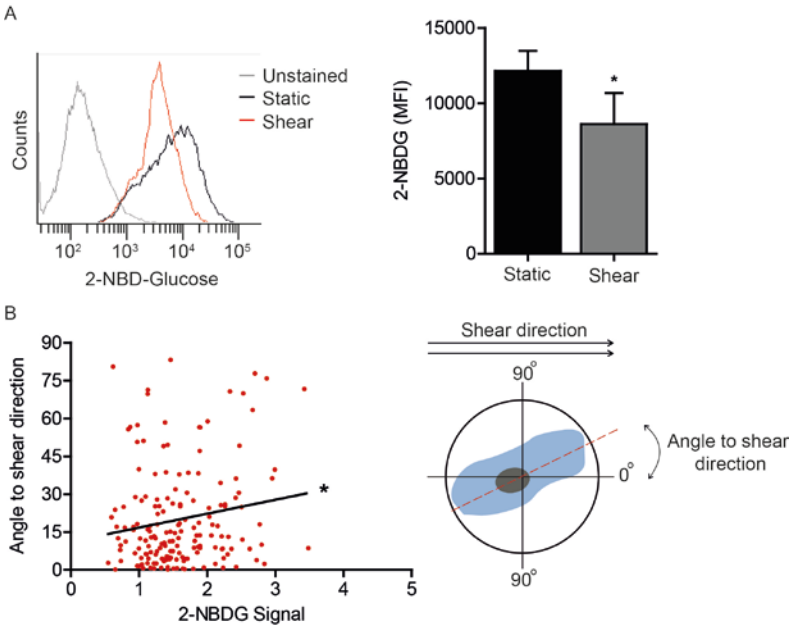

Figure IV.2. Exposure to laminar shear stress reduces uptake of glucose in ECs
(A) HUVECs cultured under static conditions or exposed to shear stress (20 dyn/cm^2 for 72hrs) were incubated with 100μM fluorescently labeled glucose analog 2-NBDG for 30min and analyzed by flow cytometry for uptake of glucose in FL-1 channel (FITC). Representative flow cytometry histogram overlay is shown in left panel and quantification of 2-NBDG uptake in cells is shown in right panel. (n=4; *p<0.05 vs. Static). (B) HUVECs on μ-slide Y shaped (Ibidi) were exposed to shear stress of 20 dyn/cm^2 for 72 hours and incubated with 1mM 2NBDG for 30min, 2NBDG uptake (signal intensity) was analyzed by confocal microscopy and

correlated with cell alignment to direction of flow. 10 images each from regions of high shear and low shear were captured and analyzed. (*p<0.05 by Pearson's correlation). Data are represented as mean ± S.E.M. 2-NBDG: 2-N-7-Nitrobenz-2-oxa-1,3-diazol-4-yl-Amino-2-Deoxyglucose, MFI: mean fluorescence intensity.

4.1 3 Lentiviral overexpression of KLF2 in HUVECs

Since overexpression of KLF2 in ECs recapitulates many effects of shear stress including induction of cellular quiescence in ECs, we used a lentiviral based transduction protocol to overexpress KLF2 in HUVECs to levels similar to that induced by shear stress and further studied the role of KLF2 in metabolic regulation of quiescent ECs. KLF2 mRNA levels are known to increase after 24 hours of its viral overexpression but the long term effects of KLF2, especially with respect to inducing an anti-inflammatory response, is at its maximum at 7 days post transduction [147]. For all of our experiments (unless stated otherwise), we used cells that were at least 7 days post transduced with mock or KLF2 lentivirus. Indeed, lentiviral KLF2 overexpression mimics the elongation of ECs as seen under flow exposure, however here they do not align in any particular direction (Fig IV.3A). In addition, an induction of KLF2 mRNA (Fig IV.3B) and protein (Fig IV.3C) to similar levels as seen upon shear stress stimulation was confirmed.

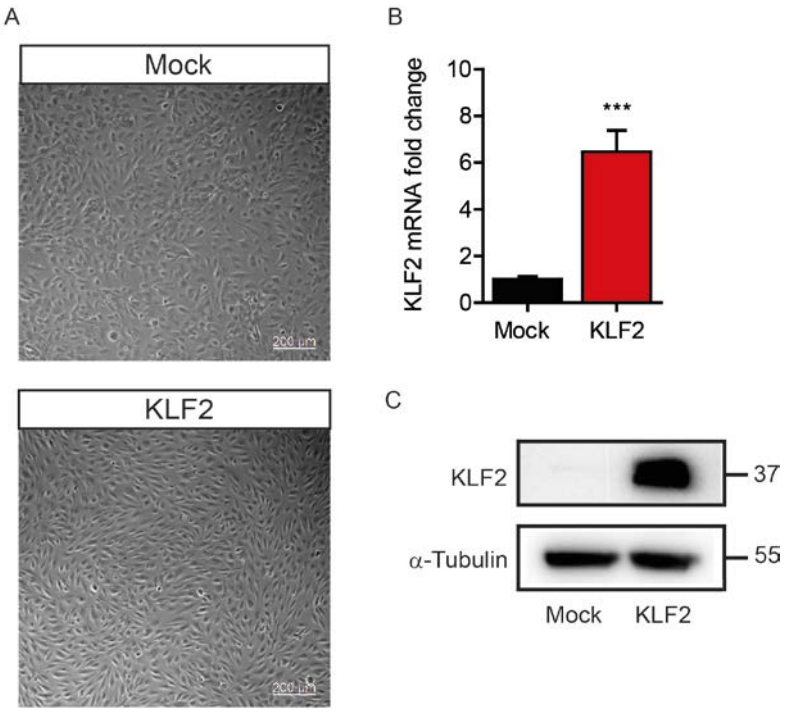

Figure IV.3. Lentiviral overexpression of KLF2 in ECs

(A) Representative images from HUVECs transduced with either mock or KLF2 overexpressing lentivirus. Images were captured 2 days post transduction. Scale bar: 200μm. (B) Total cell mRNA was isolated and relative expression levels of KLF2 mRNA, normalized to RPLP0 mRNA in mock and KLF2 overexpressing HUVECs, 7 days post transduction (n=10) (C) Mock and KLF2 overexpressing HUVECs were lysed and KLF2

protein levels were determined by immunoblot analysis. α-Tubulin protein levels served as loading control. Data are represented as mean ± S.E.M; ***p<0.001.

4.1.4 KLF2 reduces glucose uptake and subsequently allows for better bioavailability of glucose for transfer

To check if changes in glycolysis upon flow stimulation could be attributed to KLF2 induction, we measured glucose uptake in mock and KLF2 transduced HUVECs. Lentiviral overexpression of KLF2 in HUVECs also reduced glucose uptake (Fig IV.4A) in ECs. Since glucose uptake in KLF2 overexpressing cells was lower, we further investigated if this results in higher availability of glucose for transport. For this, we used a trans well assay model where mock and KLF2 cells were incubated with 2-NBD-Glucose and TMR-Dextran (control). Later, fluorescence from the media underneath the cell monolayer was measured. We confirmed an increase in glucose underneath the endothelial layer (Fig IV.4B) thus suggesting KLF2 allows for better transport and bioavailability of glucose to underlying tissues.

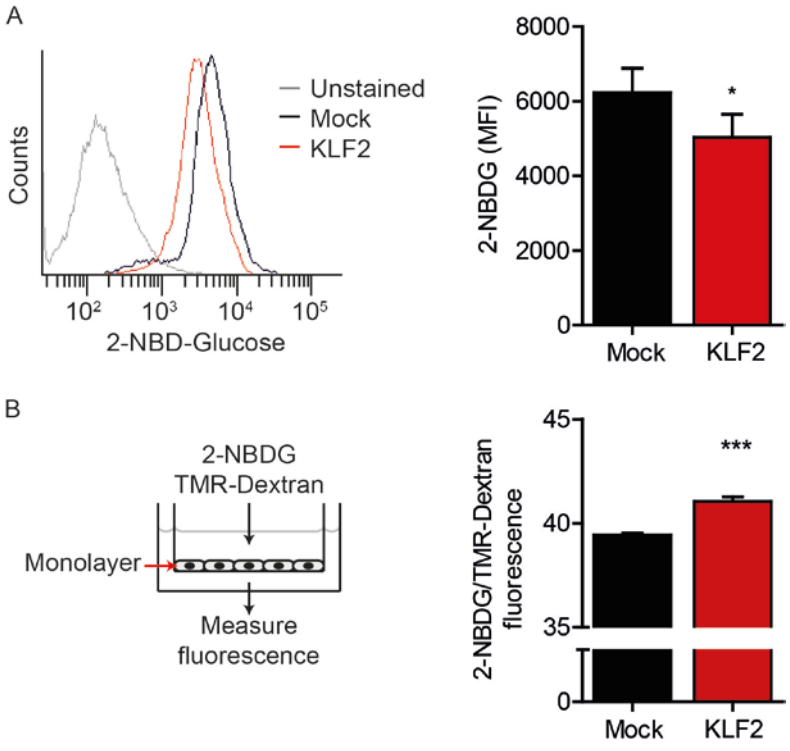

Figure IV.4. KLF2 reduces glucose uptake and consequently increases availability of glucose to underlying layers

(A) HUVECs transduced with mock or KLF2 overexpressing lentivirus were incubated with 100µM fluorescent labeled 2-NBDG for 60min and analyzed by flow cytometry for uptake of glucose in FL-1 channel (FITC). Representative flow cytometry histogram overlay is shown in left panel and quantification of 2-NBDG uptake in cells is shown in right panel. (n=6). (B) Glucose transport was measured after 60min incubation of mock and

KLF2 overexpressing HUVECs with 100µM 2NBDG and 10µM 20kDa-Dextran (internal control). Fluorescence of 2NBDG and Dextran was measured in buffer in trans well plates, beneath monolayer of ECs (n=8). Data are represented as mean ± S.E.M; *p<0.05, ***p<0.001.

4.1.5 Lentiviral shRNA-mediated silencing of KLF2 abrogates glucose uptake inhibition in HUVECs

To determine if changes observed upon shear stress exposure to ECs is KLF2 dependent; we setup a model where we transduced short hairpin lentivirus to silence KLF2 in HUVECs and subsequently exposed these cells to laminar shear stress (20 dyn/cm^2) for 72 hours. Morphologically, alignment of HUVECs in the direction of flow was abrogated in KLF2 silenced (shKLF2) sheared ECs, which indicates KLF2 dependent actin cytoskeleton remodeling by shear stress (Fig IV.5A). Real time PCR analysis showed an induction of KLF2 levels in control hairpin condition under shear stress which was abrogated upon KLF2 silencing to levels observed under static conditions (Fig IV.5B). We used the cone plate shear setup to obtain more cell material to prepare protein lysates, where shCon and shKLF2 transduced HUVECs were exposed to shear stress (12 dyn/cm^2) for 48 hours and immunoblotting of these samples confirmed inhibition of shear stress mediated induction of KLF2 at protein level in KLF2 silenced ECs (Fig IV.5C).

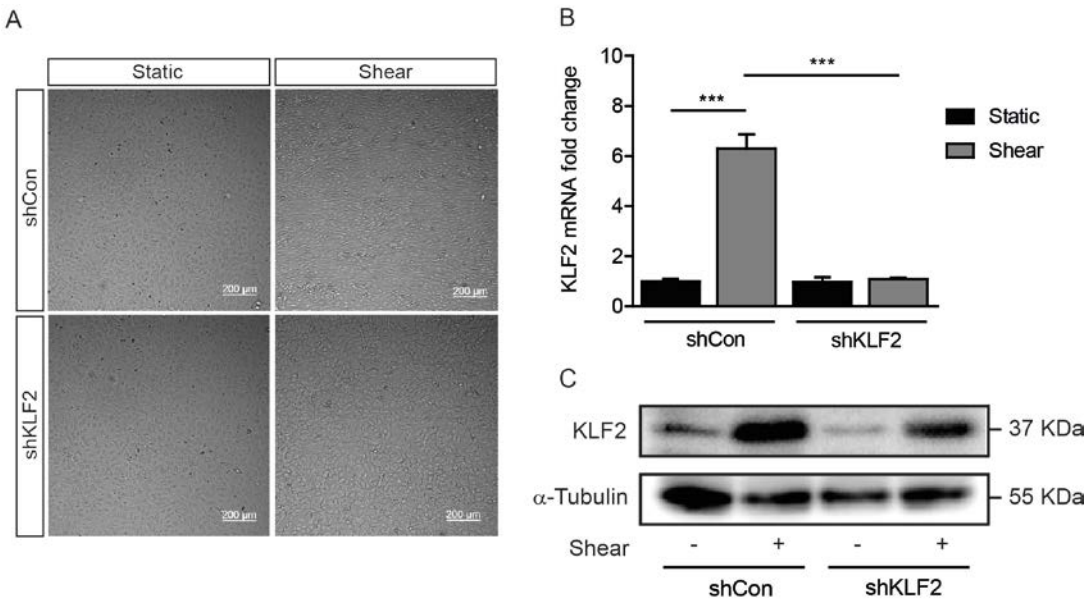

Figure IV.5. Exposure to shear stress after lentiviral knockdown of KLF2 does not induce KLF2 expression

HUVECs were transduced with shCon or shKLF2 lentivirus to knockdown KLF2 and cultured under static condition or exposed to shear stress of 20 dyn/cm^2 for 72 hours (A) Representative images showing alignment of ECs in direction of flow and abrogation of flow induced alignment upon knockdown of KLF2. Scale bar: 200µm. (B) Total mRNA was isolated and KLF2 mRNA expression was quantified by real time qPCR,

normalized to GAPDH mRNA and shown as fold change relative to static shCon transduced cells (n=3) (C) Representative immunoblot image of total cell protein lysates from HUVECs after lentiviral mediated shRNA knockdown of KLF2 and flow exposure (12 dyn/cm^2 for 48 hours) in a cone-plate viscometer, probed against antibodies for KLF2 and α-Tubulin which served as a loading control. Data are represented as mean ± S.E.M; ***p<0.001.

To assess if reduced glucose uptake after shear stimulation is dependent on KLF2, shCon and shKLF2 transduced ECs that were exposed to shear stress (20 dyn/cm^2) for 72 hours, were incubated with 2-NBDG and subsequent flow cytometry analysis was performed. We could show that the inhibition of glucose uptake by shear stress was abrogated upon knockdown of KLF2, suggesting that the reduced uptake of glucose in HUVECs induced by shear stress stimulation is KLF2 dependent.

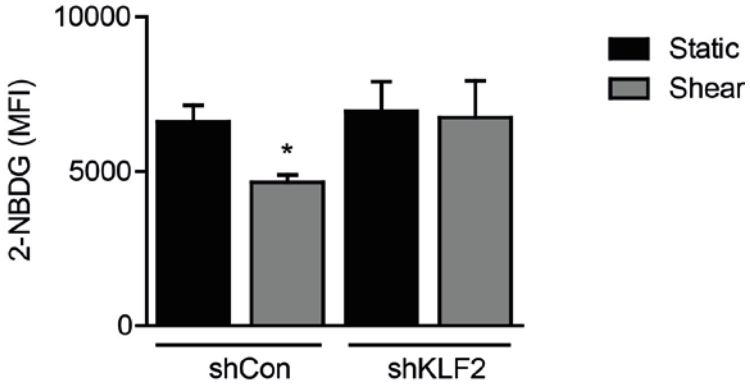

Figure IV.6. Reduced glucose uptake upon shear exposure is KLF2 dependent
HUVECs transduced with shCon or shKLF2 lentivirus were cultured under static condition or exposed to shear stress of 20 dyn/cm^2 for 72 hours. Glucose uptake in cells was analyzed by flow cytometry (FL-1 channel) after incubation with 100μM fluorescent labeled 2-NBDG for 30min (n=3). Data are represented as mean ± S.E.M; *p<0.05.

4.1.6 Endothelial specific KLF2 knockout mice show reduced glucose uptake in cardiac ECs

To study the role of KLF2 in glucose uptake *in vivo*, we first generated inducible endothelial specific KLF2 knockout mice. KLF2 flox/flox mice (provided by Dr.Sebzda, Vandelbilt University) were mated with a cre-deleter line (provided by Dr. R. Adams, Max Planck Institute for Molecular Biomedicine, Münster) expressing tamoxifen inducible cre recombinase (CreERT2) under the control of vascular endothelial cadherin promoter (Cdh5) to obtain inducible EC-specific KLF2 knockout mice. Tamoxifen injections were administered as shown (Fig IV.7A) to delete KLF2 in endothelial cells. KLF2 knockdown efficiency was confirmed in hearts of mice by real time PCR (Fig IV.7B). Hearts from wild type and knock out mice were harvested and infused with 2-NBDG via Langendorff perfusion

method. Next, hearts were digested with collagenase and endothelial cells were labeled with CD31 antibody and subsequently analyzed by flow cytometry to quantify glucose uptake (Fig IV.7C). Cardiac endothelial cells lacking KLF2 showed an increase in glucose uptake (Fig IV.7D) which concurs with our previous *in vitro* data of reduced glucose uptake upon KLF2 overexpression.

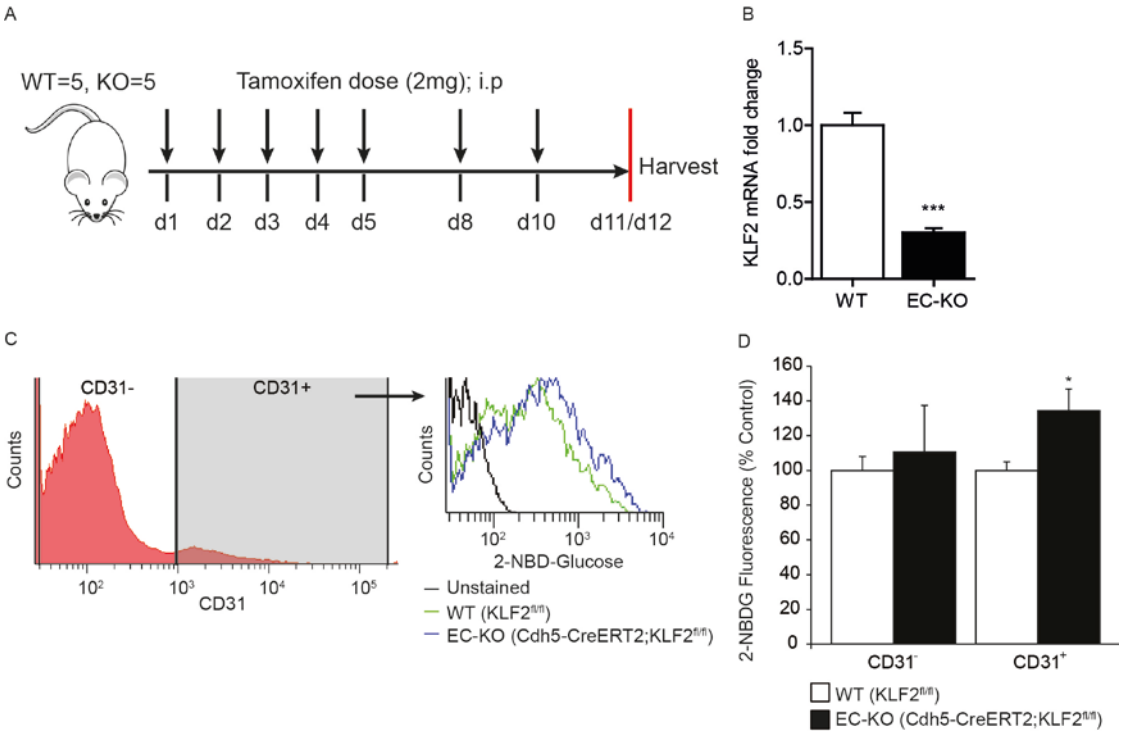

Figure IV.7. Loss of KLF2 in cardiac ECs leads to increased glucose uptake
(A) Schematic diagram showing tamoxifen injection schedule. Inducible EC-specific KLF2 knockout mice were injected intra peritoneal (i.p) with 2mg/day tamoxifen over a period of 10 days and harvested at day 11/12. (B) Total RNA from hearts of WT (KLF2 $^{fl/fl}$) and EC-KO (Cdh5-CreERT2;KLF2$^{fl/fl}$) mice was isolated and analyzed for KLF2 mRNA expression, normalized to RPLP0 mRNA levels by real time qPCR (n≥4) (C and D) *Ex vivo* 2-NBDG uptake in heart ECs of WT and EC-KO mice was analyzed by flow cytometry. Representative histogram showing CD31$^+$ endothelial cell population from Langendorff perfused hearts which were subsequently analyzed for 2-NBDG mean fluorescence and quantified (n=5). Data are represented as mean ± S.E.M; *p<0.05 vs WT CD31$^+$, ***p<0.001.

4.1.7. Role of KLF2 in endothelial cell glycolysis

Since KLF2 reduced glucose uptake in ECs, we next aimed to understand how KLF2 modulates glucose metabolism. Therefore, we used the XF Seahorse flux analyzer to determine glycolytic function in HUVECs transduced with KLF2 and mock controls. Proton excretion (pH) produced during conversion of glucose to pyruvate and eventually to lactate is measured and represented as real time extra cellular acidification rate (ECAR), which is an indirect measure of glycolysis in cells.

Initially, basal acidification rate (basal ECAR) of cells in assay medium is measured followed by an injection of glucose at saturating levels. The values measured now reflect glycolysis that is achieved by cells upon consuming injected glucose. Oligomycin addition to cells inhibits the ATP synthase of the electron transport chain inhibiting respiration, consequently pushing cells to their maximal glycolytic capacity. The difference between maximum glycolytic capacity and glycolysis measure reflects the glycolytic reserve of cells. Finally, 2-de-oxy-D glucose addition which competitively binds to enzyme hexokinase instead of glucose, inhibits glycolysis close to basal levels. Using these compounds, a glycolytic profile of cells can be achieved and each phase can be quantified accordingly.

KLF2 overexpressing cells tend to proliferate slightly slower than mock controls which may affect final ECAR result interpretation due to cell number variability and therefore we normalized the final ECAR values of both mock and KLF2 conditions to respective cell numbers measured by DAPI fluorescence. KLF2 overexpressing cells showed an interesting phenotype with a dramatic reduction in the overall glycolytic function profile (Fig IV.8A). Quantification of all phases revealed that KLF2 significantly reduces basal ECAR, glycolysis and glycolytic capacity of ECs. However glycolytic reserve was not changed by KLF2 suggesting that both mock and KLF2 overexpressing cells have the same capability to respond to an energy demand and this parameter also defines how close the glycolytic function of cell is to its theoretical maximum (Fig IV.8B). With the above results we could conclude that KLF2 indeed reduces glucose uptake and glycolytic function in ECs.

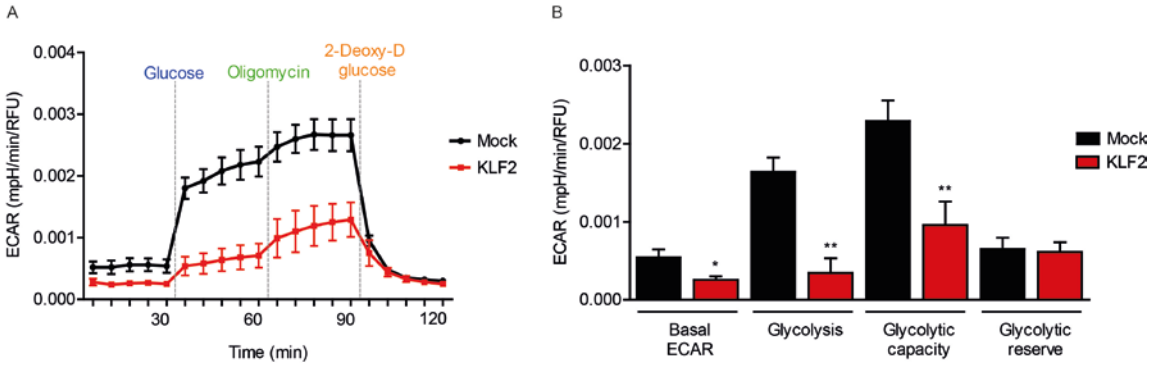

Figure IV.8. KLF2 reduces glycolytic function of ECs

HUVECs transduced with mock or KLF2 overexpressing lentivirus was analyzed by Seahorse flux analysis for glycolytic function (A) Extracellular acidification rate (ECAR) profile showing glycolytic function, vertical lines indicate the time of addition of Glucose (10mM), Oligomycin (3µM) and 2-Deoxy-D glucose (100mM) (B) Quantification of glycolytic function parameters from (A), values are normalized to DNA content determined by DAPI staining of cells (n=3). Data are represented as mean ± S.E.M; *p<0.05, **p<0.01. RFU: relative fluorescence unit.

4.2 KLF2 plays a role in mitochondrial mediated changes in respiratory metabolism

Cancer cells are known to convert glucose into lactate even with available oxygen in the environment (aerobic glycolysis), which is described as a metabolic hallmark of cancer cells- the classical Warburg effect[114,148]. It has also been shown that a shift from oxidative metabolism in somatic cells to glycolytic phenotype occurs in induced pluripotent cells (iPS) upon reprogramming[149] suggesting that different cell types adapt their metabolism to meet cellular energy demands for processes like angiogenesis and proliferation. In our study, KLF2 overexpressing cells showed a marked decrease in glycolytic metabolism and we wanted to explore if this reduction is compensated by an increase in mitochondrial respiration.

4.2.1 Shear stress and KLF2 reduce mitochondrial DNA content

We first determined if mitochondrial content is regulated by shear stress and KLF2. Using real time PCR we quantified mitochondrial DNA and nuclear DNA levels. Primers were designed to amplify mitochondrial DNA within mtND1 gene (mitochondrial encoded) and nuclear DNA within RPLP0 (nuclear coded). A ratio of mitochondrial DNA to nuclear DNA was used to interpret the relative mitochondrial DNA content. Both exposure of HUVECs to shear stress (20 dyn/cm^2) for 72 hours and KLF2 overexpression reduced mitochondrial DNA content significantly compared to their respective controls (Figs 9A and 9B). On silencing of KLF2 by short hairpin RNA, we observed an increase in mitochondrial content under static condition, however, shear mediated reduction could not be attributed to KLF2 (Fig IV.9C).

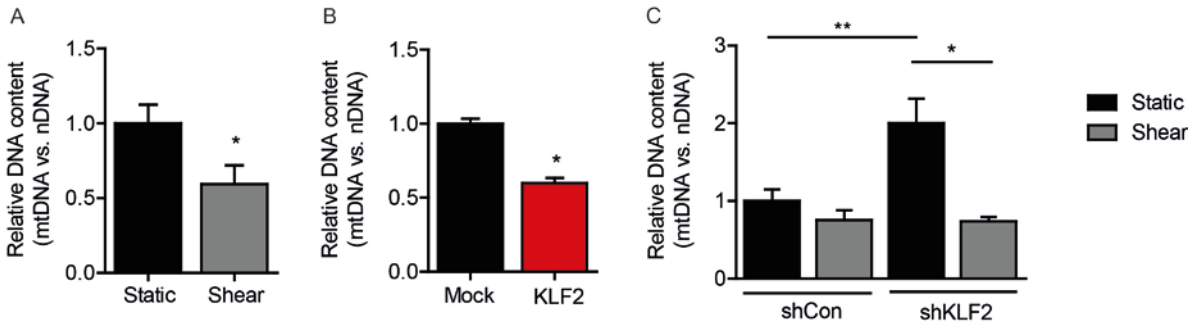

Figure IV.9. Shear stress and KLF2 reduce mitochondrial DNA content

Mitochondrial DNA content in (A) HUVECs exposed to shear stress (20 dyn/cm^2 for 72 hours) versus static control (n=4) (B) KLF2 transduced HUVECs versus mock transduced control (n=3) (C) HUVECs after lentiviral mediated shRNA knockdown of KLF2 and flow exposure (20dyn/cm^2 for 72 hours) (n=4) was measured by quantitative real time PCR of mitochondrial encoded gene ND1 (mtDNA) and nuclear encoded gene RPLP0 (nDNA). Relative levels were normalized to median values. Data are represented as mean ± S.E.M; *p<0.05, **p<0.01.

4.2.2 Shear stress and KLF2 reduce mitochondrial activity and ATP production in ECs

Having shown that flow stimulation and KLF2 reduce mitochondrial content, we next addressed the effects of KLF2 and shear stress on mitochondrial activity. We used a MTT (3-(4,5-dimethylthiazol-2-yl)-2,5-diphenyltetrazolium bromide) reduction assay that is commonly used as a measure of cell viability to assess mitochondrial activity. Upon entry into cells, the tetra zolium salt MTT passes into the mitochondria where it is reduced to insoluble formazan by mitochondrial succinate dehydrogenase. Addition of organic solvent isopropanol solubilizes formazan to a purple colored end product that is spectro-photometrically analyzed at 550 nm. Since the reduction of MTT occurs only in cells with actively functioning mitochondria (succinate dehydrogenase activity), this reduction assay reflects overall mitochondrial activity in the cell. KLF2 overexpression reduced mitochondrial activity of ECs (Fig IV.10A) and a similar inhibition trend was seen on flow stimulation (20 dyn/cm^2; 72 hours) in shControl cells. Silencing of KLF2 and subsequent shear exposure did not rescue the shear mediated reduction of mitochondrial activity suggesting that reduction of mitochondrial activity by shear stress is KLF2-independent (Fig IV.10B).

Mitochondria are the main source of ATP in cells and since we observed reduced mitochondrial content and activity due to KLF2 overexpression and shear stress exposure, we further determined changes in cellular ATP production. A luminescence based assay was used to quantify ATP produced in ECs, where cells were incubated with a luciferin-luciferase mixture. Substrate luciferin in the presence of O_2, Mg^{2+} and available ATP is converted by luciferase to oxyluciferin, CO_2, AMP and light. The luminescent light output signal is measured which represents cellular ATP that was available for the luciferase reaction. Overexpression of KLF2 and flow stimulation (20 dyn/cm^2; 72 hrs.) inhibited total cellular ATP production, yet again KLF2 silencing did not rescue the shear induced effect, thus indicating KLF2 independency (Figs IV.10C and D).

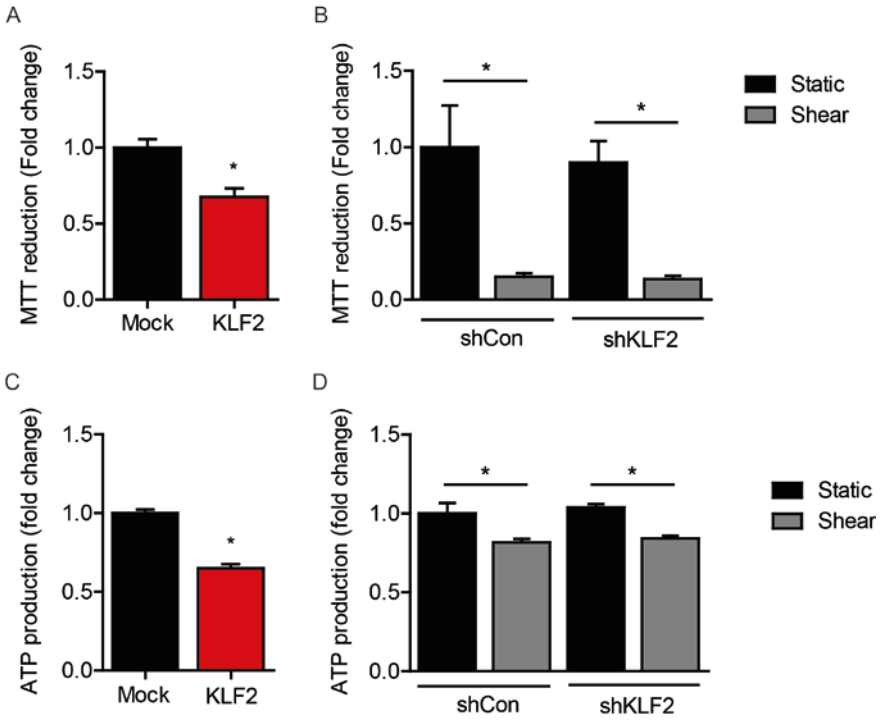

Figure IV.10. KLF2 reduces mitochondrial activity and cellular ATP production
Mitochondrial activity in (A) KLF2 or mock transduced HUVECs, normalized to median values (n=6) and in (B) HUVECs after lentiviral mediated shRNA knockdown of KLF2 and flow exposure (20dyn/cm^2 for 72 hours) (n=4) was measured by MTT reduction. Absorbance levels at 550nm levels were normalized to median values. Total cellular ATP produced in (C) KLF2 or mock transduced HUVECs (n=3) and in (D) HUVECs after lentiviral mediated shRNA knockdown of KLF2 and flow exposure (20dyn/cm^2 for 72 hours) (n=4) was quantified from luminescence output signal. Data are represented as mean ± S.E.M; *p<0.05. MTT: 3-(4,5-dimethylthiazol-2-yl)-2,5-diphenyltetrazolium bromide, ATP: adenosine triphosphate.

4.2.3 Although KLF2 reduces mitochondrial content and activity, membrane potential of mitochondria is induced upon KLF2 overexpression

Mitochondria consume most of the available O_2 in cells to fuel oxidative phosphorylation (OXPHOS) in the inner mitochondrial membrane to synthesize ATP. As the electrons from donors such as NADH and $FADH_2$ travel through complexes I-IV in the ETC, the energy released is used to pump H^+ out of the inner mitochondrial matrix thus creating an electrochemical gradient. This gradient leads to an increased mitochondrial potential ($\Delta\Psi_m$) which indicates mitochondrial health. In our experiments, overexpression of KLF2 resulted in an increase in mitochondrial membrane potential in HUVECs and we confirmed this with two separate assays. In the first assay, we measured 5,5′,6,6′-tetrachloro-1,1′,3,3′-tetraethylbenzimidazolocarbo-cyanine iodide (JC1) dye accumulation in cells, which indicates a mitochondrial membrane potential dependent accumulation in the mitochondria, determined

by a shift from (PE) red aggregate formation to (FITC) green monomers of JC1 in mitochondria (Fig IV.11A). In the second assay we analyzed tetramethylrhodamine, methyl ester (TMRM) fluorescence in cells which allows for determining mitochondrial permeability transition and membrane depolarization (Fig IV.11B). Silencing KLF2 and exposing these cells to shear stress did not inhibit the shear mediated increase in membrane potential (Fig IV.11C). Therefore we conclude that the effect of shear stress on mitochondrial membrane potential is likely independent of KLF2, in other words, both KLF2 and shear stress maintain mitochondrial integrity by separate mechanisms.

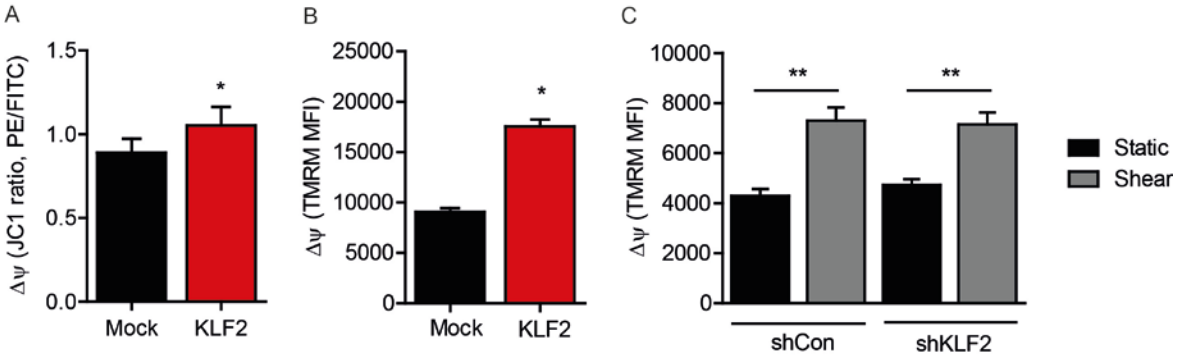

Figure IV.11. KLF2 induces mitochondrial membrane potential but shear mediated induction is independent of KLF2

Mitochondrial membrane potential ($\Delta\Psi_m$) in mock or KLF2 overexpressing HUVECs was assessed by flow cytometry analysis of (A) JC1 fluorescence ratio: PE red channel/FITC green channel (n=10) and (B) TMRM fluorescence intensity (n=3). (C) HUVECs after lentiviral silencing of KLF2 and subsequent exposure to flow (20 dyn/cm^2 for 72 hours) were analyzed by flow cytometry for TMRM fluorescence intensity (n=4). Data are represented as mean ± S.E.M; *p<0.05, **p<0.01. JC1: 5,5′,6,6′-tetrachloro-1,1′,3,3′-tetraethylbenzimidazolocarbo-cyanine iodide, PE: phycoerythrin, FITC: fluorescein isothiocyanate, TMRM: Tetramethylrhodamine, methyl ester, MFI: mean fluorescence intensity.

In addition, we performed immunofluorescence staining to visualize mitochondrial morphology in mock and KLF2 overexpressing cells. Using Mito-tracker staining we could specifically observe mitochondria morphology and localization; DAPI was used to stain nuclei of ECs. Microscopic analysis showed no apparent differences in the morphology or localization of mitochondria by KLF2 (Fig IV.12).

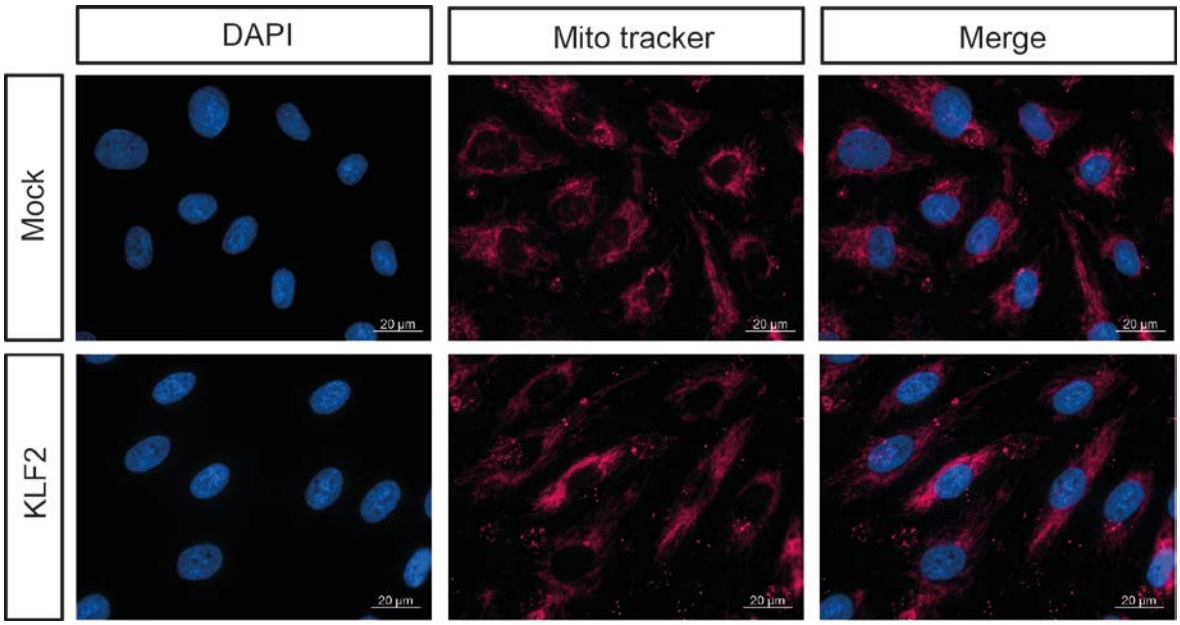

Figure IV.12. Mitochondrial morphology and localization are not affected by KLF2
HUVECs transduced with mock or KLF2 overexpressing lentivirus were fixed and immunofluorescence was performed. Images indicate mitochondria stained with Mito tracker (magenta) and nuclei stained with DAPI (blue). Representative images (63x) are shown here. Scale bar: 20µm.

4.2.4 KLF2 reduces oxygen consumption leading to decreased mitochondrial respiration in ECs

After defining that KLF2 indeed reduces mitochondrial activity without compromising mitochondrial integrity, we next used seahorse flux analysis to determine how KLF2 modulates mitochondrial function. Real time oxygen consumption rate (OCR) of cells, a direct measure of respiration is the read out from seahorse flux analyses and it is sequentially determined.

First, basal respiration of cells indicating the energy demand of cells under baseline conditions is measured, followed by addition of oligomycin. Oligomycin inhibits ATP synthase (Complex V) and the decrease in OCR reflects the amount of basal respiration that was used for ATP production by cells. Next, addition of carbonyl cyanide-4 (trifluoromethoxy) phenylhydrazone (FCCP), an uncoupler that collapses the proton gradient across the mitochondrial membrane leads to disruption of mitochondrial membrane potential. This allows for unlimited flow of electrons in the ETC resulting in maximal oxygen consumption by complex IV. Using maximal OCR, spare respiratory capacity of cells which is the difference between maximal respiration and basal respiration was calculated. Spare respiratory capacity of cells reflects their ability to respond to increased energy demand.

Finally, introducing a combination of Antimycin A, a complex III inhibitor and Rotenone, a complex I inhibitor, completely inhibits mitochondrial respiration. Using these compounds, a mitochondrial function profile of samples can be achieved and each phase quantified accordingly.

KLF2 overexpressing cells showed reduction in OCR in the overall mitochondrial function profile (Fig IV.13A). Quantification of individual parameters revealed that KLF2 significantly reduces basal respiration and ATP production. Maximal respiratory capacities of KLF2 and mock transduced controls did not appear to differ significantly suggesting that both conditions can achieve the same maximal rate of respiration. Interestingly, spare respiratory capacity of ECs was slightly induced by KLF2 suggesting that KLF2 overexpressing cells indeed still have the ability to function and respond to high energy demand of the environment when required, similar to levels of mock controls. Collectively, seahorse analyses show that KLF2 overexpression leads to lower respiratory metabolism in ECs.

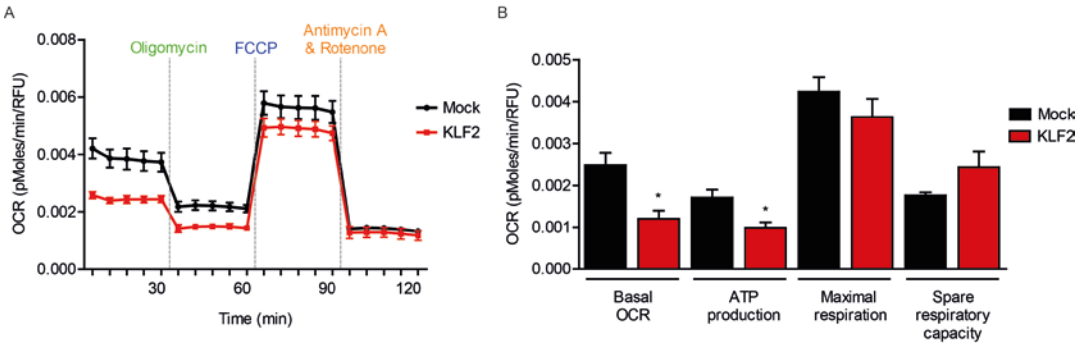

Figure IV.13. KLF2 reduces mitochondrial respiration in ECs
HUVECs transduced with mock or KLF2 overexpressing lentivirus was analyzed by Seahorse flux analysis for mitochondrial respiration. (A) Oxygen consumption rate (OCR) profile showing mitochondrial respiration function, vertical lines indicate the time of addition of Oligomycin (3µM), FCCP (1µM), Antimycin A (1.5µM) and Rotenone (3µM). (B) Quantification of mitochondrial respiration parameters from (A), values are normalized to DNA content determined by DAPI staining of cells (n=3). Data are represented as mean ± S.E.M; *p<0.05. RFU: relative fluorescence unit.

4.3 KLF2 confers an anti-apoptotic and anti-senescent phenotype to the endothelium

4.3.1 KLF2 slightly delays proliferation and protects endothelial cells from apoptosis

After establishing that KLF2 reduces metabolic activity of ECs, we next speculated whether KLF2 mediated reduction in metabolism induces cell death and therefore performed assays to

analyze proliferation and apoptosis. Mock and KLF2 transduced cells were incubated with BrdU and analyzed by flow cytometry for incorporation of BrdU, which allows for quantification of cell population in different phases of cell cycle. KLF2 overexpression in ECs slightly reduced the number of cells in G2/M phase accompanied by an increase in S phase cell population (Fig IV.14A) indicating that KLF2 slightly reduces cell proliferation.

Using two different assays we addressed whether KLF2 overexpression was driving ECs into apoptosis. First, we used fluorescence based caspase 3/7 activity assay and confirmed that upon KLF2 overexpression cells have reduced apoptosis (Fig IV.14B). Since apoptosis could be caspase independent, we further performed Annexin V staining and flow cytometry analysis to measure caspase independent apoptosis. Here too, KLF2 overexpression reduced apoptosis in ECs (Fig IV.14C). Thus we could conclude that KLF2 is indeed anti-apoptotic and rather presents a vasoprotective characteristic to ECs.

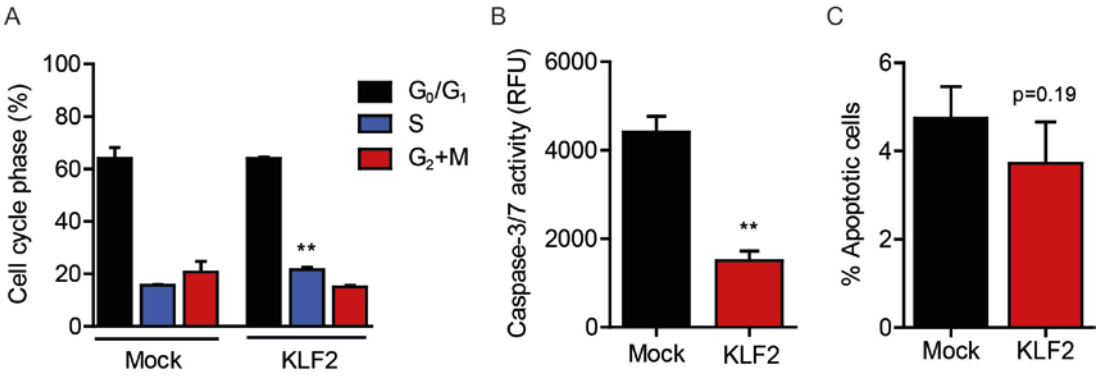

Figure IV.14. KLF2 reduces proliferation of ECs but does not induce apoptosis
(A) Proliferation of mock and KLF2-transduced HUVECs measured by flow cytometric BrdU incorporation analysis at 45 min after addition of BrdU (n=3). (B) Apoptosis measured by Caspase-3/7 activity in mock and KLF2 transduced HUVECs by fluorescence based assay (n=3). (C) Apoptotic [early (Annexin V^+, $7AAD^-$) and late (Annexin V^+, $7AAD^+$)] cells represented as % of total cells, measured by Annexin V staining by flow cytometry in mock and KLF2 transduced HUVECs. (n=5). Data are represented as mean ± S.E.M; **p<0.01. RFU: relative fluorescence unit.

4.3.2 KLF2 inhibits senescence in ECs

To exclude the possibility that KLF2 reduces metabolic activity in ECs by inducing senescence, we performed acidic beta galactosidase staining assay in mock and KLF2 transduced ECs to determine senescent cells expressing pH-dependent beta galactosidase activity. KLF2 overexpression in ECs reduced the number of beta-gal positive cells compared to mock controls, (Fig IV.15 A and B) indicating that KLF2 prevents induction of senescence. In addition, using real time PCR, we quantified expression of senescence marker p21, where

KLF2 overexpression reduced p21 mRNA levels in ECs. In summary, we confirmed KLF2 to be anti-senescent and that the reduced proliferation and metabolic activity seen on KLF2 overexpression is not caused due to augmented senescence.

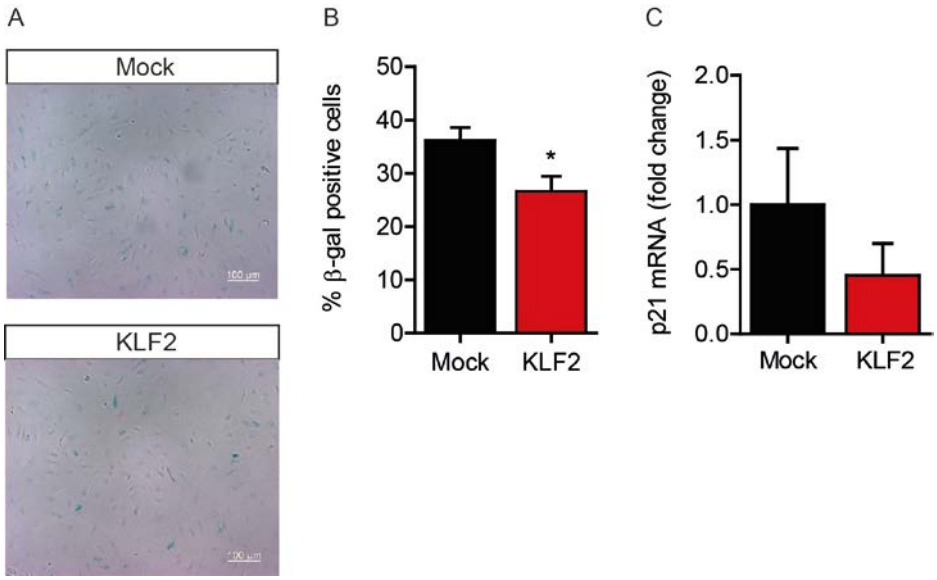

Figure IV.15. KLF2 protects ECs against senescence
(A) Representative images (10x) of β-gal positive stained cells counted after 24 hour incubation of acidic β-gal staining mixture in mock and KLF2 transduced cells to analyze senescence. 5 random image fields were analyzed per condition. Scale bar: 100μm. (B) % of β-gal positive cells among total number of cells in image field (n=3). (C) Total RNA from mock and KLF2 transduced HUVECs were isolated and analyzed for p21 mRNA expression normalized to RPLP0 mRNA (n=4). Data are represented as mean ± S.E.M; *p<0.05.

4.3.3 Overexpression of KLF2 maintains NAD levels and does not induce a metabolic shift towards mitochondrial respiration

For efficient metabolic and mitochondrial homeostasis, maintenance of NAD^+ levels in the cells is crucial. Both NAD^+ and NADH serve as metabolic co-factors in oxido-reductase reactions of glycolysis and mitochondrial respiration. A balance between availability and breakdown of nutrients in cells largely determines NAD^+/NADH ratio[150]. To study the consequence of KLF2 mediated reduction of metabolic activity on NAD^+ levels, we analyzed concentration of NAD^+ in mock and KLF2 transduced cells. NAD^+ concentration was determined in a lactate dehydrogenase cycling reaction where the NADH formed during the reaction reduced MTT formazan reagent to a colored product whose intensity was colorimetrically measured at 565 nm. The intensity of measurement indicates the NAD^+ concentration in the cell sample. KLF2 overexpression did not change the NAD^+ concentration in ECs (Fig IV.16A). Thus we could conclude from this assay, that KLF2 indeed maintains the mitochondrial “fitness” in ECs.

ECAR/OCR ratio derived from seahorse flux analyses helps in understanding dependency of cells on glycolysis over respiration and if there occurs a shift from one pathway to other. We determined levels of basal ECAR and basal respiration rates which was used to represent ECAR/OCR ratio in mock and KLF2 transduced cells. Here, we observed no difference in the ratio between mock controls and KLF2 overexpressing cells (Fig IV.16B) suggesting that KLF2 does not induce a shift from glycolytic to oxidative metabolism to compensate for the decrease in glycolytic function. This is due to reduction in both glycolysis and respiration capacities of cells by KLF2. These results are consistent with measurements of glycolytic function in 4.1.7 and mitochondrial respiration in 4.2.4, showing a similar decrease in both pathways after KLF2 overexpression.

In order to understand the preference of ECs to glycolytic or oxidative metabolism, we additionally compared and analyzed metabolism of other cell types such as HL-1 cardio myocytes and HEK293FT. On comparison of ECAR/OCR of HUVECs, HL-1 and HEK cultures we could conclude that HEK cultures are highly glycolytic which helps in deriving the much needed energy demand for their high proliferation rate. HUVECs also exhibit ECAR/OCR ratios similar to that of HEKs indicating an intermediate phenotype that are more dependent on glycolysis than respiration for energy metabolism. In contrast, HL-1 cardiomyocytes show a more respiratory phenotype compared to HUVECs and HEKs (Fig IV.16C).

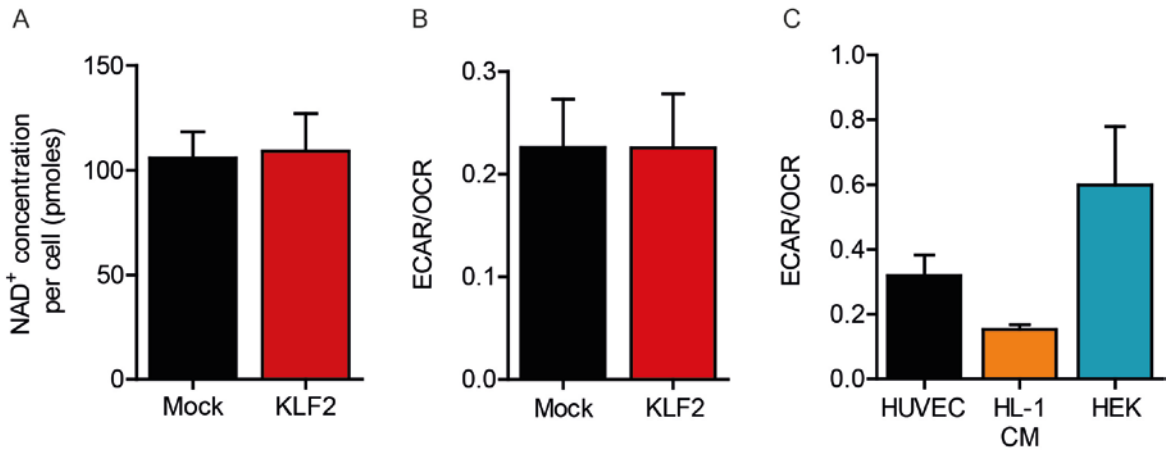

Figure IV.16. KLF2 does not alter NAD levels and maintains glycolysis to respiration ratio

(A) HUVECs transduced with mock or KLF2 overexpressing lentivirus was analyzed for NAD^+ concentration, measured by colorimetric measurement at 565nm. Final sample concentrations were calculated against NAD^+ standard curve (n=5). (B) Ratio of basal ECAR and basal respiration rates measured by Seahorse flux analysis in mock and KLF2 transduced HUVECs (n=3) (C) Ratio of basal ECAR and basal respiration rates in HUVECs, HL-1 CMs and HEK cell lines, measured by seahorse flux analysis (n≥3). Data are represented as mean ± S.E.M.

Collectively the above results indicate that KLF2 reduces both glycolytic and respiratory metabolism without affecting cell integrity in terms of apoptosis, senescence or a drastic metabolic shift. We next set out to determine the mechanism by which KLF2 down regulates metabolism in HUVECs.

4.4 Phospho kinase array gives insights into post translational modifications by KLF2

To investigate how KLF2 reduces metabolic activity in ECs, we initially performed phospho kinase proteome profiling to study KLF2 mediated post translational modifications. Lysates from mock and KLF2 transduced cells were analyzed and the array data revealed significant regulation of (3/45 induced) and (4/45 repressed) phospho proteins by KLF2 as depicted in Fig IV.17.

WNK1, ERK 1/2, STAT3 and eNOS had increased phosphorylation under KLF2 overexpression. WNK1 (upstream activator of ERK5) and ERK 1/2 are both important MAP kinases which are implicated in cell cycle regulation, growth and differentiation. STAT3 phosphorylation at Ser727 has been shown to be induced by shear stress in ECs via the ERK 1/2 pathway, in turn leading to inhibition of Tyr-705 phosphorylation[151]. eNOS is vital for regulating vascular reactivity and tone, and it has been described to be directly activated by KLF2 in terms of gene expression and activity[51]. Here, we indeed see an increase in phosphorylation of eNOS by KLF2 which perhaps contributes to its increased activity.

Proteins that showed strong reduction in phosphorylation under KLF2 overexpression were JNK, c-Jun, beta-catenin, HSP60 and AMPKα1. KLF2 has been previously described to inhibit JNK and downstream target c-Jun phosphorylation in an actin cytoskeleton dependent manner[94,147]. HSP60 is implicated in mitochondrial protein import and macromolecular assembly where it functions as a chaperone. Studies also report HSP60 to be a regulator of T-cell mediated inflammation[152] and *in vivo* KLF2 seems to repress HSP60 expression in monocytes in the context of arthritis[153]. AMPKα1 has been implicated to be activated transiently upon shear stimuli and is a proven upstream regulator of ERK5-MEF2C signaling in turn inducing KLF2 expression[154]. Since from our array profile, AMPKα1 phosphorylation was repressed to the highest extent and it is known to be a cellular metabolic sensor, we chose this protein to perform further experiments to check its involvement in KLF2 mediated reduction in metabolism of ECs.

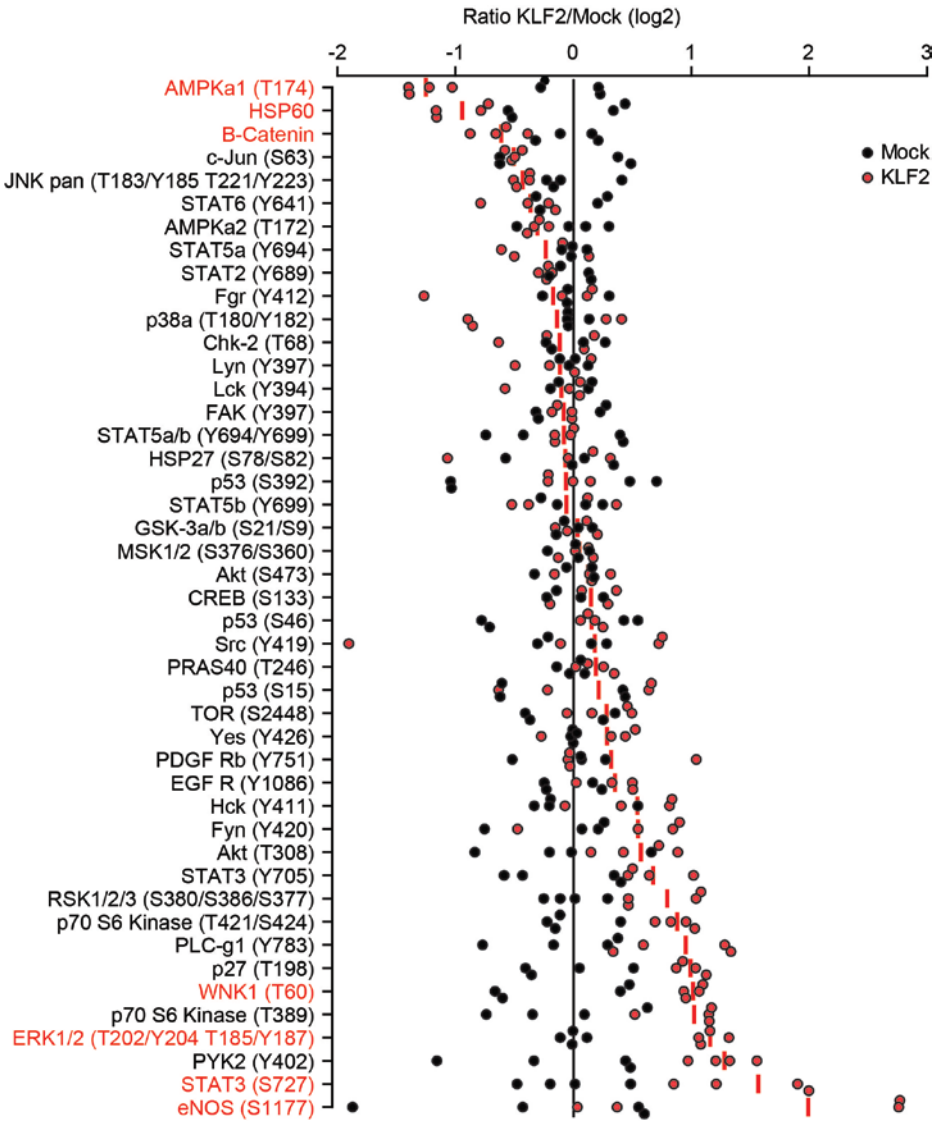

Figure IV.17. Phospho-kinase array reveals many proteins with differential phosphorylation patterns upon KLF2 over expression

Phospho-kinase array profile showing phosphorylation levels of proteins in KLF2 transduced HUVEC versus mock transduced controls. Code in parenthesis indicates site of phosphorylation and those highlighted in red represent proteins with significant changes in levels as analyzed by two way ANOVA. Data is represented as ratio of phosphorylation levels in KLF2 transduced HUVECs to mock controls and log 2 transformed (n=4).

4.5 Role of AMPKα1 in KLF2 mediated regulation of endothelial metabolism

4.5.1 KLF2 regulates AMPKα1 phosphorylation

AMPK has been previously described to act upstream of KLF2, where an increase in its phosphorylation activity was apparent upon shear exposure[154]. Here, we describe the regulation of AMPK activity as a downstream target of KLF2. In our study, we observed no significant changes in AMPKα1 gene expression (Fig IV.18A) or AMPKα protein levels (Fig

IV.18B) upon KLF2 overexpression. It is likely that KLF2 regulates AMPKα1 at a post translational level. To confirm data obtained from phospho-kinase profile of reduced phosphorylation of AMPKα1 subunit by KLF2, we performed an ELISA to measure phosphorylated AMPKα1 (threonine 174; T174) activity with mock and KLF2 transduced cells. KLF2 indeed reduces p-AMPKα1 activity compared to mock control (Fig IV.18C).

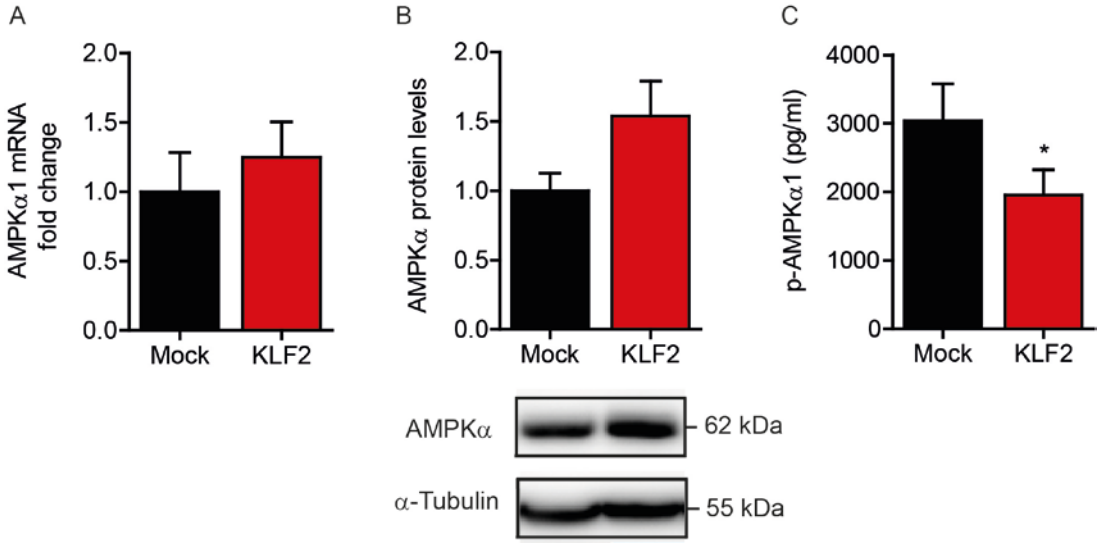

Figure IV.18. KLF2 indeed reduces phosphorylation of AMPKα1

(A) Total RNA was isolated from mock and KLF2 transduced HUVECs and AMPKα1 mRNA expression levels was quantified by real time qPCR and normalized to RPLP0 mRNA (n=4) (B) Cell lysates from mock and KLF2 transduced HUVECs were analyzed by immunoblot and probed for antibodies against total AMPKα protein and α-Tubulin, which served as a loading control. Representative blot is shown here. Protein levels of AMPKα was quantified and normalized to α-Tubulin signal (n=4). (C) Phosphorylated-AMPKα1 (T174) levels was measured in mock and KLF2 transduced cell lysates by ELISA and final sample concentrations were calculated against p-AMPKα1 standard curve (n=3). Data are represented as mean ± S.E.M; *p<0.05.

4.5.2 Loss of AMPKα1 in ECs does not contribute to reduction in glycolytic metabolism

Since KLF2 reduced AMPKα1 function, this could potentially explain the mechanism by which KLF2 down regulates glycolysis. To test this hypothesis, we used a siRNA mediated knock down approach. We used two siRNA targeting AMPKα1; siAMPKα1 (1) and siAMPKα1 (2) and upon transfection in HUVECs achieved a knockdown efficiency of 60-80%. This was confirmed at mRNA level at 24 hours post transfection by real time PCR. A universal non –specific siRNA was used as control.

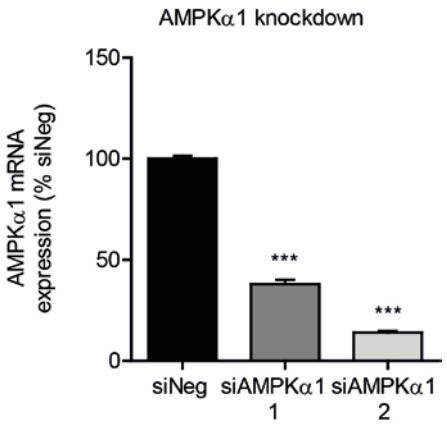

Figure IV.19. Knockdown of AMPKα1 in HUVECs

HUVECs were transfected with 67nM of control siRNA (siNeg) or two different siRNA directed against AMPKα1 (siAMPKα1; 1 and 2) and 24 hours after transfection, total RNA was isolated and AMPKα1 mRNA levels were measured by real time qPCR and normalized to RPLP0 mRNA (n=3). Data are represented as mean ± S.E.M; ***p<0.001.

We next analyzed uptake of glucose in control cells and after silencing of AMPKα1 by flow cytometry after an hour incubation of cells with 2-NBDG. Loss of AMPKα1 using both siRNAs did not affect glucose uptake in HUVECs (Fig IV.20A). In addition, we performed seahorse flux analysis to study glycolytic function and results revealed that ECs lacking AMPKα1 do not change significantly in basal ECAR levels, glycolysis or maximum glycolytic capacity (Fig IV.20A and B). The above data suggests that AMPKα1 does not play a role in controlling endothelial cell glycolysis and reduction of AMPKα1 phosphorylation by KLF2 therefore does not explain the KLF2 mediated reduction of glycolysis.

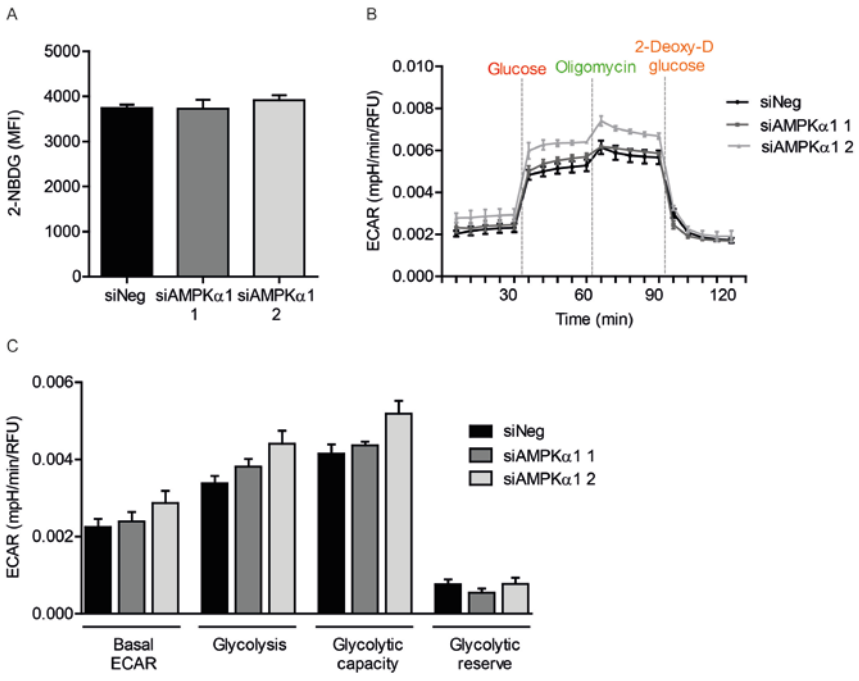

Figure IV.20. Knockdown of AMPKα1 does not explain the inhibitory effect of KLF2 on metabolism

48 hours after transfection with siNeg or siAMPKa1 (67nM), HUVECs were analyzed for (A) Glucose uptake by flow cytometry analysis of 2-NBDG fluorescence (n=3) (B) ECAR glycolytic profile by seahorse flux analysis, vertical lines indicate the time of addition of Glucose (10mM), Oligomycin (3µM) and 2-Deoxy-D glucose (100mM) (C) Glycolytic function parameters quantified from (B) and levels normalized to DNA content determined by DAPI staining (n=3). Data are represented as mean ± S.E.M. MFI: mean fluorescence intensity, ECAR: extra cellular acidification rate, RFU: relative fluorescence unit.

4.6 Role of nitric oxide and hypoxia in metabolic regulation of ECs by KLF2

Results from the phospho kinase array experiments (Fig IV.17) show eNOS phosphorylation to be induced upon KLF2 overexpression. This is in agreement with previous reports that KLF2 binds to the promoter of endothelial nitric oxide synthase (eNOS) and trans activates eNOS gene expression and activity in bovine aortic endothelial cells (BAECs)[51]. eNOS is required for generation of vasoprotective NO and in turn to maintain the vascular tone. NO is known to be a competitive inhibitor of complex I (cytochrome C oxidase) in the electron transport chain with oxygen and thus inhibits mitochondrial respiration[155,156]. NO has also been reported to inhibit glycolysis by reducing GAPDH activity[157]. This led us to question whether the increase in NO availability on KLF2 overexpression leads to inhibition of glycolysis and oxygen consumption. To test this, we used an inhibitor of NO, Nω-nitro-L-arginine methyl ester hydrochloride (L-NAME) in mock and KLF2 transduced HUVECs. Interestingly, KLF2 overexpressing cells with NO inhibition by L-NAME (4 hours; 1mM) did not increase their acidification rate (Fig IV.21A) or respiration levels (Fig IV.21B), suggesting that NO is not involved in KLF2 mediated reduction in mitochondrial respiration and glycolysis.

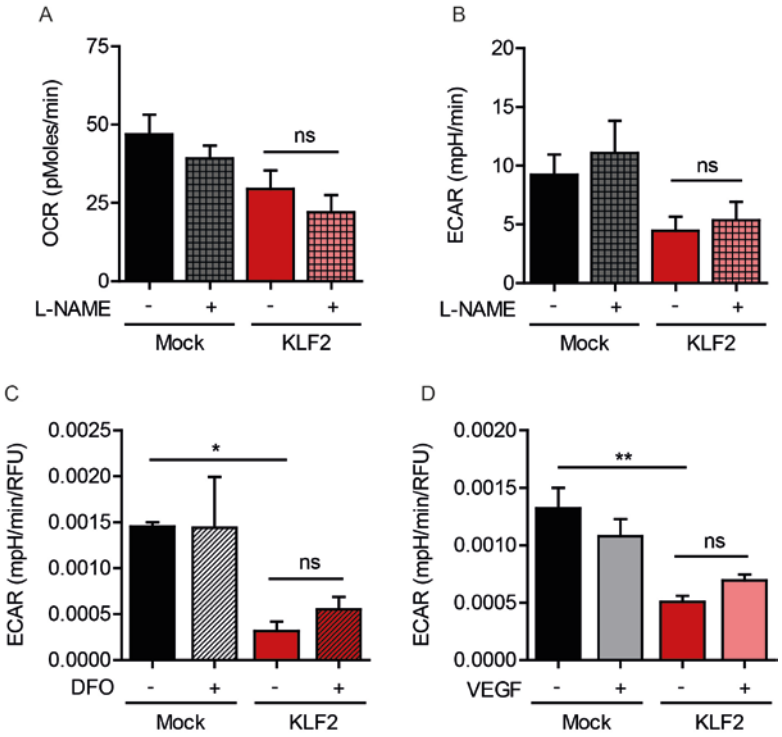

Figure IV.21. Inhibition of NO, hypoxic mimicking nor VEGF stimulation explains the inhibitory effect of KLF2 on metabolism

HUVECs transduced with mock and KLF2 overexpressing lentivirus were treated with 1mM L-NAME for 4 hours and analyzed for (A) basal acidification rate and (B) basal mitochondrial respiration by seahorse flux analysis (n=4). HUVECs transduced with mock and KLF2 overexpressing lentivirus were treated with (C) 100μM of DFO for 24 hours (n=3) and (D) 50 ng/ml of VEGF for 24 hours (n≥3) and quantified for glycolysis by seahorse flux analysis, values were normalized to DNA content determined by DAPI staining. Data are represented as mean ± S.E.M; *p<0.05, **p<0.01. L-NAME: N ω-nitro-L-argininemethyl ester hydrochloride, DFO: desferrioxamine, VEGF: vascular endothelial growth factor.

As other possible mediators involved in KLF2 dependent glycolytic inhibition, we focused on HIF1α activation and vascular endothelial growth factor (VEGF) stimulation that are inducers of glycolysis in ECs[111,158] and the observation that KLF2 is a negative regulator of hypoxia induced angiogenesis and VEGF mediated angiogenesis[97,98]. We treated mock and KLF2 overexpressing HUVECs with desferrioxamine (DFO; 24 hours; 100μM), a hypoxia mimicking agent and analyzed ECAR levels by seahorse flux analysis. Rescue of HIF1α activation by DFO in KLF2 overexpression conditions did not increase glycolysis to levels seen in mock controls (Fig IV.21C); indicating KLF2 induced glycolytic inhibition is HIF1α independent. Stimulation of mock and KLF2 conditions with VEGF (24 hours; 50ng/ml) also did not significantly increase glycolysis in KLF2 overexpressing HUVECs (Fig IV.21D) confirming that VEGF signaling does not play a role in KLF2 mediated glycolysis inhibition of ECs.

4.7 RNA sequencing analysis reveals key glycolytic genes regulated by shear stress

4.7.1 Shear stress down regulates gene expression of key glycolytic genes

As an unbiased approach to understand regulation of metabolism related genes we performed RNA sequencing of cells cultured under static conditions and those exposed to shear stress of 20 dyn/cm^2 for 72 hours. Analysis of RNA sequencing data revealed an interesting pattern of down regulation of most enzymes involved in glycolysis (see Table IV.1). A color coded graphical representation of the regulated genes in glycolytic metabolism is shown in Fig IV.22.

Briefly, an up regulation of glucose transporters (SLC2A) was seen and a reduction in gene expression of hexokinase, the first critical enzyme catalyzing an irreversible reaction of glycolysis, was apparent upon shear stimulation. The other crucial rate limiting checkpoints of glycolysis that determines the flux of the reaction is conversion of fructose-6-phosphate (F6P) to fructose-1,6-bisphosphate (F1,6BP), catalyzed by phosphofructokinase (PFK). The conversion of F6P to fructose-2,6-bisphosphate (F2,6BP) requires the activity of PFKFB rate limiting enzymes and the product F2,6 BP is an allosteric activator of PFK. The expression of both PFKP (platelet isoform expressed in ECs) and PFKFB3 (highly expressed isoform in ECs), the two most potent stimulators of glycolysis, was indeed reduced by shear stress suggesting a reduction in glycolytic flux of ECs.

Shear stress also reduced gene expression of aldolases which are implicated in high glucose induced cellular dysfunction[159]. Additionally, other glycolytic enzymes like PGK1, PGAM, enolases and LDHB were also down regulated by shear stress. However, expression of PKM, LDHA and LDHC genes were slightly upregulated by shear stress.

From the RNA sequencing data we could conclude that the expression profile of rate limiting glycolytic genes was significantly reduced in ECs by shear stress. We further selected a few candidates to elucidate the mechanism of glycolytic metabolism inhibition by shear stress.

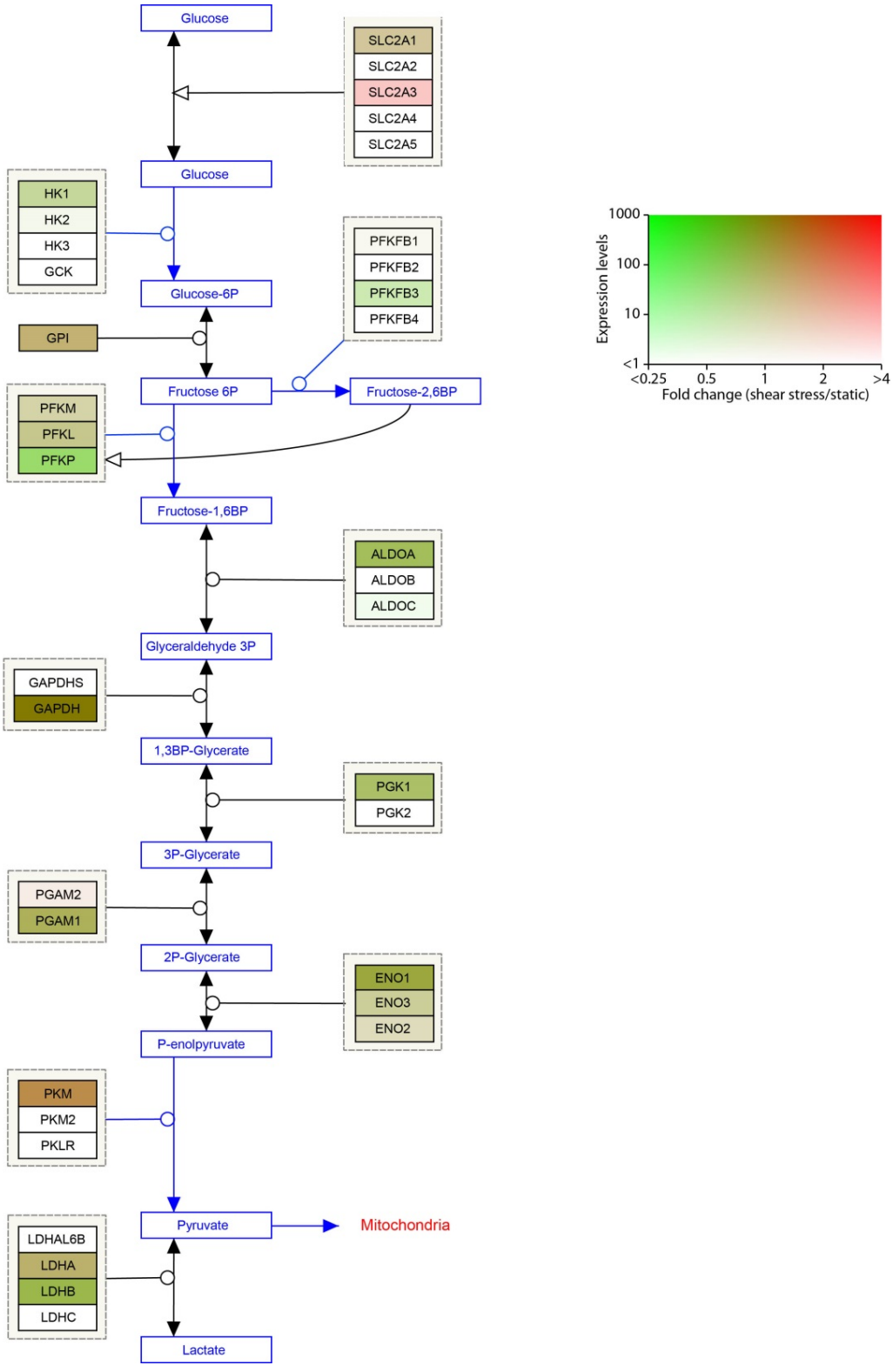

Figure IV.22. RNA sequencing of static and shear exposed ECs

Graphical representation of RNA sequencing profile analysis from shear stress stimulated HUVECs (20 dyn/cm^2 for 72 hours) and static control RNA, showing expression levels of genes in the glycolytic pathway. Data is represented as fold change versus static controls that corresponds to color coded legend.

HGNC ID	HGNC symbol	Description	Fold change	DEG_RPKM	p-value
11005	SLC2A1	solute carrier family 2 (facilitated glucose transporter), member 1	1.36	0.607	0.186
11006	SLC2A2	solute carrier family 2 (facilitated glucose transporter), member 2	1.40	0.101	0.500
11007	SLC2A3	solute carrier family 2 (facilitated glucose transporter), member 3	2.52	0.889	0.035
11009	SLC2A4	solute carrier family 2 (facilitated glucose transporter), member 4	-1.07	0.134	0.852
11010	SLC2A5	solute carrier family 2 (facilitated glucose/fructose transporter), member 5	1.11	0.099	0.650
4922	HK1	hexokinase 1	-1.24	0.534	0.276
4923	HK2	hexokinase 2	-1.40	0.521	0.114
4925	HK3	hexokinase 3 (white cell)	1.62	0.177	0.388
4195	GCK	glucokinase (hexokinase 4)	-1.62	0.177	0.310
4458	GPI	glucose-6-phosphate isomerase	1.24	0.542	0.136
8877	PFKM	phosphofructokinase, muscle	-1.09	0.317	0.519
8876	PFKL	phosphofructokinase, liver	-1.01	0.025	0.864
8878	PFKP	phosphofructokinase, platelet	-1.93	0.831	0.011
8872	PFKFB1	6-phosphofructo-2-kinase/fructose-2,6-biphosphatase 1	-1.74	0.247	0.360
8873	PFKFB2	6-phosphofructo-2-kinase/fructose-2,6-biphosphatase 2	1.40	0.291	0.324
8874	PFKFB3	6-phosphofructo-2-kinase/fructose-2,6-biphosphatase 3	-1.79	0.716	0.032
8875	PFKFB4	6-phosphofructo-2-kinase/fructose-2,6-biphosphatase 4	-1.11	0.172	0.742
414	ALDOA	aldolase A, fructose-bisphosphate	-1.23	0.538	0.005
417	ALDOB	aldolase B, fructose-bisphosphate	-1.27	0.171	0.519
418	ALDOC	aldolase C, fructose-bisphosphate	-2.58	0.801	0.103
24864	GAPDHS	glyceraldehyde-3-phosphate dehydrogenase, spermatogenic	1.42	0.345	0.202
4141	GAPDH	glyceraldehyde-3-phosphate dehydrogenase	1.24	0.553	0.084
8896	PGK1	phosphoglycerate kinase 1	-1.20	0.503	0.231
8898	PGK2	phosphoglycerate kinase 2	-1.04	0.097	0.912
8889	PGAM2	phosphoglycerate mutase 2 (muscle)	1.92	0.683	0.086

8888	PGAM1	phosphoglycerate mutase 1 (brain)	-1.05	0.133	0.569
3350	ENO1	enolase 1, (alpha)	-1.10	0.364	0.213
3353	ENO2	enolase 2 (gamma, neuronal)	1.17	0.402	0.535
3354	ENO3	enolase 3 (beta, muscle)	-1.05	0.125	0.763
9021	PKM	pyruvate kinase, muscle	1.64	0.739	0.198
9020	PKLR	pyruvate kinase, liver and RBC	-2.06	0.177	0.019
21481	LDHAL6B	lactate dehydrogenase A-like 6B	-7.61	0.393	0.139
6535	LDHA	lactate dehydrogenase A	1.29	0.591	0.012
6541	LDHB	lactate dehydrogenase B	-1.32	0.611	0.318
6544	LDHC	lactate dehydrogenase C	2.27	0.177	0.018

Table IV.1. RNA sequencing data from sheared and static HUVECs
Quantification data from RNA sequencing profile of shear stress exposed cells (20 dyn/cm^2 for 72 hours) versus static control. Total RNA was isolated from cells, sequence libraries were prepared and deep sequencing data was mapped as previously described[138]. DEG: differential expression gene, RPKM: reads per kilobase per million.

4.7 2 Confirmation of RNA sequencing data

In order to confirm the regulation of glycolytic genes by shear stress, we validated the data from RNA sequencing by performing real time qPCR. We focused on the first three rate limiting enzymes of glycolysis namely HK2, PFK1 and PFKFB3. Gene expression results showed significant down regulation of HK2, PFK1 and PFKFB3 upon exposure to shear stress (20 dyn/cm^2) for 72 hours when compared to static controls (Fig IV.23A) which is similar to that detected by RNA sequencing. To investigate whether KLF2 has a similar effect on glycolytic genes, we analyzed for gene expression in mock and KLF2 transduced cells by real time qPCR where a similar inhibition of HK2, PFK1 and PFKFB3 was observed at mRNA level by KLF2 (Fig IV.23B).

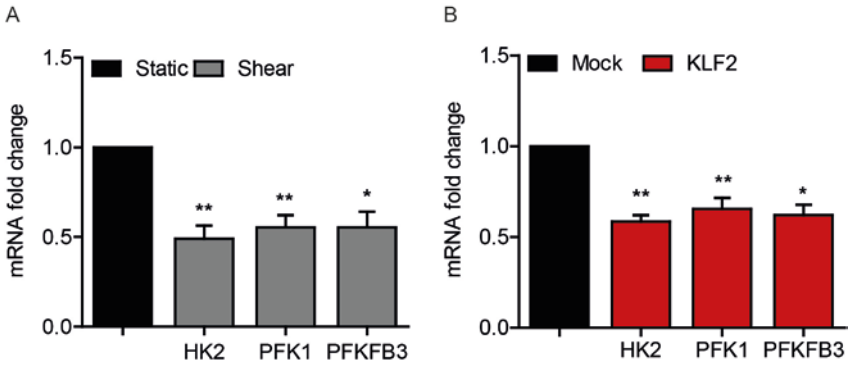

Figure IV.23. Shear stress and KLF2 reduce expression of glycolytic genes
(A) mRNA expression of HK2, PFKFB3 and PFK1 normalized to GAPDH expression in shear stress stimulated HUVECs (20 dyn/cm^2 for 72 hours) versus static controls (n≥6) (B) mRNA expression of HK2, PFKFB3 and

PFK1 normalized to RPLP0 expression in KLF2 transduced HUVECs versus mock transduced controls (n≥3). Data are represented as mean ± S.E.M; *p<0.05, **p<0.01.

Next, we determined the regulation of HK2, PFK1 and PFKFB3 protein by KLF2. Lysates from mock and KLF2 transduced cells were prepared and analyzed by immunoblotting to determine protein levels. Antibodies against HK2, PFK1 and PFKFB3 were used and the expression level of α-Tubulin was used as a control to normalize respective protein levels. Upon KLF2 overexpression, a reduction in HK2 protein (Fig IV.24A), PFK1 protein (Fig IV.24B) and PFKFB3 protein levels (Fig IV.24C) was confirmed. These data indicate repression of key glycolytic genes i.e. HK2, PFK1 and PFKFB3 by shear stress and KLF2.

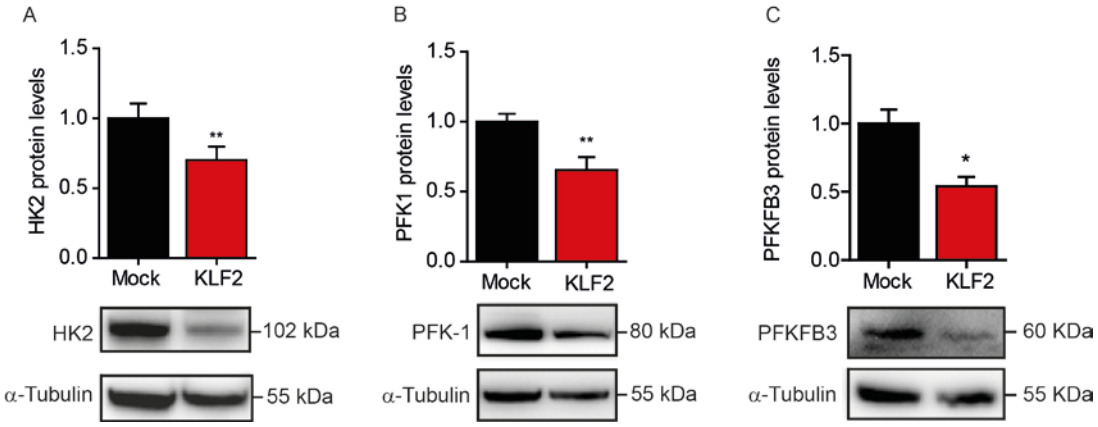

Figure IV.24. KLF2 down regulates glycolytic genes at protein level

Total cell protein lysates from mock and KLF2 transduced cells were analyzed by immunoblotting and probed against antibodies for (A) HK2 (n=4), (B) PFK1 (n=8) and (C) PFKFB3 (n=4), and α-Tubulin which served as a loading control. Respective protein levels were quantified and normalized to α-Tubulin signal intensity. Representative blot images are shown here. Data are represented as mean ± S.E.M; *p<0.05, **p<0.01.

4.7.3 Shear stress mediated reduction in glycolytic gene expression is KLF2 dependent

As mentioned previously, many of the shear stress effects could be attributed to KLF2. We observed repression of glycolytic gene set HK2, PFKFB3 and PFK1 by shear stress as well as KLF2 overexpression. To test whether shear stress mediated repression of the glycolytic gene set is KLF2 dependent; we used shKLF2 lentivirus to silence KLF2 in HUVECs and further subjected them to shear stress (20 dyn/cm^2 for 72 hours). qPCR analysis from these samples revealed that reduction seen in expression of HK2 (Fig IV.25A), PFK1 (Fig IV.25B) and PFKFB3 (Fig IV.25C) mRNA upon shear exposure is abrogated when KLF2 is silenced. The effect was significant for PFK1 and PFKFB3 expression; for HK2 mRNA a trend in the same

direction was observed. Thus, we concluded that shear stress reduces PFK1 and PFKFB3 expression in a KLF2-dependent manner.

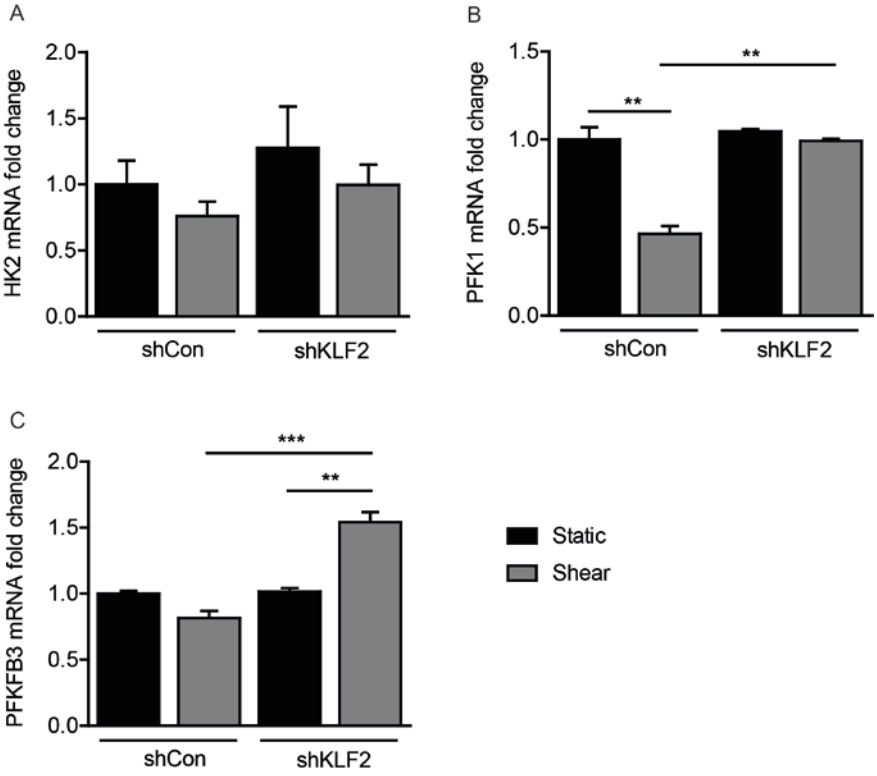

Figure IV.25. Repression of glycolytic genes by shear stress is KLF2 dependent
Total RNA was isolated from HUVECs after lentiviral silencing of KLF2 and subsequent exposure to flow (20 dyn/cm^2 for 72 hours). mRNA expression levels of (A) HK2 (B) PFK1 and (C) PFKFB3 were quantified by real time qPCR and normalized to GAPDH mRNA levels (n≥3). Data are represented as mean ± S.E.M; **p<0.01, ***p<0.001.

4.8 Role of HK2, PFK1 and PFKFB3 in KLF2 mediated glycolytic metabolism of endothelium

4.8.1 HK2 knockdown in ECs does not recapitulate KLF2 mediated glycolysis reduction

After confirming that shear stress and KLF2 regulate expression of the three key glycolytic genes, we next set out to determine which genes down regulate glycolysis to the same levels as KLF2 in HUVECs. We used two separate siRNAs targeted against HK2 in HUVECs, siHK2 (1) and siHK2 (2). A knockdown efficiency of 80% on mRNA level (24 hours post transfection) was achieved in both cases (Fig IV.26A), confirmed by real time PCR. Next, we performed seahorse analyses to determine glycolytic function after knockdown of HK2 in

HUVECs. Assay was performed 48 hours post transfection. Loss of HK2 did not change basal ECAR, glycolysis or other parameters of glycolysis measurement (Fig IV.26B) and thus did not recapitulate the reduction in glycolytic function observed on overexpression of KLF2 (Fig IV.8). Although KLF2 reduces HK2 mRNA and protein levels, it appears that HK2 in not involved in KLF2 mediated reduction in glycolysis.

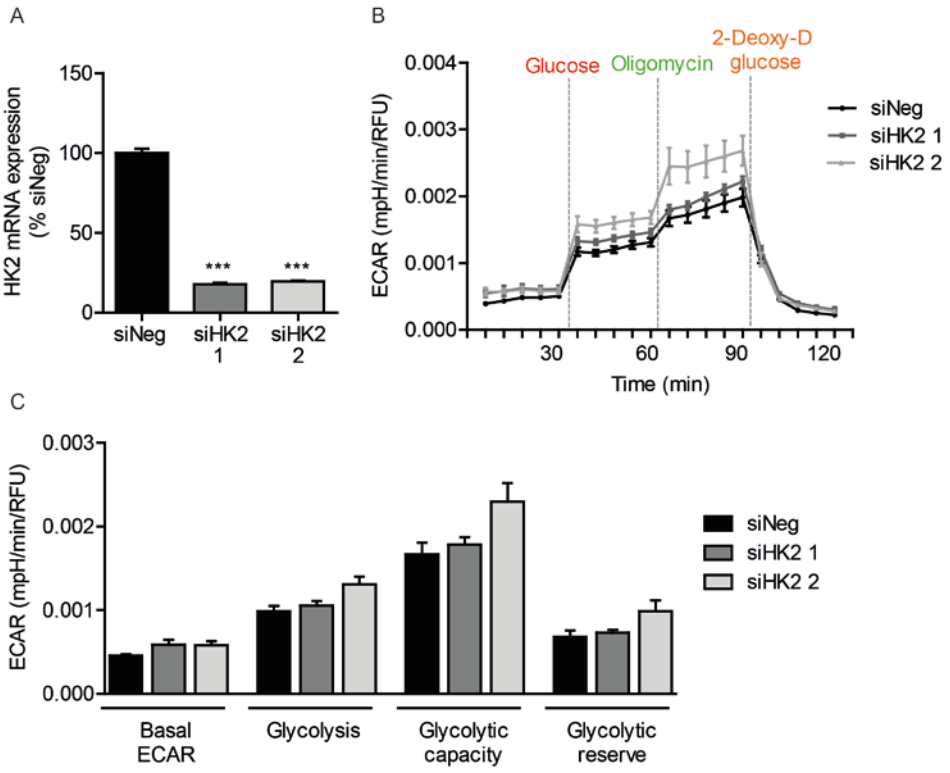

Figure IV.26. HK2 is not involved in KLF2 mediated reduction in metabolism

HUVECs were transfected with 67nM of control siRNA (siNeg) or two different siRNA directed against HK2 (siHK2; 1 and 2). (A) 24 hours after transfection, total RNA was isolated and HK2 mRNA levels were measured by real time qPCR, expression normalized to RPLP0 mRNA (n=3). (B) ECAR glycolytic profile was analyzed 48 hours after transfection by seahorse flux analysis, vertical lines indicate the time of addition of Glucose (10mM), Oligomycin (3µM) and 2-Deoxy-D glucose (100mM) (C) Glycolytic function parameters were quantified from (B), normalized to DNA content determined by DAPI staining (n=3). Data are represented as mean ± S.E.M; ***p<0.001.

4.8.2 PFK1 is not involved in KLF2 mediated glycolysis reduction in ECs

We performed siRNA mediated knock down of the second target PFK1, a crucial flux determinant of glycolysis. Using two separate siRNA against PFK1 we observed 85-90% knockdown of PFK1 mRNA levels at 24 hours after transfection, confirmed by real time qPCR (Fig IV.27A). Surprisingly, cells were still viable after such a drastic knockdown of PFK1. Furthermore, we performed seahorse analyses for glycolysis which revealed no

significant changes in basal ECAR, glycolysis and other parameters on knockdown of PFK1 in HUVECs (Fig IV.27B and C). In spite of reduced expression of PFK1 due to KLF2 overexpression, loss of PFK1 in HUVECs per se did not reduce glycolysis in ECs indicating that PFK1 is perhaps not involved in KLF2 mediated glycolysis reduction.

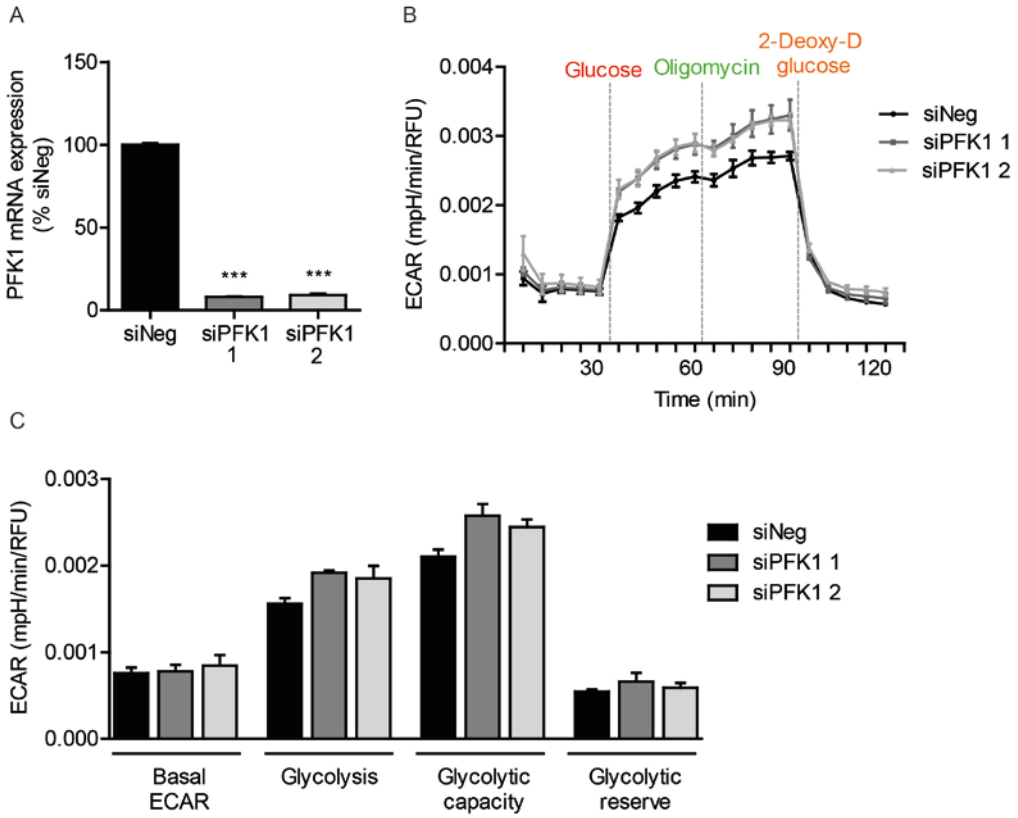

Figure IV.27. PFK1 is not involved in KLF2 mediated reduction in metabolism

HUVECs were transfected with 67nM of control siRNA (siNeg) or two different siRNA directed against PFK1 (siPFK1; 1 and 2). (A) 24 hours after transfection, total RNA was isolated and HK2 mRNA levels were measured by real time qPCR, expression normalized to RPLP0 mRNA (n=3). (B) ECAR glycolytic profile was analyzed 48 hours after transfection by seahorse flux analysis, vertical lines indicate the time of addition of Glucose (10mM), Oligomycin (3µM) and 2-Deoxy-D glucose (100mM) (C) Glycolytic function parameters were quantified from (B), normalized to DNA content determined by DAPI staining (n=3). Data are represented as mean ± S.E.M; ***p<0.001.

4.8.3 Loss of PFKFB3 in ECs shows a glycolytic phenotype similar to KLF2 overexpression

To study the role of PFKFB3 in our study, we knocked down PFKFB3 in HUVECs using two different siRNA against PFKFB3. We observed 80-85% reduction in expression of PFKFB3 on mRNA level after 24 hours of transfection (Fig IV.28A). We also confirmed knockdown on protein level, 48 hours post transfection (Fig IV.28B). Next, we checked glycolytic function by seahorse flux analyses and interestingly, we observed a drastic reduction in

glycolytic function (Fig IV.28C) and upon quantification we confirmed a decreasing trend in basal ECAR and significant decrease in glycolysis and maximum glycolytic capacity (Fig IV.28D). The decrease in glycolytic function was comparable to the glycolytic profile observed under KLF2 overexpression (Fig IV.8). These results led us to the hypothesis that KLF2 reduces glycolytic function in a PFKFB3 dependent manner.

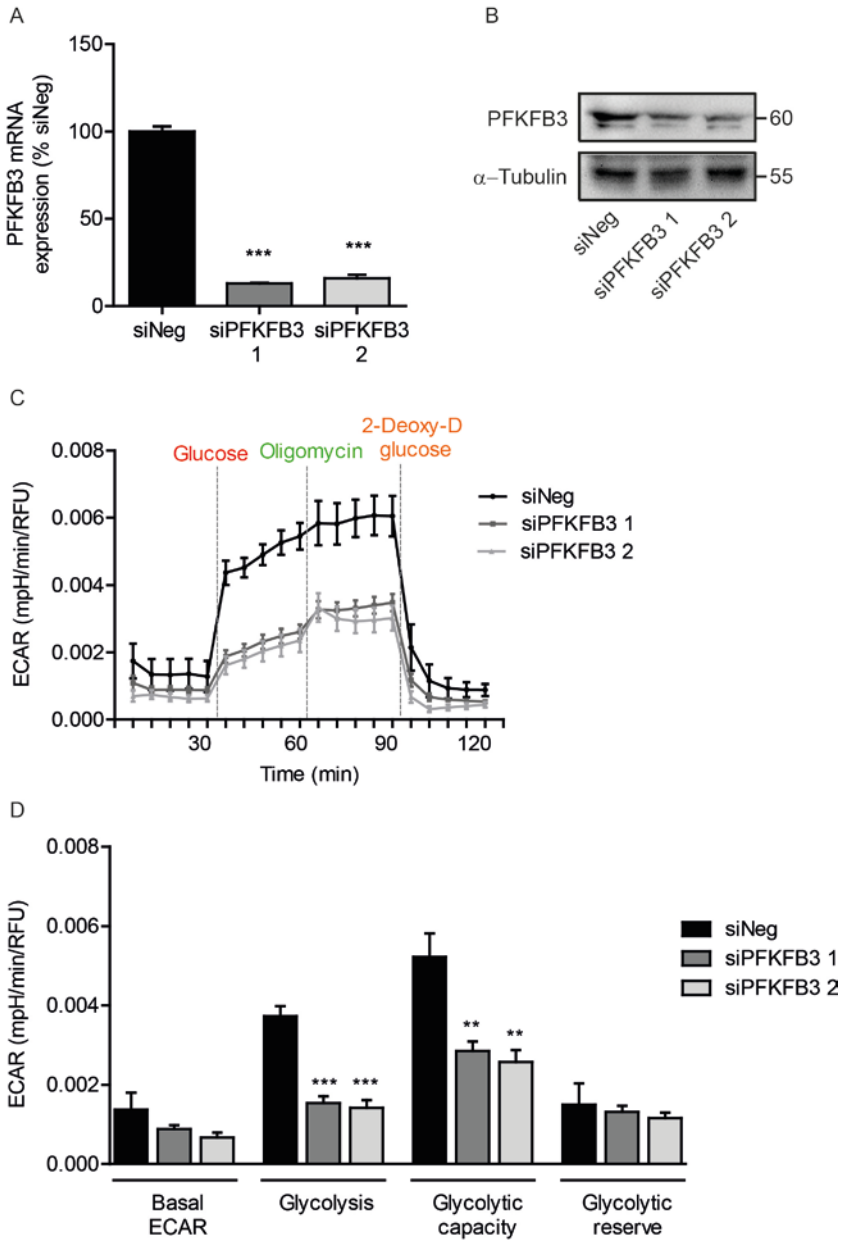

Figure IV.28 Knockdown of PFKFB3 recapitulates the effects seen upon KLF2 overexpression

HUVECs were transfected with 67nM of control siRNA (siNeg) or two different siRNA directed against PFKFB3 (siPFKFB3; 1 and 2). (A) 24 hours after transfection total RNA was isolated and PFKFB3 mRNA levels were measured by real time qPCR (n=3) (B) Representative immunoblot analysis of total cell protein lysates harvested 48 hours after transfection, probed against antibodies for PFKFB3 and α-Tubulin which served as a loading control. (C) ECAR glycolytic function profile was analyzed 48 hours after transfection by Seahorse

flux analysis, vertical lines indicate the time of addition of Glucose (10mM), Oligomycin (3µM) and 2-Deoxy-D glucose (100mM) (D) Quantification of glycolytic function parameters from (C), normalized to DNA content determined by DAPI staining (n≥3). Data are represented as mean ± S.E.M; **p<0.01, ***p<0.001.

4.8.4 Localization of PFKFB3 in ECs

We next investigated localization of PFKFB3 in endothelial cells transduced with mock and KLF2 lentivirus. Immunofluorescence staining was performed to visualize PFKFB3 localization and expression, Phalloidin dye was used to stain actin filaments and DAPI for nuclei staining. Microscopy analysis revealed no significant differences in localization of PFKFB3 by KLF2. In both mock and KLF2 transduced cells, nuclear and peri-nuclear localization of PFKFB3 was observed. Indeed, actin filament rearrangement and elongated morphology was apparent in KLF2 overexpressing cells (Fig IV.29). Previous studies have reported similar perinuclear localization of PFKFB3 in HUVECs in addition to expression in lamellopodia in actively proliferating cells[111].

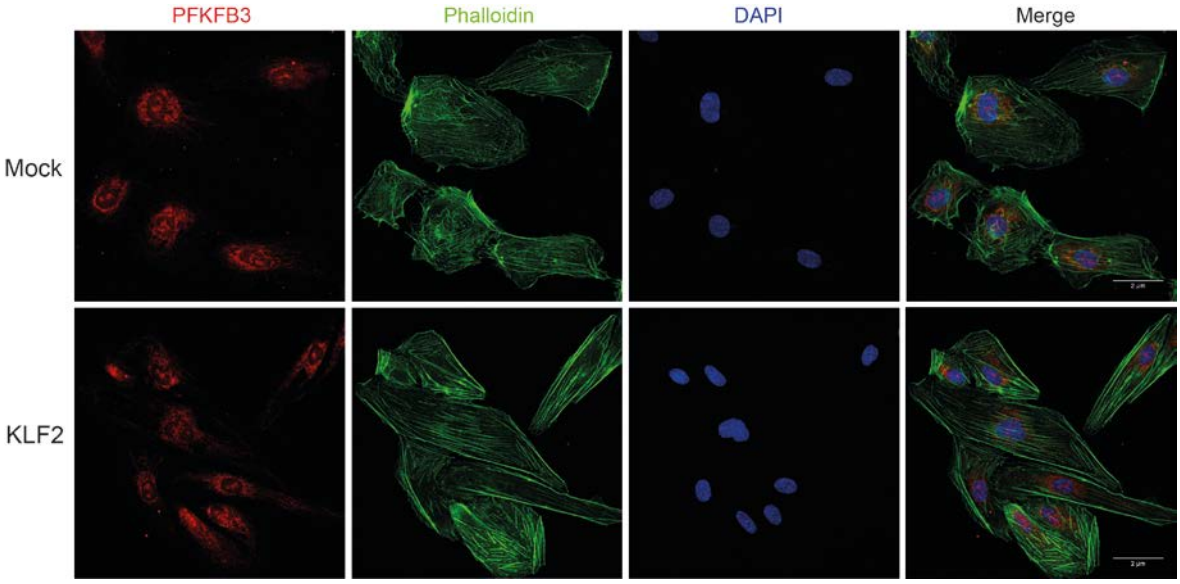

Figure IV.29. Localization of PFKFB3 in mock and KLF2 transduced cells
HUVECs transduced with mock and KLF2 overexpressing lentivirus were fixed and immunostained for endogenous PFKFB3 (red), phalloidin (green) was used to visualize actin filaments and DAPI (blue) was used to stain nuclei. Representative images (63x) are shown here. Scale bar: 2µm.

4.8.5 Shear stress repression of PFKFB3 in evident even at rates higher than 20 dyn/cm^2

To understand the regulation of PFKFB3 by shear stress, we tested PFKFB3 mRNA expression in ECs that were exposed to different rates of shear stress. µ-slide I Slides with same culture area but different volume capacity (0.8 luer, 0.4 luer and 0.2 luer; Ibidi) were

used and thus HUVECs seeded in these slides were exposed to shear stress of 10, 20 and 30 dyn/cm^2 respectively. qPCR analysis of KLF2 and PFKFB3 mRNA levels (Fig IV.30A and B) showed that at 10dyn/cm^2, shear stress that is sensed by ECs experiencing turbulent flow, mRNA levels of PFKFB3 is not changed. However at 20 dyn/cm^2, KLF2 was up regulated by 8 fold and this indeed reduced PFKFB3 expression significantly as seen in our previous experiments. When ECs are exposed to even higher shear stress of 30 dyn/cm^2, we indeed observe KLF2 induction to 7 fold, which still maintains the repression of PFKFB3 mRNA. These data confirm that at low shear stress experienced by ECs under disturbed flow, PFKFB3 expression is not regulated and hence similar to that seen under static controls. However, upon exposure to shear stress ≥20 dyn/cm^2, expression of PFKFB3 is inhibited by atheroprotective flow accompanied by KLF2 induction.

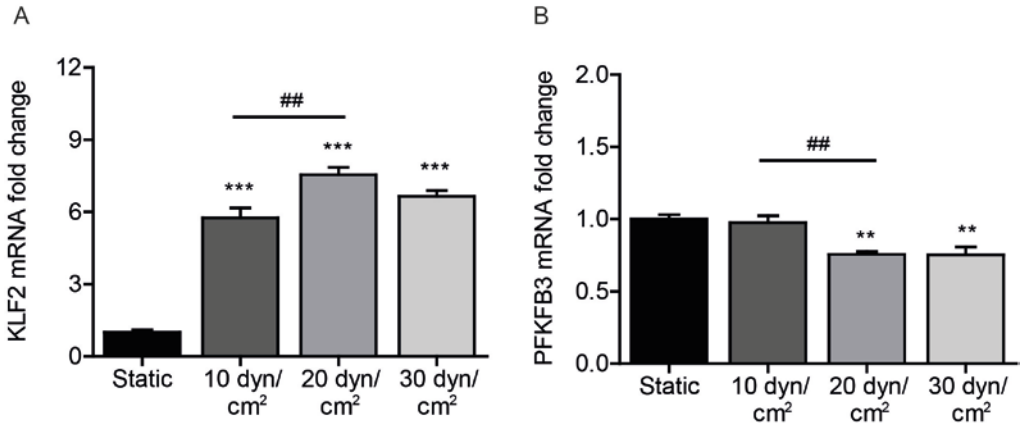

Figure IV.30. Shear stress higher than 20dyn/cm^2 also repress PFKFB3 expression
HUVECs were exposed to different shear stress rates of 10, 20 and 30 dyn/cm^2 for 72 hours or kept under static conditions (control). Total RNA was isolated and mRNA expression levels of (A) KLF2 and (B) PFKFB3 was quantified by real time qPCR, normalized to GAPDH mRNA levels (n=4). Data are represented as mean ± S.E.M; **p<0.01 vs static, ***p<0.001 vs static, ##p<0.01.

4.9 Mechanism of PFKFB3 mediated glycolysis inhibition by KLF2

4.9.1 Promotor analysis of PFKFB3 revealed putative KLF binding sites

To investigate the mechanism of PFKFB3 inhibition by KLF2, we performed *in silico* promotor analysis of PFKFB3 using rVISTA 2.0 web browser (http://rvista.dcode.org) to identify Sp1/KLF binding sites. Two evolutionary conserved regions in the short isoform of

PFKFB3 gene were identified in its promotor (Fig IV.31A) by ECR browser DCODE platform[139] and we focused on the 757 bp long region (chr10: 6244721-6245477) marked within a red box in Fig IV.31A. In rVISTA, eleven conserved transcription binding sites for Sp1, Sp1_Q2, Sp1_Q4 and Sp1_Q6 transcription factors was predicted in the 757bp conserved region. An enlarged picture of this region is depicted in Fig IV.31B. A conserved sequence of 312bp that included the predicted binding site for Sp1/KLF was chosen to design promotor constructs for luciferase assay.

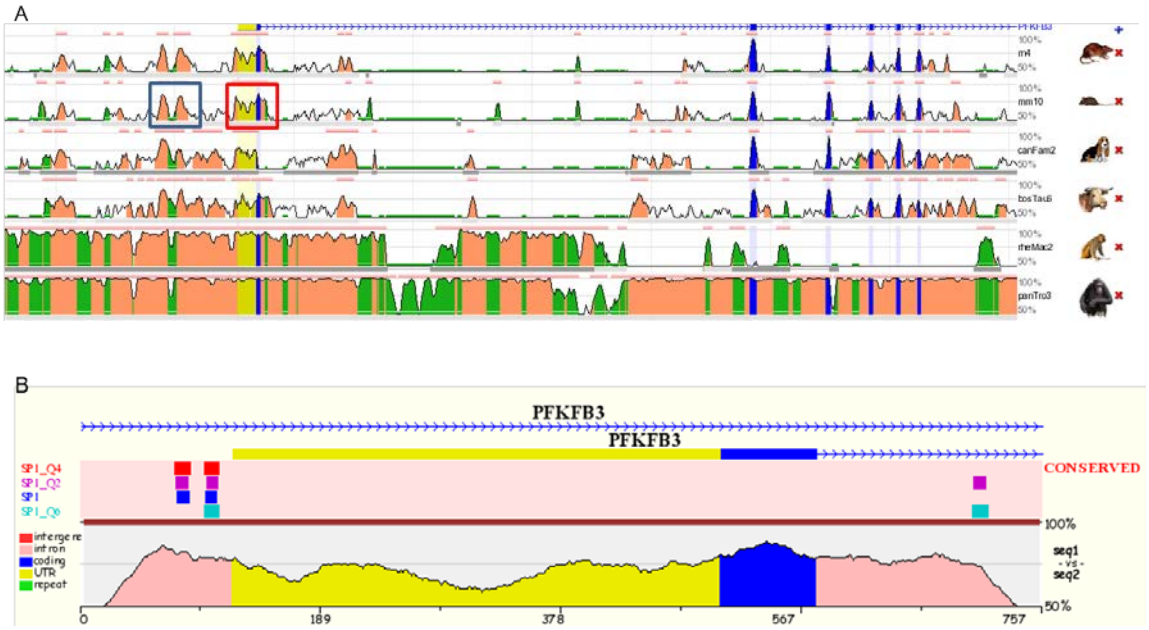

Figure IV.31. Sp1 putative binding sites on the promotor of PFKFB3
(A) Graphical representation showing two evolutionary conserved regions (marked within blue and red boxes) in PFKFB3 promotor (adapted from rVISTA 2.0, http://rvista.dcode.org/) (B) Enlarged region contained within the red box from (A) showing putative conserved Sp1 family/KLF transcription factor binding sites on PFKFB3 promotor.

4.9.2 KLF2 binds and represses the PFKFB3 promotor

We next established a luciferase reporter assay to study whether KLF2 binds directly to the conserved Sp1/KLF binding site in PFKFB3 promoter to regulate PFKFB3 expression. We cloned the 312 bp conserved sequence of PFKFB3 promoter in front of firefly luciferase gene in a luciferase reporter vector (pGL4.10 [*luc2*] from Promega). This luciferase reporter construct served as the wild type control and a mutant construct was also used, where the putative binding site of KLF in the PFKFB3 promoter was mutated from –CCCGCCC- to –AATTAAC-. Partial sequences of PFKFB3 promoter constructs are shown in Fig IV.32A, which were used as the wild type construct (WT) and binding site mutated construct (mutant). Along with the firefly luciferase constructs, we also transfected renilla firefly plasmid (pGL

4.74 [*hRluc*] from Promega), which served as an expression control for fluorescence measurements. Luciferase activity was measured for the wild type reporter and mutated reporter constructs in HUVECs transduced with mock and KLF2 overexpressing lentivirus and normalized to Renilla firefly activity. We found that luciferase activity is significantly reduced in KLF2 transduced HUVECs compared to mock controls when transfected with the wild type reporter construct. The repression was abrogated in KLF2 transduced cells when they were transfected with the mutated version of the reporter construct (Fig IV.32B). These results confirmed that KLF2 inhibits expression of PFKFB3 via transcriptional repression in ECs.

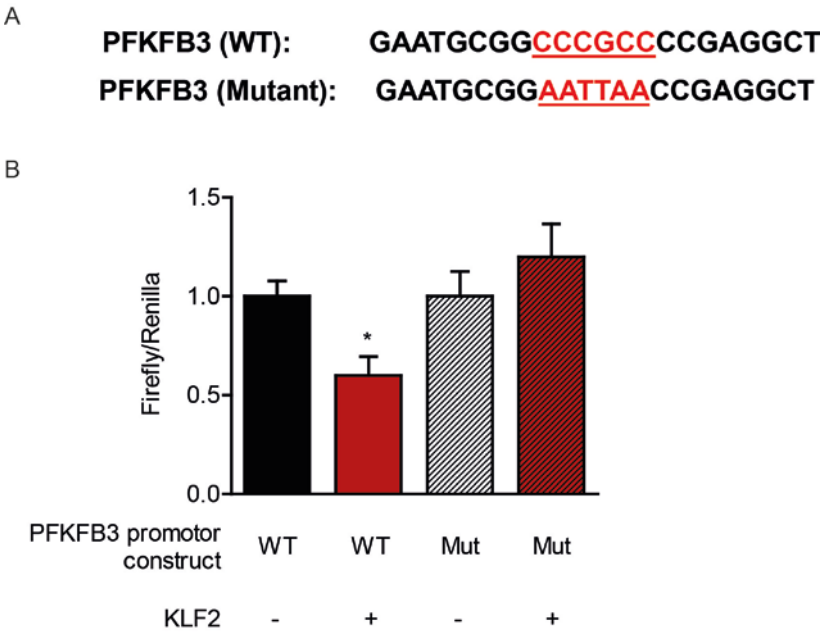

Figure IV.32. Luciferase assay confirms direct binding of KLF2 on PFKFB3 thus leading to its repression

(A) Partial sequence of PFKFB3 promoter constructs of wild type (WT) Sp1/KLF binding site and mutated (mut) binding site (highlighted in red) cloned into firefly luciferase reporter plasmids. (B) HUVECs transduced with mock or KLF2 overexpressing lentivirus were transfected with renilla firefly plamid (control) and firefly luciferase plasmid with PFKFB3 promoter region bearing wild type (WT) KLF2 binding site or mutated (mut) version of KLF2 binding site and 24 hours post transfection luciferase promoter activity was assessed (n=6). Data are represented as a ratio of firefly luciferase and Renilla (control) activity and as mean ± S.E.M; *p<0.05.

4.9.3 Lentiviral overexpression of PFKFB3 in ECs

Thus far, we could show that KLF2 inhibits glycolysis via repression of PFKFB3 promotor expression. We next investigated whether gain of function of PFKFB3 could overcome the inhibitory effect of KLF2 on glycolytic metabolism and glycolysis driven angiogenesis in general. To study this, we cloned a PFKFB3 overexpressing construct that was used for

lentiviral overexpression of PFKFB3 in HUVECs. We achieved a stable overexpression of PFKFB3 up to 6-8 fold compared to mock controls which was consistent and stable even at 2 weeks post transduction. We devised an experimental setup of HUVECs transduced with mock control, KLF2 only, PFKFB3 only and both PFKFB3 and KLF2 virus overexpression simultaneously. We confirmed overexpression of KLF2 and PFKFB3 on mRNA levels after 7 days of transduction in culture, by real time qPCR analysis. As seen in Fig IV.33, KLF2 overexpression induced KLF2 mRNA to 12-15 fold and in this condition PFKFB3 expression was repressed by 50%. On PFKFB3 overexpression, an induction of 6-8 fold of PFKFB3 mRNA was observed, KLF2 levels were unaffected. In cultures overexpressing both KLF2 and PFKFB3, 12-15 fold of KLF2 induction was seen as earlier and PFKFB3 mRNA was upregulated by 4-5 fold (Fig IV.33).

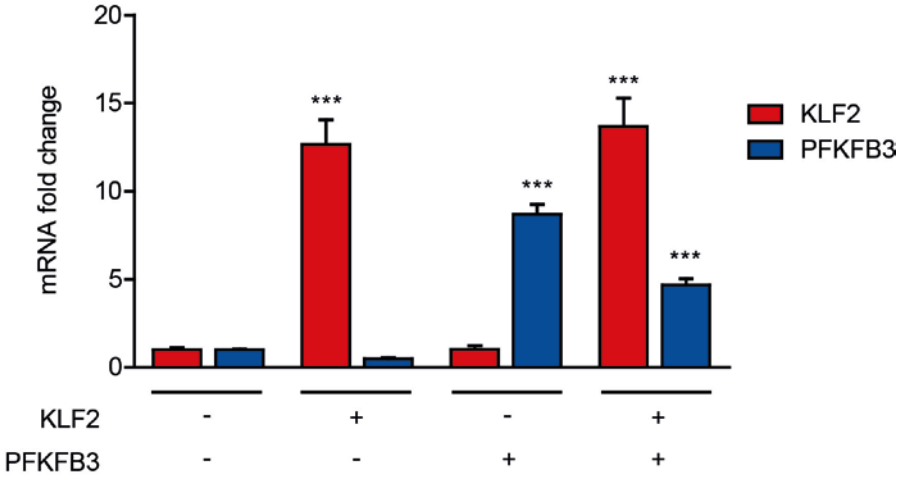

Figure IV.33. Lentiviral Overexpression of PFKFB3 and KLF2

HUVECs were transduced with lentivirus to overexpress KLF2, PFKFB3 or both KLF2 and PFKFB3 simultaneously. Total cell mRNA was isolated and analyzed for expression of KLF2 and PFKFB3 by real time qPCR, normalized to RPLP0 mRNA and expressed as fold change versus mock controls (n=6). Data are represented as mean ± S.E.M; ***p<0.001.

4.9.4 PFKFB3 partially rescues KLF2-mediated inhibition of glycolysis

PFKFB3 overexpression in ECs has been shown to increase glycolytic flux and in turn sprouting of ECs *in vitro*[111]. After establishing simultaneous overexpression of KLF2 and PFKFB3 in the same culture, we performed seahorse flux analyses to determine whether PFKFB3 can rescue KLF2 inhibition of glycolysis. ECAR analysis indeed showed an increase in glycolytic function parameters (Fig IV.34A). Quantification revealed that basal ECAR levels were slightly higher upon PFKFB3 overexpression alone. The reduction seen in basal

ECAR by KLF2 could not be compensated by overexpression of PFKFB3 (Fig IV.34B). Glycolysis was significantly upregulated by PFKFB3 overexpression alone, and KLF2 mediated repression was partially rescued by PFKFB3 when overexpressed along with KLF2 (Fig IV.34C) suggesting that KLF2 indeed reduces glycolysis by repression of PFKFB3. Similar trend was seen with respect to glycolytic capacity (Fig IV.34D); however the results were not significant. Glycolytic reserve remained unchanged by PFKFB3 which was similar to that seen in earlier experiments with KLF2 overexpression (Fig IV.34E).

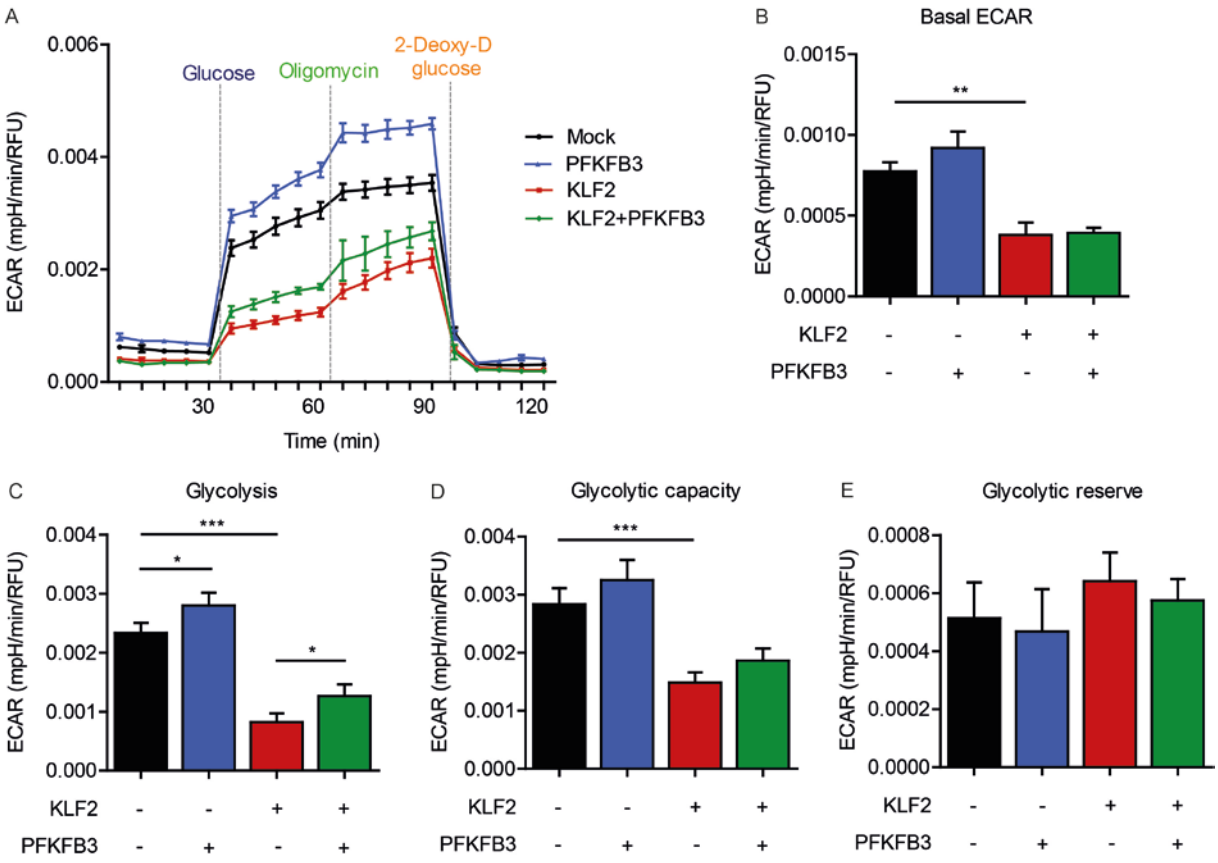

Figure IV.34. PFKFB3 overexpression partially rescues inhibitory effect of KLF2 on glycolysis

(A) Representative ECAR glycolytic function profile in HUVECs transduced with KLF2, PFKFB3 or both KLF2 and PFKFB3 overexpressing lentivirus, analyzed by seahorse flux analysis where vertical lines indicate the time of addition of Glucose (10mM), Oligomycin (3µM) and 2-Deoxy-D glucose (100mM). Quantification of glycolytic function parameters (B) basal ECAR (C) glycolysis (D) maximum glycolytic capacity and (E) glycolytic reserve from ECAR profile shown in (A) compared to mock control and normalized to DNA content determined by DAPI staining (n=7). Data are represented as mean ± S.E.M; *p<0.05, **p<0.01, ***p<0.001.

4.9.5 PFKFB3 rescues anti-angiogenic effect of KLF2

KLF2 has been described to exert an anti-angiogenic effect on the endothelium[91,97]. PFKFB3 expression and localization is important for motility and proliferation of migrating cells thus

proving crucial in glycolytic dependent angiogenesis[111]. In order to understand the functional role of PFKFB3 in combination with KLF2 overexpression, we studied angiogenesis by two different *in vitro* models. The assays described below were performed with cells that overexpressed mock, KLF2, PFKFB3 or both KLF2 and PFKFB3 simultaneously. We first tested both assays with cells that had been overexpressing KLF2 for seven days, but did not observe any initiation of angiogenesis since KLF2 thoroughly inhibits angiogenesis in these conditions (7 days post transduction) in HUVECs (data not shown). Since KLF2 overexpression (mRNA) has been previously shown to be induced strongly even at 24hours after transduction[147], we started the below described angiogenic assays with HUVECs transduced with mock, KLF2 or/and PFKFB3 at 24hrs post transduction.

We used a spheroid sprouting assay, which is a well-established 3 dimensional (3D) model of angiogenesis that mimics the behavior of endothelial cells during sprouting angiogenesis. Briefly, HUVECs 24 hours post transduction, were first allowed to form aggregates (spheroids) and further embedded in an extracellular matrix to form endothelial cell sprouts. After 24 hours, endothelial sprouting was analyzed by microscopy and cumulative sprout length was calculated. Representative photomicrographs of spheroids are shown in Fig IV.35A. Cells overexpressing KLF2 indeed showed minimal sprouting which was significantly lower compared to mock controls. PFKFB3 overexpression alone increased sprout formation in ECs and its simultaneous overexpression with KLF2 could significantly increase sprout length, thus partially rescuing the inhibitory effect of KLF2 on EC sprouting (Fig IV.35B).

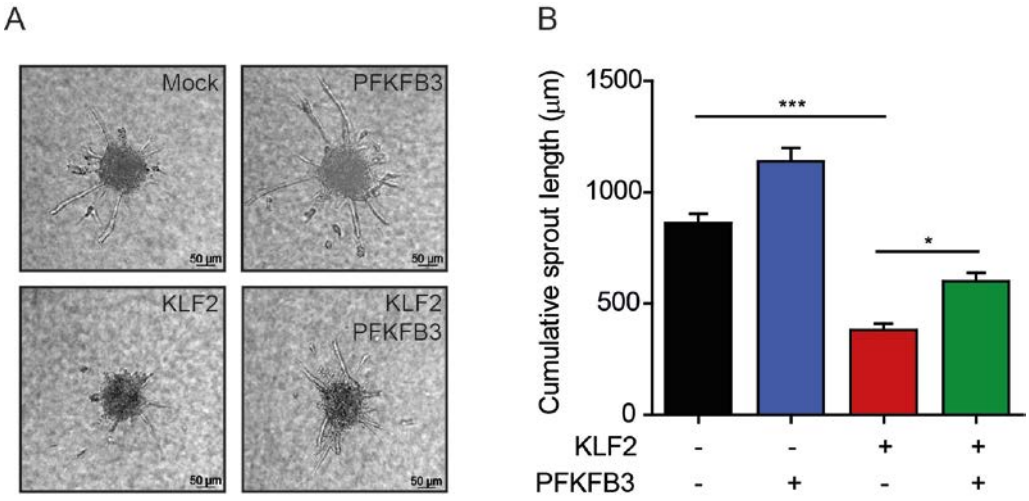

Figure IV.35. PFKFB3 rescues anti-angiogenic phenotype of KLF2 in spheroid formation assay

HUVECs transduced with mock, KLF2, PFKFB3 or both KLF2 and PFKFB3 lentivirus for 24 hours were allowed to form spheroids in a 3D matrix over 24 hours. (A) Representative images of spheroids from mock, KLF2, PFKFB3 or both KLF2 and PFKFB3 overexpressing conditions. Scale bar: 50µm. (B) 10 sprouts were imaged and analyzed per condition and cumulative sprout length was quantified (n=3). Data are represented as mean ± S.E.M; *p<0.05, ***p<0.001.

In a second model for functional analysis of PFKFB3 in an angiogenic context, we used a 2 dimensional (2D) tube formation assay. 24 hours after transduction, HUVECs were seeded on a matrigel basement membrane matrix and allowed to form endothelial tubes. After 24 hours, tube formation was analyzed by microscopy and cumulative tube length was calculated. Similar to results obtained from spheroid sprouting assay, KLF2 overexpression in ECs inhibited tube formation significantly (Fig IV.36). Overexpression of PFKFB3 only slightly increased tube length. However when PFKFB3 was overexpressed along with KLF2, it could indeed induce better tube formation in ECs thus confirming PFKFB3 can reverse the anti-angiogenic effect of KLF2. In summary, repression of PFKFB3 by KLF2 was overcome by PFKFB3 overexpression in *in vitro* functional angiogenic models.

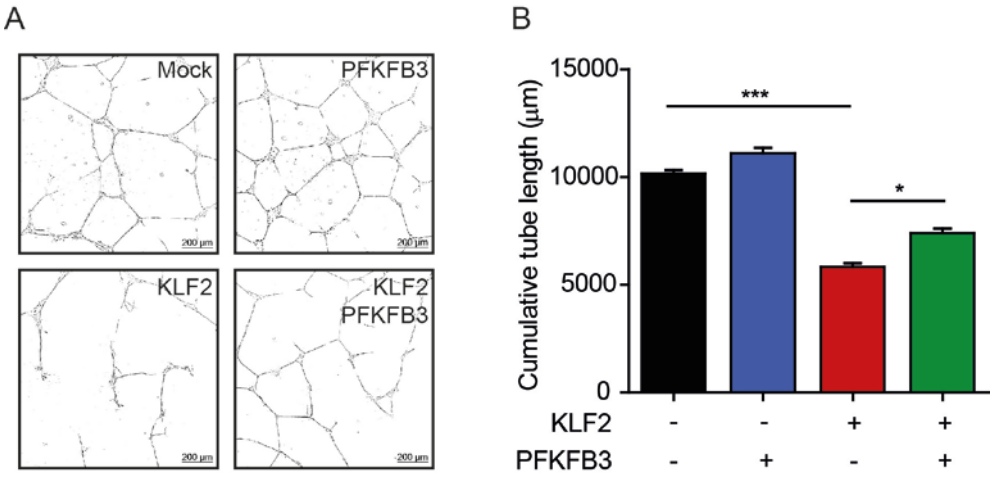

Figure IV.36. PFKFB3 rescues anti-angiogenic phenotype of KLF2 in tube formation assay

HUVECs transduced with mock, KLF2, PFKFB3 or both KLF2 and PFKFB3 lentivirus for 24 hours were allowed to form endothelial tube network in a 2D matrix over 24 hours. (A) Representative images of tube formation from mock, KLF2, PFKFB3 or both KLF2 and PFKFB3 overexpressing conditions. Scale bar: 200µm. (B) 5 random microscopic fields were imaged and analyzed per condition and cumulative tube length was quantified (n=4). Data are represented as mean ± S.E.M; *p<0.05, ***p<0.001.

4.10 Loss of KLF2 in mouse ECs leads to induction of angiogenesis which is abrogated upon PFKFB3 inhibition

To confirm the involvement of PFKFB3 dependent glycolysis as well as the role of KLF2 in *in vivo* angiogenesis, we used the aortic ring outgrowth model to analyze endothelial

sprouting angiogenesis in mice. Inducible endothelial specific KLF2 knockout mice were administered with tamoxifen for 7 days over a 2 week period as previously described (Fig IV.7A) to delete KLF2 in endothelial cells. Briefly, aorta from wild type and knockout mice were harvested, adventitial tissue removed and short segments of aorta were embedded in collagen and further cultured in DMEM medium for 7 days. A pharmacological inhibitor of PFKFB3, 3-PO was added at 50µM during culture. The tissue was stained with Isolectin B4 to visualize endothelial sprouts and analyzed by microscopy and cumulative sprout length was calculated.

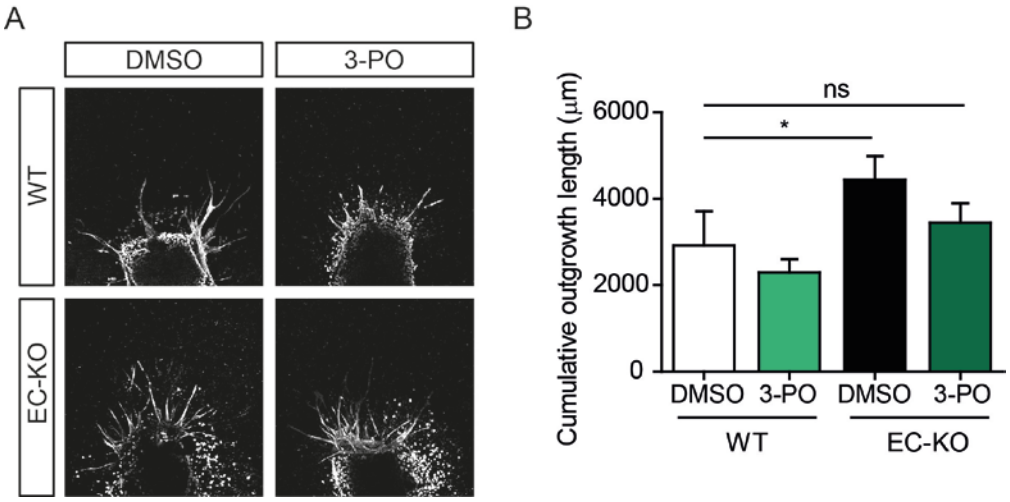

Figure IV.37. Loss of KLF2 in ECs of mice leads to increased sprouting which is abrogated upon inhibition of PFKFB3

Endothelial sprouts from aorta of WT (KLF2 $^{fl/fl}$) and EC-KO (Cdh5-CreERT2;KLF2$^{fl/fl}$) mice were treated with or without 50µM 3-PO and allowed to develop in collagen matrix over 7 days and stained with Isolectin B4. (A) Representative images of endothelial sprouts formation are shown (B) Cumulative outgrowth length was quantified from 3 aortic rings per condition. (n=6). Data are represented as mean ± S.E.M; *p<0.05. DMSO: dimethylsulfoxide, 3-PO: 3-(3-pyridinyl)-1-(4-pyridinyl)-2-propen-1-one.

Representative photomicrographs of sprouts from embedded aorta rings are shown in Fig IV.37A. Loss of KLF2 in endothelial cells in mice significantly increased sprout formation under basal conditions (DMSO). Inhibition of PFKFB3 by 3-PO reduced sprouting in wild type tissue and additionally inhibited the increase in sprouting in EC-KO tissue (Fig IV.37B). Taken together, these data suggest that KLF2 is indeed anti-angiogenic *in vivo* and the increase in sprouting seen upon loss of KLF2 is partially PFKFB3 dependent.

4.11 KLF2 mediated inhibition of glycolytic metabolism in ECs leads to attenuated inflammatory response

KLF2 has been previously described to function as an anti-inflammatory factor[51]. We investigated whether glycolysis inhibition in ECs by KLF2 contributed to its anti-inflammatory properties. To this end, mock and KLF2 overexpressing HUVECs were stimulated with 10ng/ml TNF-α for 24hr or 48hr and glucose uptake was measured. TNF-α stimulation increased glucose uptake in mock transduced HUVECs after 24hr and 48hr treatment, while KLF2 inhibited the inflammation mediated increase in glucose uptake (Fig IV.38A). Seahorse flux analysis revealed that TNF-α treatment significantly increased glycolysis in mock HUVECs at 24 hr treatment, and KLF2 repressed this inflammation induced increase in glycolysis (Fig IV.38B).

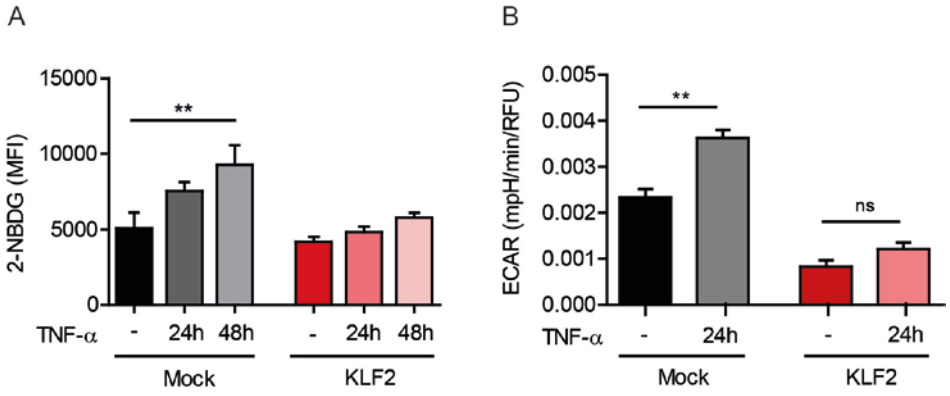

Figure IV.38. KLF2 inhibits inflammation induced glucose uptake and glycolysis

(A) Mock and KLF2 transduced HUVECs were treated with 10ng/ml TNF-α for 24hr or 48hr and glucose uptake was analyzed by flow cytometry after incubation with 100μM fluorescent 2-NBDG for 60min (n=6) (B) Mock and KLF2 transduced HUVECs were treated with 10ng/ml TNF-α for 24hr and analyzed by seahorse flux analyzer for glycolysis, values are normalized to DNA content determined by DAPI staining of cells (n≥3). Data are represented as mean ± S.E.M; **p<0.01. MFI: mean fluorescence intensity; RFU: relative fluorescence unit.

To correlate glycolysis and inflammatory responses physiologically, we inhibited glycolysis in HUVECs using glycolysis inhibitor 2-Deoxy-D-glucose (2DG) for 1 hour, in a dose dependent manner (0.5mM, 10mM and 50mM) and subsequently stimulated these cells with 10ng/ml TNF-α for 2hrs. Our results revealed that treatment of HUVECs with TNF-α indeed increased expression of VCAM1, E-selectin and ICAM1 mRNA. However, inhibition of glycolysis by 2DG and subsequent stimulation with TNF-α, significantly reduced VCAM-1 and E-selectin levels when compared to TNF-α stimulated condition without 2DG treatment (Fig IV.39), suggesting that ECs having reduced glycolytic metabolism are protected from TNF-α induced inflammatory insult.

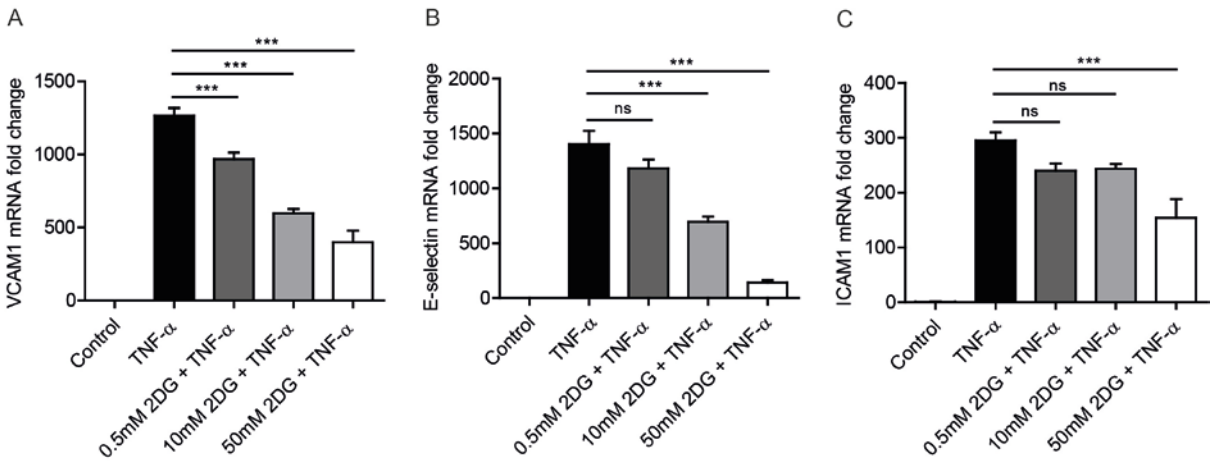

Figure IV.39. Inhibition of glycolysis by 2DG treatment elicits attenuated inflammatory response

HUVECs were incubated for 1hr with varying doses of 2DG (0.5mM, 10mM and 50mM) and further treated with 10ng/ml TNF-α for 2hours. Total mRNA was isolated and expression of (A) VCAM1 (B) E-selectin and (C) ICAM1 was analyzed by real time qPCR. Gene expression was normalized to RPLP0 mRNA and expressed as fold change versus untreated HUVEC controls (n≥7). Data are represented as mean ± S.E.M; ***p<0.001.

Since our previous results showed KLF2 inhibits EC glycolytic metabolism by repression of PFKFB3, we checked whether PFKFB3 was involved in KLF2 mediated anti-inflammatory response that involves reduced glycolysis. Stimulation of mock and KLF2 transduced HUVECs with 10ng/ml TNF-α for 24hr or 48hr increased PFKFB3 mRNA levels in mock controls but strikingly, the repression of PFKFB3 levels by KLF2 under unstimulated conditions was no longer evident under TNF-α stimulation, in that a significant increase in PFKFB3 mRNA levels was observed in KLF2 overexpressing ECs (Fig IV.40A). Using siRNA against PFKFB3 we confirmed that inflammation induced glycolysis was independent of PFKFB3 since knockdown of PFKFB3 did not reduce glycolysis when stimulated with TNF-α (Fig IV.40B). Thus, we could confirm that attenuation of inflammation induced glycolysis by KLF2 was PFKFB3 independent.

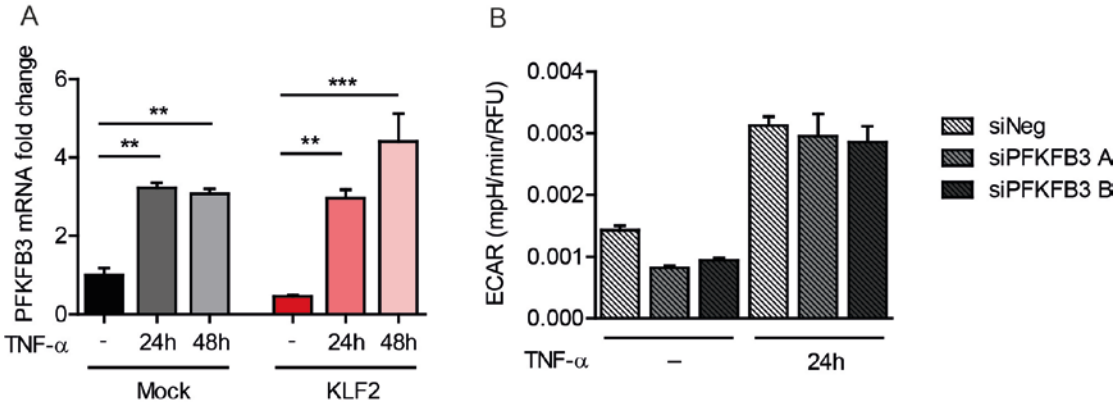

Figure IV.40. Inhibition of inflammation induced glycolysis by KLF2 is PFKFB3 independent

(A) Mock and KLF2 transduced HUVECs were treated with 10ng/ml TNF-α for 24hr or 48hr and mRNA expression of PFKFB3 was quantified by real time qPCR and normalized to GAPDH mRNA, expressed as fold change versus untreated mock controls (n≥4) (B) 24 hours after transfection with siNeg or siPFKFB3 (67nM), HUVECs were treated with 10ng/ml TNF-α for 24hr and analyzed by seahorse flux analysis for glycolysis (48 hours post transfection), values normalized to DNA content that was determined by DAPI staining of cells (n=3). Data are represented as mean ± S.E.M; **p<0.01, ***p<0.001. RFU: relative fluorescence unit.

5. DISCUSSION

5.1. Coupling flow mediated angiogenesis and endothelial metabolism

The vascular endothelium is a highly dynamic structure where endothelial cell sub types (tip, stalk and phalanx) rapidly adapt to the changing environment. Under hypoxic conditions, quiescent ECs migrate and proliferate to form new vessels by angiogenesis thereby vascularizing the tissue. After the new vessels are established, the endothelium returns to a quiescent state to maintain homeostasis. Recent studies have highlighted the role of metabolism in ECs that is crucial during this angiogenic and quiescent state switching. Laminar shear stress via flow-dependent transcription factor KLF2 confers an atheroprotective effect on the endothelium by inducing cellular quiescence. The main aim of this thesis was to investigate whether laminar shear stress and KLF2 play a role in regulating metabolism of ECs, and if this contributes to their pro-quiescence effects. Mechanistically, we determined how ECs rewire their metabolic state upon flow exposure to subsequently change from an angiogenic to quiescent state. This study adds a new dimension to the relationship between hemodynamics and cellular quiescence involving metabolic regulation of ECs, in the field of vascular biology.

Our initial data demonstrated that exposure of HUVECs to prolonged laminar flow alters morphology of ECs, where cells aligned in the direction of flow and appeared elongated. Shear stress exposure leads to reorganization of F-actin cytoskeleton[160], redistribution of FAKs[161], formation of short stress fibers mediated by KLF2-JNK pathway[147], all of which contribute to the change in morphology. Cytoskeleton remodeling is also reported to work as an adaptive mechanism since it allows for transmission of shear stress force to ECs[162]. Our data showed a significant increase in mRNA and protein levels of flow-induced transcription factor KLF2 after long term LSS exposure, which is in agreement with previous *in vitro* and *in vivo* studies[62,80,103]. Upon knockdown of KLF2 and subsequent flow exposure, EC alignment was abolished and shear stress induced upregulation of KLF2 was abrogated. *In situ* experiments in porcine aorta show that failure of ECs to align in direction of blood flow is evident in regions experiencing disturbed flow and hence serves as an indication for regions prone to atherosclerosis[163]. In addition to shear stimulated HUVECs, we also used HUVECs

overexpressing KLF2 (to levels similar to that seen on shear stimulation) to study metabolic functions in ECs.

5.1.1 Role of laminar flow and KLF2 in endothelial glycolytic metabolism

ECs derive a majority of their energy to fuel proliferation and migration during angiogenesis via glycolytic metabolism, instead of relying on mitochondrial respiration, pentose phosphate pathway (PPP), amino acid metabolism or fatty acid oxidation. In spite of having immediate access to oxygen from blood stream, ECs metabolize glucose to lactate (anaerobic glycolysis), instead of glucose oxidation in the mitochondria. Since glycolysis is the main energy generating pathway to maintain cellular functions in ECs[112], we first determined the effect of laminar flow and KLF2, on glycolytic EC metabolism. Our data revealed that exposure of ECs to shear stress reduced glucose uptake in HUVECs. The results are consistent with a previous study, where shear stress (20 dyn/cm^2) exposure to brain ECs reduced glucose consumption in a time dependent manner, maximum reduction seen at 72 hours post exposure[164]. In our data, the reduction in glucose uptake by shear stress was dependent on KLF2. Indeed, overexpression of KLF2 reduced glucose uptake. In addition to reducing glucose uptake in ECs, KLF2 overexpression led to improved glucose transport through the ECs to the underlying layer, which led us to speculate that shear mediated reduction in glucose consumption in ECs leads to better bioavailability of glucose for adjacent tissue. In order to investigate effect of KLF2 on glucose uptake *in vivo*, we used inducible endothelial-specific KLF2 knockout mice and wild type controls. Knockdown of KLF2 in ECs was confirmed in intimal ECs (data not shown) and in the heart. Our results showed increased glucose uptake in cardiac ECs lacking KLF2. This data is in concurrence with our *in vitro* finding that KLF2 overexpression reduces glucose uptake in HUVECs.

As glucose consumption in ECs was reduced by shear stress and KLF2, we probed further to determine glycolysis rates in these cells. Technically, Seahorse flux analysis on shear stimulated cells using our experimental pump setup could not be performed due to cell number limitation and hence only glucose uptake was analyzed in shear stimulation conditions. Shear stress has been described to reduce lactate dehydrogenase (LDH) activity, an indicator of lactate production after 72 hours exposure of shear stress in brain ECs, in a time dependent manner[164]. On the contrary, Suarez and colleagues showed that coronary flow (20ml/min and 25ml/min) acting via EC glycocalyx induced glycolytic flux in Langendorff

perfused guinea pig hearts[165]. The increased flux could be due to the initial short term flow exposure (120 min) as opposed to our long term shear stress exposure conditions. In our present work, KLF2 overexpression in ECs reduced 1) EC basal acidification rate 2) glycolysis occurring after glucose supplementation at saturating levels and 3) maximum glycolytic capacity of ECs. Since the spare respiratory capacity of cells overexpressing KLF2 remained unchanged, we conclude that although KLF2 inhibits glycolysis, the cells have the same ability to respond to an energy demand as mock controls. Our data fits well with the understanding of quiescent EC metabolism where quiescent ECs have about 40% reduction in glycolysis compared to dividing cells[111]. ECs are thought to use the rest 60% energy derived from glycolysis for maintaining homeostasis, barrier functions, trans-endothelial transport, glycocalyx deposition and matrix production[8,166].

5.1.2 Role of laminar flow and KLF2 in EC mitochondrial respiration

To determine whether shear stress and KLF2 lead to a switch from glycolytic to oxidative metabolism, to compensate for the reduced glycolysis, we performed assays to study mitochondrial respiration in these ECs. Mitochondria poorly contribute to ATP production in proliferating ECs[116]; however they function as signaling molecules modulating oxidative stress, heme synthesis, calcium signaling and apoptosis[167]. Our data reveal that morphology and localization of mitochondria were not affected by KLF2, however mitochondrial DNA content and activity was reduced by shear stress and KLF2. Since PGC1α plays an important role in inducing mitochondrial biogenesis[167], we speculated whether it could be a potential molecule in regulating shear stress and KLF2 mediated decrease in mitochondrial content. However, we did not see a regulation of PGC1α on mRNA level by KLF2 or shear stress (data not shown), although Chen et al. report that laminar shear stress (12 dyn/cm^2) induces PGC1α mRNA levels and in turn mitochondrial biogenesis in ECs[168]. Induction of PGC1α was mediated through activation of SIRT1 and AMPK pathway. Interestingly, activity of SIRT1 is dependent on NAD^+ levels in the environment and stimulation of HUVECs with shear stress was reported to increase cellular NAD^+ levels. In our study, we did not measure cellular NAD^+ levels in shear exposed ECs, nonetheless, KLF2 did not alter cellular NAD^+ levels. Furthermore, shear stress and KLF2 reduced total ATP production in ECs. This is concurrent with the observation that proliferation requires about 30% increase in ATP production in comparison to quiescent levels[169] and both shear stress and KLF2 are quiescence inducing factors. The shear stress mediated effect on mitochondrial content, activity and ATP production were independent of KLF2.

Proper mitochondrial function is essential to maintain mitochondrial homeostasis and protect against cardiovascular diseases. Mitochondrial membrane potential ($\Delta\Psi_m$) is an indicator of the mitochondrial function, its energy state and consequently cell viability. During myocardial reperfusion injury, $\Delta\Psi_m$ in myocytes is reduced leading to apoptosis or necrosis in worse conditions[170]. In the present work, we show that although shear stress and KLF2 reduce mitochondrial DNA content and activity, it does not compromise mitochondrial function since our data demonstrate $\Delta\Psi_m$ to be slightly induced upon shear stress stimulation and KLF2 overexpression. Our finding is in line with the data from Li et al., where shear stress dynamically increased $\Delta\Psi_m$ in human arterial ECs, in a MnSOD dependent manner and the effect diminished 4 hours after shear stress exposure was ceased. Overall, by inducing $\Delta\Psi_m$, LSS adds another mechanism to the array of its protective function exerted on ECs. Mitochondrial membrane depolarization or hyperpolarization (drop in $\Delta\Psi_m$) leads to excessive ROS production and cell damage[167], which is prevented by KLF2 and shear stress by maintaining a relatively high $\Delta\Psi_m$. The shear stress induced increase in $\Delta\Psi_m$ was KLF2 independent. Most of the mitochondrial assays show KLF2 independent effects of shear stress. It could be that other shear-induced pathways such as that mediated by Nrf2 plays a role in shear mediated regulation of mitochondrial metabolism. KLF2 and shear stress both have been described to reduce oxidative stress in ECs through the Nrf2 pathway[68]. However, further work needs to be performed to understand the precise role of shear stress and its mechanism of action in regulating EC respiratory metabolism.

Our data reveal that KLF2 reduces basal respiration and mitochondrial ATP production in ECs. This diminished production of ATP from mitochondria measured by seahorse flux analysis concurs with our earlier data that KLF2 reduces overall cellular ATP production. Of note, maximal respiration and spare respiratory capacities of ECs were not affected by KLF2 suggesting that the cells can push their respiration maximum to the same extent as mock controls in energy demanding conditions. Reduced mitochondrial respiration in KLF2 overexpressing ECs is explained by lower mitochondrial DNA content and activity in these cells. Although, quiescent ECs are directly exposed to blood flow and hence high oxygen levels, they exhibit low oxidative metabolism. This is particularly beneficial in reducing ROS production and protect against oxidative damage. In addition, lower oxygen consumption by ECs allows for better transport of oxygen to underlying tissue[24]. The reduction in mitochondrial respiration of ECs by KLF2 may not play a significant role in angiogenesis, since results from De Bock et al. show that blocking mitochondrial respiration with

oligomycin or antimycin A, does not affect vessel sprouting in ECs[111]. Taken together, reduction in glycolytic metabolism by KLF2 probably has a larger impact on overall reduced metabolic activity of ECs and therefore we focused on elucidating the mechanism of glycolytic inhibition by KLF2.

5.1.3 KLF2 protects ECs from apoptosis and senescence

Our data show that KLF2 inhibits apoptosis, despite reducing metabolic activity of ECs. However, no direct link between inhibition of glycolysis acting as a causative factor for reduced apoptosis could be drawn from our study. Moreover, the increase in mitochondrial membrane potential by KLF2, may partially contribute to the anti-apoptotic phenotype via the classical mitochondrial apoptotic pathway[115]. Previous studies show that LSS reduces proliferation by inhibiting cell cycle related genes at early time point of flow exposure[48,49], whereas disturbed or turbulent flow to increases EC turnover[171,172]. Furthermore, KLF2 has been described to reduce cell proliferation[173]. Our data revealed that KLF2 slightly delayed EC proliferation by arresting cells in S phase and reducing total number of ECs in the mitotic population. The data are in agreement with previous work where reduced glucose consumption led to reduction in proliferative capacity of cells[174]. Our results revealed that KLF2 protected ECs from senescence confirmed by acidic beta galactosidase staining and expression levels of p21 senescence marker. Unterluggauer et al. report that senescence leads to decrease in cellular ATP production in HUVECs[133], but although KLF2 overexpression reduced ATP levels in ECs, it did not induce senescence and we thus excluded that KLF2 mediated metabolic down regulation is caused by senescence. Collectively, we could show that KLF2 did not drive ECs into apoptosis or senescence.

5.1.4 KLF2 effects are independent of AMPKα1

To decipher the mechanism by which KLF2 inhibits metabolism in ECs, a phospho kinase array was performed to screen for candidates that were modified at a post-translational level by KLF2. Among significantly regulated phospho proteins was AMPKα1, whose phosphorylation levels was reduced by KLF2. AMPK functions as a metabolic master switch that helps cells to sense and adapt their energy status to the changing environment. Previous studies have highlighted the link between metabolic stress and vascular function where they demonstrate AMPK to be induced by laminar flow, which subsequently phosphorylates to activate eNOS and increases NO availability[175–177]. Both AMPKα1 and AMPKα2 subunits play similar important roles in EC function. Young et al. demonstrate that activation of

AMPK is required for expression of KLF2 in mouse vasculature and that AMPK functions as an upstream kinase of ERK5 in the shear induced ERK5/MEF2 pathway that leads to KLF2 induction[154]. In our study, we investigated the downstream effect of KLF2 on AMPK and our data demonstrated that overexpression of KLF2 reduced AMPKα1 phosphorylation (Thr 174), which was confirmed by ELISA. However, KLF2 did not significantly alter mRNA or protein levels of AMPKα1. It appears that inactivation of AMPKα1 by KLF2 works as a feedback loop in the flow induced ERK5/MEF2C/KLF2 mechanotransduction cascade. We questioned whether KLF2 regulates glycolysis through AMPKα1 function. Knockdown of AMPKα1 in HUVECs did not recapitulate the reduction in glycolytic metabolism as seen under KLF2 overexpression conditions and hence we inferred that KLF2 mediated glycolysis repression is likely independent of AMPKα1 in ECs. Interestingly, Nagata et al. show that hypoxia activates AMPK by phosphorylation and that AMPK is essential for EC migration and angiogenesis in response to VEGF and under hypoxic conditions, but not under normoxia[178]. Indeed, our *in vitro* data partly supports their findings, wherein under normoxic conditions, AMPKα1 does not seem to be involved in glycolysis mediated angiogenesis.

5.1.5 Involvement of nitric oxide and hypoxic signaling in KLF2 mediated inhibition of endothelial metabolism

KLF2 has been shown to induce eNOS expression and subsequent release of NO in ECs. Previous reports have revealed NO to be a competitive inhibitor of cytochrome oxidase, the terminal enzyme of mitochondrial respiratory chain, thus inhibiting oxygen consumption in isolated nerve terminals from rat brain[156]. Additionally, Bereta and colleagues described NO to inhibit glycolysis in ECs by reducing GAPDH activity upon cytokine stimulation, which is compensatory to increased GAPDH mRNA expression and stability[157]. We questioned whether the increased NO release by KLF2 leads to inhibition of glycolysis and mitochondrial respiration in our study. Inhibition of NO by L-NAME, did not lead to an increase in either respiration or glycolysis, suggesting that KLF2 mediated metabolic reduction is NO independent.

Upregulation of glycolysis to produce energy for tumor growth in response to low oxygen is a trademark characteristic in cancer cells. Hypoxia induces glycolysis in human glioblastoma cells by promoting binding of HIF1α to the promotor of PFKFB3[158]. VEGF stimulation has been shown to increase PFKFB3 levels and glycolysis in tip endothelial cells[111]. Interestingly, KLF2 inhibits HIF1α expression, limits accumulation of HIF1α protein and subsequent

hypoxia mediated angiogenesis[98]. In addition, KLF2 reduces secretion of VEGF under hypoxia and inhibits expression of VEGFR2 by binding to its promoter[97]. Thus, KLF2 inhibits both hypoxia and VEGF signaling, which we speculated to be potential mechanisms by which KLF2 reduces glycolysis. To address involvement of these pathways, we stimulated KLF2 overexpressing ECs with VEGF or hypoxia mimicking agent (DFO), but did not observe an increase in glycolysis levels. Therefore, we concluded that KLF2 mediated glycolysis inhibition is independent of hypoxia and VEGF signaling.

5.1.6 Inhibition of key glycolytic genes by shear stress and KLF2

From our RNA sequencing data of shear stimulated versus static controls, it was evident that multiple genes in the glycolytic pathway were regulated by shear stress. Genes regulated significantly were GLUT3, LDHA and LDHC (upregulated) and aldolase A, HK2, PFK1, PFKFB3 and pyruvate kinase, liver and RBC isoform (down regulated). We focused particularly on HK2, PFK1 and PFKFB3 since HK2 and PFK1 catalyze rate limiting steps in glycolytic pathway and PFKFB3 is an allosteric activator of the product of PFK1 reaction. Hexokinases convert glucose to glucose-6-phosphate (G6P) and HK2 is described to be highly induced during tumorigenesis and a variety of stimuli such as HIF1α, AKT signaling, ATP/ADP levels have been implicated in regulating HK2 expression[179]. KLF2 is known to inhibit HIF1α, which induces HK2 and could be one of the mechanisms through which KLF2 reduces HK2 expression. PFK is the second vital flux determining enzyme in the pathway that catalyzes the conversion of fructose 6 phosphate to fructose 1, 6 bisphosphate. It is induced in response to hypoxia and oncogene activation, and in highly glycolytic proliferative cells [180,181]. In contrast to our data, Desai et al. report that shear stress (20 dyn/cm^2) exposure of 3 or 7 days in brain arterial endothelial cells does not change expression levels of hexokinase or PFK. An increase in GAPDH and PDH expression and decrease in LDHA levels was observed in their results, but no physiological relevance was stated[174]. PFKFB catalyzes the rate limiting step of glycolysis and PFKFB3 isoform has a higher kinase activity than other isoforms and thus allows for more efficient accumulation of F2,6 BP. Collectively, PFK1 and PFKFB3 are the most potent stimulators of glycolysis. We confirmed the sequencing data using qPCR analysis, where shear stress indeed inhibited gene expression of HK2, PFK1 and PFKFB3. Notably, KLF2 overexpression in ECs reduced HK2, PFK1 and PFKFB3 mRNA and protein levels. Shear stress mediated reduction in glycolytic gene expression was KLF2 dependent.

Loss of function experiments with the three glycolytic genes in HUVECs was performed to check whether silencing of the genes would lead to glycolysis reduction, similar to levels that was observed under KLF2 overexpression. HK2 and PFK1 knockdown in ECs did not recapitulate the reduction in glycolysis, whereas loss of PFKFB3 in ECs showed a glycolytic phenotype similar to KLF2 overexpression. A reduction of 60% in glycolysis was seen upon siRNA knockdown of PFKFB3, an inhibition effect similar to that seen by KLF2 overexpression (80% reduction). Our results conform to published data from De Bock et al., where siRNA and shRNA against PFKFB3 in HUVECs reduced glycolysis, although by a moderate 35-40%. Additionally, glycolysis inhibition due to PFKFB3 silencing was described in other EC types such as human arterial and microvascular ECs and murine angiosarcoma and hemangioma cells[111]. PFKFB3 loss has also been shown to reduce glycolysis in tumor cells [182,183].

5.1.7 KLF2 represses PFKFB3 transcriptionally to inhibit glycolysis and angiogenesis

Since our data showed reduction of PFKFB3 mRNA and protein levels by KLF2, we set out to investigate the mechanism by which KLF2 regulates PFKFB3 in ECs. KLF2 has been reported to activate or repress transcription of many genes by actively binding to Sp1/KLF sites in gene promotors. Transcription activation of eNOS and TM genes by KLF2 is well documented[51,90]. Hara et al. describe KLF2 to transcriptionally repress hTERT expression in human T cells[184]. Another study by Sebzda et al. reveals that KLF2 transcriptionally represses chemokine receptors CCR3 and CCR5 in T cells, receptors that are crucial for naive T cell migration[185]. KLF2 negatively regulates WEE1, a gene implicated in DNA damage induced apoptosis in ovarian cancer cells[186]. We performed *in silico* promotor analysis and identified evolutionary conserved transcription factor binding sites of Sp1/KLF on PFKFB3 promotor. Through a luciferase assay, with wild type and mutated binding sites, we confirmed repression of PFKFB3 expression by KLF2. Direct binding of KLF2 on PFKFB3 promotor could be assessed by performing a chromatin immunoprecipitation (ChIP) assay.

In order to rescue the glycolysis inhibited KLF2 phenotype *in vitro*, using a gain of function approach, we tested the hypothesis that overexpression of PFKFB3 could reverse KLF2 mediated inhibition of glycolysis. To this end, we established stable overexpression (6-8 fold) of PFKFB3 by lentivirus transduction in ECs. PFKFB3 mRNA levels were reduced to 4-5 fold when overexpressed along with KLF2 in the same condition, which suggests that KLF2

inhibits PFKFB3 expression by additional mechanisms than just transcriptional repression. Indeed, overexpression of PFKFB3 in ECs alone was capable of increasing glycolysis in ECs, which is in agreement with previous studies that highlight PFKFB3 overexpression to induce glycolytic flux in ECs, in addition to promoting a more tip like phenotype (high glycolysis) by overruling Notch signals that induce a stalk phenotype[111]. Upon overexpression of KLF2 and PFKFB3 simultaneously, a significant increase in glycolysis was observed indicating that PFKFB3 partially rescues KLF2-mediated inhibition of glycolysis. We next determined the functional role of PFKFB3 overexpression in the KLF2 phenotype by using two angiogenic assays, namely, 2D tube formation and 3D spheroid sprouting assay. Our data showed inhibition of tube formation and sprouting by KLF2. The anti-angiogenic function of KLF2 seen in our data concurs with previous studies which confirm KLF2 to negatively regulate angiogenesis in a HIF1α dependent manner[98] or by inhibition of VEGFR2 expression and activity[97]. KLF2 has also been described to reduce migration capacity of ECs in *in vitro* scratch wound assay via chemorepulsant SEMA3F induction[91]. Notably, PFKFB3 over expression in HUVECs increased endothelial sprouting and tube formation in our results. The data are in agreement with the findings from De Bock and colleagues, where overexpression of PFKFB3 in ECs induced glycolysis and promoted sprouting, whereas loss of PFKFB3 in ECs led to reduced sprout formation *in vitro* and genetic deletion of PFKFB3 led to hypo branching in mice retina and impaired vascular development in zebrafish[111]. Indeed embryonic stem cells lacking PFKFB3 (impaired tip and stalk functions) do not contribute to dorsal aorta formation when implanted in mosaic blastocysts indicating that PFKFB3 driven glycolysis is important for vessel formation during embryogenesis[187]. PFKFB3 blockade by 3-PO led to impaired vascular development in retina of mice[109]. Both these studies indicate that glycolysis driven angiogenesis is important during development stages.

Interestingly, PFKFB3 overexpression only partly rescued the anti-angiogenic effect of KLF2 when both proteins were overexpressed simultaneously. Indeed, KLF2 inhibits various factors to induce an anti-angiogenic effect and inhibition of PFKFB3 mediated glycolysis is just one of them. Therefore, overexpression of PFKFB3 alone did not completely rescue the KLF2 phenotype. siRNA mediated knockdown of PFK1 and HK2 did not have any effect on EC glycolysis and therefore we speculate that neither proteins contribute significantly to the rescue of the KLF2 phenotype. We conclude that PFKFB3 has a greater role to play in EC glycolytic metabolism, however, *in vivo* role of flow mediated PFKFB3 needs to be established. At first hint, KLF2 heterozygous mice show increased capillary density[98], which

is perhaps due to increased glycolysis driven by higher PFKFB3 expression. It would be interesting to study the expression of PFKFB3 in aorta of mice to check if we could correlate increased PFKFB3 expression in atheroprone regions where reduced KLF2 levels are observed due to disturbed flow exposure.

To further investigate the role of KLF2 and PFKFB3 in controlling the endothelial phenotype in mice, we performed *ex vivo* aortic ring assay to assess angiogenesis. Loss of KLF2 in ECs increased sprouting, thus confirming that KLF2 is indeed anti-angiogenic. Remarkably, inhibition of PFKFB3 by 3-PO, a pharmacological inhibitor, reversed the pro-angiogenic phenotype observed in EC-specific KLF2 knockout mice. These results are in agreement with our *in vitro* gain of function data from tube formation and spheroid sprouting assay and emphasize that PFKFB3 via glycolysis induction proves to be a pro-angiogenic factor. By inhibiting PFKFB3-mediated glycolysis, KLF2 represses angiogenesis and consequently leads ECs towards a quiescent state. In retrospect, examining the role of KLF2 in angiogenesis *in vivo* in a hind limb ischemia (HLI) model would be an interesting experiment, where one would expect better recovery after injury in KLF2 EC-KO mice. Also, whether overexpression of PFKFB3 would rescue impaired angiogenesis in vascular disease models needs further investigation.

In a therapeutic context, Schoors et al. demonstrate that pharmacological inhibition of PFKFB3 by 3-PO reduced pathological angiogenesis in ocular and inflammation models[109]. 3-PO effects were non-cytotoxic and reversible owing to its short half-life (30 min). In another study, treatment of adult mice with 3-PO for 15 days, confirmed that PFKFB3 inhibition by 3-PO occurs only in proliferating and migrating ECs during pathological angiogenesis and does not affect ECs in other organs such as heart, kidney or retinal vasculature where established vessels and quiescent ECs are abundant, nor did it affect heart function[187]. 3-PO treatment caused minor systemic changes, however no permanent adverse effects were seen in mice indicating that the blockade of pathological angiogenesis *in vivo* by 3-PO is due to partial and transient inhibition of PFKFB3 driven glycolysis[187]. Since, 3-PO blocks only hyper metabolism of sprouting ECs, it could be used as a potential drug for anti-glycolytic therapy, where a partial (30-40%) and transient decrease in glycolysis is sufficient to block angiogenesis only in rapidly proliferating ECs, tumor cells or activated T cells and not affecting homeostatic functions of quiescent ECs. From our data, KLF2 induces a similar reduction in PFKFB3 driven glycolysis due to which it could work as an attractive target for

anti-angiogenic therapy through its glycolysis inhibition effects. This could be particularly beneficial in combating inflammation during atherosclerosis and other inflammatory disorders, since they are characterized by increased angiogenesis. Blocking EC angiogenesis during tumor growth by inhibiting glycolysis is another possible application, since cancer cells rely on blood vessels for oxygen and nutrient transport.

Conceivably, there are mechanisms, independent of PFKFB3, by which KLF2 reduces glycolytic metabolism since KLF2 inhibits several other proteins involved in glycolysis. One of the mechanisms through which KLF2 regulates multiple pathways is via paracrine effects such as those involving the communication between ECs and SMCs through KLF2-mediated release of atheroprotective microRNAs[141]. In other experiments, KLF2 overexpression in ECs inhibited growth factor activin A secretion into cell supernatants in a PFKFB3 independent manner (data not shown), adding to the knowledge of KLF2 functioning as an anti-proliferative factor. Furthermore, activin A levels in EC specific KLF2 knockout mice plasma was induced, which is in concurrence with the *in vitro* data (unpublished data from Dr. Yosif Manavski, Institute of Cardiovascular Regeneration, Frankfurt). Zhou et al. show that activin-dependent HIF1α signaling is crucial for maintaining a high glycolytic rate to sustain pluripotency of human epiblast stem cells (EpiSCs)[188]. Their findings could hint towards a possible role of activin mediated effect on glycolytic EC metabolism, where KLF2 indirectly inhibits glycolysis through activin A. Another secondary effect of KLF2 on metabolism is perhaps mediated by ROS, which is important for maintaining vascular homeostasis and increased ROS is indeed detrimental to ECs and leads to cardiovascular diseases. Previous studies showed that ROS regulates secretion of growth factors from ECs. Of note, KLF2 and shear stress reduce ROS generation in ECs which could lead to their inhibitory effects on growth factor (activin A) secretion and downstream inhibition of glycolytic metabolism. Whether, the ROS mediated decrease in growth factor secretion causes inhibition of metabolism or vice-versa is not clear. Taken together, these results suggest KLF2 reduces glycolytic metabolism in more ways than repression of PFKFB3 alone, which could explain only partial rescue of KLF2 metabolic phenotype by PFKFB3 overexpression.

To sum up, through this study we have shown laminar shear stress induced transcription factor KLF2 to modulate metabolism of endothelial cells by repressing glycolytic and respiratory metabolism. Mechanistically, laminar flow via KLF2 reduces glycolysis in ECs by repressing the promotor of PFKFB3, an enzyme catalyzing the rate limiting step of glycolysis.

KLF2 also inhibited oxidative metabolism, however the precise mechanism remains to be elucidated. Inhibition of glycolysis by KLF2 led to reduced angiogenesis and promoted an atheroprotective quiescent endothelium.

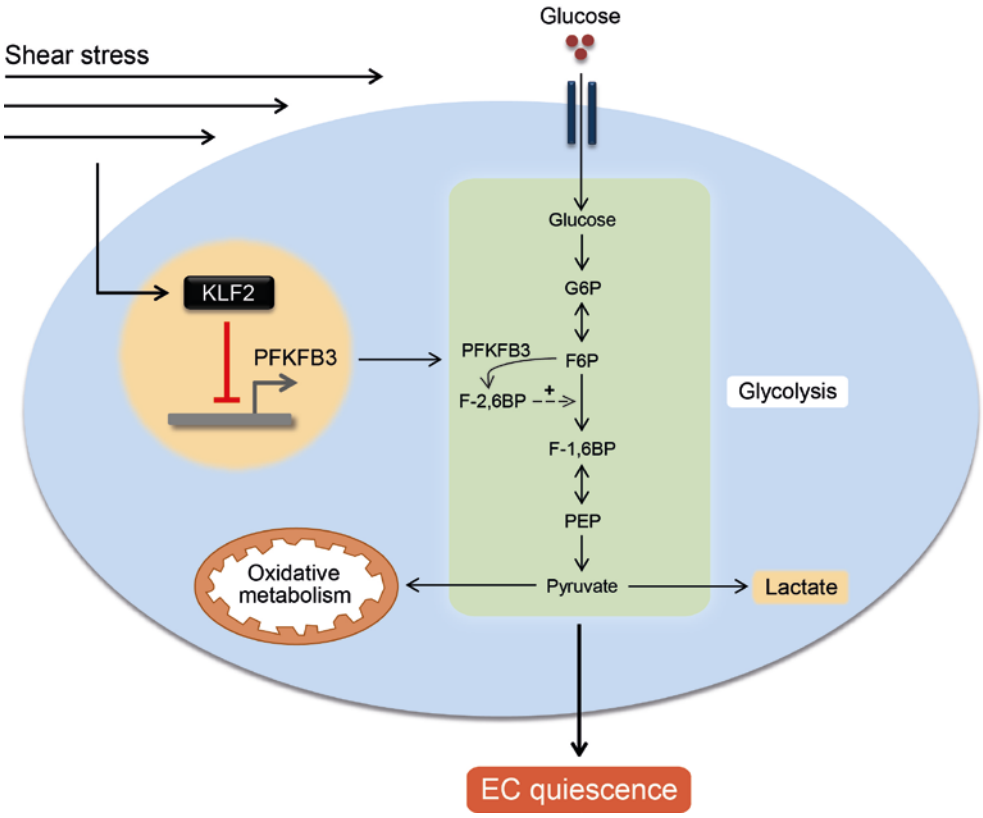

Figure V.1. Schematic representation of the mechanism by which hemodynamic forces regulate endothelial metabolism.

Laminar shear stress acting on endothelial cells induces KLF2 upregulation which leads to reduced glucose consumption and repression of PFKFB3, a determinant of glycolytic flux in ECs. Reduction in glycolytic metabolism through PFKFB3 and attenuation of mitochondrial respiration (oxidative metabolism) by additional mechanisms lead to a quiescent metabolic state of ECs resulting in arrest of angiogenesis.

5.2. Role of glycolysis in eliciting an inflammatory response

KLF2 has been implicated in promoting an anti-inflammatory phenotype to the endothelium by attenuating NFκB pathway and inhibiting pro-inflammatory molecules VCAM1 and E-selectin gene expression[51]. Additionally, KLF2 also inhibits formation of pro-inflammatory AP1 complex[94] by interfering with phosphorylation of c-Jun and ATF2 in ECs[93]. In other cell types, KLF2 induces quiescence of various leukocyte populations[189] and myeloid specific KLF2 prevents atherosclerotic development[190]. We investigated whether downregulation of EC metabolism by KLF2 had any implications on EC response to inflammatory insults. Stimulation of mock and KLF2 transduced ECs with 10ng/ml TNF-α increased glucose uptake and glycolysis in mock controls, however, KLF2 inhibited the inflammation induced

increase in both glucose uptake and glycolysis. TNF-α stimulation has been previously described to induce glycolytic metabolism in breast epithelial cells[191], colorectal cancer cells[192] and in skeletal muscle via HIF1α activation[193]. Indeed, in ECs, KLF2 has been described to inhibit HIF1α expression and perturbs its stability and function[98], which could explain the mechanism through which it inhibits TNF-α induced glycolysis. This is a relevant finding that could explain the causal link between glycolysis inhibition and inflammatory response in vascular endothelium since aerobic glycolysis has been described to be essential for immune responses in T cells and dendritic cells[194,195].

To understand how inflammatory responses in ECs are affected by their intrinsic metabolic capacities, we inhibited glycolysis in ECs using 2DG in a dose dependent manner for 1 hour and stimulated them with TNF-α for 2 hours. As a read out, mRNA levels of inflammatory marker genes VCAM1, E-selectin and ICAM1 was quantified. VCAM1, E-selectin and ICAM1 are endothelial adhesion molecules that promote rolling and adhesion of leukocytes to ECs in the arterial intima and are critical mediators of endothelial dysfunction. While ICAM1 is expressed rather broadly i.e., expressed in lesion protected areas as well as regions of aorta not affected by atherogenesis, VCAM1 is highly expressed in regions pre-disposed to atherosclerosis and contributes more significantly to the initiation of atherosclerosis[196]. Our results demonstrated significant increase in expression of VCAM1, E-selectin and ICAM1 when stimulated with TNF-α, which concurs with previous studies showing induction of pro-inflammatory genes upon cytokine stimulation[197]. Strikingly, in conditions where 2DG treatment inhibited glycolysis prior to TNF-α stimulation, a significant decrease in mRNA expression levels of VCAM1 and E-selectin was seen, in a dose-dependent manner. However, repression of ICAM1 did not follow the same trend as VCAM1 or E-selectin induction. In support of our data, a study from Chiu et al. shows that VCAM1 and ICAM1 are differentially regulated by shear stress upon induction by TNF-α treatment in ECs, where shear stress attenuates VCAM1 and E-selectin levels but induces ICAM1 expression[198]. Indeed, KLF2 overexpression in HUVECs inhibited IL-1β dependent upregulation of VCAM1 and E-selectin but not ICAM1[51]. Overall, the results indicate that ECs with lower glycolytic metabolism are protected from inflammatory activation induced by TNF-α. Therefore, reduction in glycolysis of ECs by KLF2 (described in the earlier part of the thesis) which in turn leads to an attenuated inflammatory activation, adds a new metabolic aspect that could explain how KLF2 functions as an anti-inflammatory factor in endothelial cells.

Our earlier data confirmed that KLF2 reduces EC glycolytic metabolism by directly repressing PFKFB3 expression. We next questioned whether this reduction in glycolysis which elicited an attenuated inflammatory activation, was mediated by PFKFB3. Treatment of mock and KLF2 transduced ECs with TNF-α increased PFKFB3 mRNA to similar levels (3-4 fold) in both conditions, indicating that the repression of PFKFB3 mRNA by KLF2 under baseline is not present anymore upon TNF-α stimulation. Furthermore, loss of PFKFB3 in HUVECs which led to reduced glycolysis under unstimulated conditions was abolished upon TNF-α stimulation, in that an increase in glycolysis was observed even after loss of PFKFB3 suggesting that TNF-α induced glycolysis effect was independent of PFKFB3. On the contrary, study from Tawakol et al. show that hypoxia and PFKFB3 induce glycolytic flux in macrophages and in turn upregulate its pro-inflammatory activity[199]. However, in our experimental setup, PFKFB3 did not play a crucial role in EC response to inflammation induced glycolysis. The data also hints that inhibition of inflammation induced glycolysis inhibition by KLF2 does not involve PFKFB3 and is probably mediated by other targets of KLF2.

These initial data linking inflammatory activation and EC glycolytic metabolism raises further questions such as how oxidative metabolism is regulated upon TNF-α stimulation? Can we expect a compensatory reduction in oxidative metabolism due to the marked increase in glycolysis upon TNF-α stimulation? What does the increase in glycolysis mean physiologically to the ECs in terms of inflammatory process? Thus far, based on our data we can speculate that glycolysis inhibition could serve as a potential anti-inflammatory approach in the context of endothelial dysfunction. Furthermore, since PFKFB3 is not involved in KLF2 mediated reduction in inflammatory induced glycolysis, it would be interesting to study whether the other two glycolytic genes PFK1 or HK2, that are also down regulated by KLF2, contribute to this effect. Further work is required to uncover the underlying mechanism by which KLF2 reduces inflammation induced glycolysis and henceforth confers an anti-inflammatory effect by regulating EC metabolism.

6. CONCLUSION

Flow hemodynamics play an important role in maintaining endothelial function and laminar shear stress (LSS) induces an atheroprotective and quiescent phenotype to the vascular endothelium via multiple pathways, in part mediated by flow induced transcription factor KLF2. Angiogenic cues promote endothelial sprouting from quiescent pre-existing vessels to form a new vascular network, which is stabilized and functional after recruitment of mural cells, basement membrane formation and blood perfusion. Recent studies have highlighted the role of metabolism in ECs as a crucial mediator of angiogenesis. Whether laminar flow and KLF2 are involved in regulating metabolism to promote EC quiescence has not been studied so far.

Here, we demonstrate that laminar flow and KLF2 regulate endothelial cell metabolism by inhibiting glycolytic and oxidative metabolism. LSS exposure and KLF2 lentiviral overexpression in HUVECs reduced glucose uptake *in vitro*. Moreover, KLF2 increased glucose availability to the underlying layer, which led us to speculate that regions in vessels experiencing atheroprotective flow (high KLF2 expression) promote better availability of glucose to adjacent tissues. Furthermore, in endothelial specific KLF2 knockout mice (EC-KO) increased uptake of glucose in cardiac ECs lacking KLF2 was observed. KLF2 induced a metabolic state of ECs with low glycolytic and respiratory metabolism, which we speculate to be one of the key features of a less energy consuming quiescent endothelium. We next addressed the mechanism by which KLF2 reduced EC glycolysis using RNA sequencing data from shear stress exposed and static control HUVECs. Shear stress reduced expression of key glycolytic genes HK2, PFK1 and PFKFB3 in a KLF2 dependent manner. KLF2 binding sites on PFKFB3 promotor were identified and repression of PFKFB3 promotor activity by KLF2 was confirmed. We demonstrated that PFKFB3 knockdown reduced glycolysis in ECs, similar to levels seen under KLF2 overexpression. Lentiviral overexpression of PFKFB3 along with KLF2 partially reversed the KLF2 mediated glycolysis inhibition. Importantly, we could show that PFKFB3 reversed the KLF2 mediated reduction in endothelial sprouting and network formation *in vitro*, both angiogenic processes that rely on glycolysis. *Ex vivo* aortic ring assay showed an increase in endothelial sprouting from aortas from EC-KO mice which was partially inhibited by PFKFB3 inhibition, confirming that the anti-angiogenic phenotype of KLF2 is PFKFB3 dependent. We could thus demonstrate that KLF2 functions as an anti-

angiogenic factor by exerting its effect on glycolysis via PFKFB3 repression and consequently promotes quiescence in the vascular endothelium.

Secondly, since KLF2 reduced glycolysis and is a well-known anti-inflammatory factor, we explored the possibility that glycolysis plays a role in KLF2 mediated inhibition of endothelial inflammation. Attenuating glycolysis by inhibitor 2DG in ECs reduced expression of inflammatory marker genes, after TNF-α stimulation, highlighting that ECs with reduced glycolysis capacity are resistant to inflammatory insults and therefore glycolytic inhibition could serve as a potential anti-inflammatory strategy. Indeed, KLF2 overexpression reduced TNF-α induced glucose uptake and glycolysis in a PFKFB3 independent manner. The mechanism through which KLF2 inhibits inflammation induced glycolysis remains to be studied.

In summary, this study provides insights in how PFKFB3, a key glycolysis regulator is physiologically regulated by laminar flow via flow induced KLF2. Moreover, we describe a novel molecular mechanism where atheroprotective laminar flow mediates the switching of ECs from an angiogenic state to a quiescent functional endothelium via regulation of glycolytic endothelial metabolism governed by PFKFB3 down regulation.

7. ZUSAMMENFASSUNG

Endothelzellen bilden die innerste Schicht von Blutgefäßen und sind wesentlich für die Aufrechterhaltung der Gefäßhomöostase. Durch den Blutfluss induzierte laminare Schubspannung vermittelt einen atheroprotektiven und quieszenten Phänotyp in Endothelzellen, welcher zum Teil durch die Hochregulation des Transkriptionsfaktors „Krüppel like factor 2 (KLF2)“ vermittelt wird. Das vaskuläre Endothel ist ein dynamischer Zellverbund, die sich flexibel an sich ändernde Umweltbedingungen anpassen können. Unter hypoxischen oder proinflammatorischen Bedingungen migrieren und teilen sich sonst quieszente Endothelzellen um neue Blutgefäße zu formen und so das Gewebe zu vaskularisieren. Sogenannte „tip“ Zellen migrieren an vorderster Front gefolgt von proliferierenden „stalk“-Zellen. Nachdem neue Gefäße etabliert sind, kehren Endothelzellen in einen quieszenten Zustand zurück („Phalanxzellen“) um die Gefäßhomöostase zu wahren.

Jüngste Studien hoben die Wichtigkeit des Metabolismus in der Regulation der Angiogenese hervor. Das Ziel dieser Studie war zu untersuchen, ob laminare Schubspannung und KLF2 eine Rolle in der Regulation des Metabolismus von Endothelzellen spielen und ob diese Regulation eine Rolle in der Induktion eines quieszenten Zustandes von Endothelzellen durch laminare Schubspannung und KLF2 spielt.

Die Rolle von laminarer Schubspannung und KLF2 in glykolytischem und respiratorischem Metabolismus

Anhaltende laminare Schubspannung bewirkt eine signifikante Hochregulation von KLF2 auf mRNA- und Proteinebene in humanen Nabelschnurendothelzellen (HUVECs). Die „short hairpin“ RNA (shRNA)-vermittelte Depletion von KLF2 verhindert die Ausrichtung der Endothelzellen entlang der Flussrichtung des umgebenden Mediums. Zur Untersuchung der metabolischen Aktivität wurden zusätzlich HUVECs verwendet, welche KLF2 zu einem Niveau überexprimierten, welches dem des durch laminare Schubspannung induzierten Niveaus entsprach. Erste Daten wiesen auf eine Reduktion in der Aufnahme von Glukose sowohl durch laminare Schubspannung, als auch durch die Überexpression von KLF2 in kultivierten HUVECs hin. Es konnte gezeigt werden, dass diese Reduktion unter laminarer Schubspannung abhängig von KLF2 ist. KLF2 führte außerdem zu einem verbesserten Glukosetransport durch Endothelzellen in einem modifizierten Boyden-Kammer Experiment.

Um den Effekt von KLF2 auf die Glukoseaufnahmefähigkeit *in vivo* zu überprüfen, wurden Mäuse, mit einem induzierbaren, endothelspezifischen Knockout von KLF2 genutzt. Es konnte gezeigt werden, dass kardiale Endothelzellen ohne KLF2 mehr Glukose aufnehmen. Die Überexpression von KLF2 in kultivierten HUVECs führte des Weiteren zu einer Reduktion sowohl in der basalen als auch in der maximalen Glykolysekapazität.

Zudem wurde der Einfluss von laminarer Schubspannung und KLF2 auf die Mitochondrien untersucht. Die Daten zeigen, dass der Anteil an mitochondrialer DNA in der Zelle, sowie deren Aktivität unter laminarer Schubspannung und KLF2 Überexpression reduziert waren. Des Weiteren sorgten laminare Schubspannung und KLF2 Überexpression für eine Reduktion in der Produktion von ATP in Endothelzellen. Obwohl laminare Schubspannung und KLF2 Überexpression eine Reduktion an mitochondrialer DNA und deren Aktivität bewirkten, war das mitochondriale Membranpotential durch laminare Schubspannung und KLF2 Überexpression sogar leicht erhöht. Außerdem konnte gezeigt werden, dass KLF2 lediglich die basale Respiration in Endothelzellen negativ beeinflusst, während weder die maximale, noch die respiratorische Reservekapazität beeinflusst werden.

Aufklärung des Mechanismus der Inhibition der Glykolyse durch KLF2

RNA Sequenzierungsdaten von HUVECs unter laminarer Schubspannung im Vergleich zu Kontrollzellen unter statischen Bedingungen zeigten, dass verschiedene Gene aus dem glykolytischen Stoffwechselweg durch laminare Schubspannung herunterreguliert wurden. Für die nachfolgenden Experimente fokussierten wir auf die Umsatzrate limitierenden Enzyme Hexokinase 2 (HK2), Phosphofructokinase 1 (PFK1) und 6-phosphofructo-2-kinase/fructose-2.6-biphosphatase 3 (PFKFB3). Die RNA Sequenzierungsdaten wurden durch qPCR Experimente bestätigt, die eine negative Regulation von HK2, PFK1 und PFKFB3 durch laminare Schubspannung zeigten. Die Überexpression von KLF2 in HUVECs reduzierte die Expression der drei genannten Enzyme sowohl auf mRNA-, als auch auf Proteinebene. Um zu überprüfen, ob der Verlust eines der Enzyme zu einer Reduktion in der glykolytischen Funktion, wie sie nach Überexpression von KLF2 beobachtet wurde, führt, wurde jeweils eines der Enzyme in HUVECs depletiert. Weder der Verlust von HK2, noch von PFK1 führten zu einer Reduktion der Glykolyse, während der Verlust von PFKFB3, ähnlich der Überexpression von KLF2, zu einer 60%igen Reduktion der glykolytischen Funktion führte. Zur Aufklärung des Mechanismus der Regulation von PFKFB3 durch KLF2,

wurde eine *in silico* Analyse der Promotorregion des Enzyms durchgeführt, im Zuge derer evolutionär konservierte Bindestellen der Transkriptionsfaktorenfamilie Sp1/KLF identifiziert wurden. Ein Luciferase Assay mit dem PFKFB3 Promoter zeigte eine Repression der Expression von PFKFB3 durch KLF2, welche durch die Mutation der Sp1/KLF Bindungsstelle aufgehoben wurde.

Die Hypothese, dass die Überexpression von PFKFB3 die KLF2 vermittelte Inhibition der Glykolyse umkehrt, wurde im Folgenden *in vitro* getestet. Es wurde eine stabile, 6- bis 8-fache Überexpression von PFKFB3 in HUVECs erreicht. In der Tat erhöhte die Überexpression von PFKFB3 die Glykolyse in HUVECs. Die Überexpression von PFKFB3 verhinderte zudem die KLF2 induzierte Hemmung der Glykolyse. In funktionellen Angiogenese-Assays konnte gezeigt werden, dass KLF2 sowohl die Bildung von ein Netzwerk durch Endothelzellen, als auch die Ausprossung von Endothelzellen inhibiert. Durch Überexpression von PFKFB3 konnten die KLF2 vermittelten anti-angiogenetischen Effekte teilweise umgekehrt werden und es konnte eine Zunahme sowohl der Fähigkeit zur Bildung von ein Netzwerk, als auch der Aussprossung gezeigt werden. Da weder HK2, noch PFK1 eine signifikante Rolle in der Umkehrung der durch KLF2 vermittelten Effekte zeigten, wurde geschlussfolgert dass PFKFB3 eine wichtige Rolle in der Glykolyse in Endothelzellen spielt.

Um die Rolle von KLF2 und PFKFB3 in der Regulation des endothelialen Phänotyps in Mäusen weiter zu untersuchen, wurde ein *ex vivo* aortic ring Assay zur Untersuchung der Angiogenesekapazität durchgeführt. Der endothelzell-spezifische Verlust von KLF2 erhöhte die Ausprossung von Endothelzellen, was die anti-angiogenetische Funktion von KLF2 bestätigt. Interessanterweise führte die Inhibition von PFKFB3 durch den pharmakologischen Inhibitor 3-(3-pyridinyl)-1-(4-pyridinyl)-2-propen-1-one (3-PO) zu einer Umkehrung des pro-angiogenetischen Phänotyps der endothelzell-spezifischen $KLF2^{-/-}$ Mäuse. Diese Ergebnisse stimmen mit den *in vitro* Überexpressions-Daten überein und bestätigen, dass PFKFB3 durch Induktion der Glykolyse ein pro-angiogenetischer Faktor ist. KLF2 inhibiert Angiogenese durch die Inhibition der PFKFB3 vermittelten glykolytischen Funktion und führt in Endothelzellen durch diesen Mechanismus zu einem quieszenten Zustand.

Die Rolle der Glykolyse in der Auslösung einer Entzündungsreaktion

KLF2 wurde bereits als ein anti-inflammatorischer Faktor beschrieben. In der vorliegenden Studie wurde nun zudem untersucht, ob die KLF2 vermittelte Reduktion des Endothelzellmetabolismus eine Rolle in der Reaktion von Endothelzellen auf inflammatorische Stimuli spielt. Die Stimulierung von Mock transduzierten und KLF2 überexprimierenden HUVECs mit dem proinflammatorischen Zytokin „tumor necrosis factor –alpha“ (TNF-α) erhöhte die Aufnahme von Glukose und die Glykolyse in den Mock transduzierten Kontrollzellen, wobei KLF2 die durch Inflammation verursachten Effekte in den KLF2 überexprimierenden Zellen inhibierte. Um zu verstehen wie die Glykolyse inflammatorische Reaktionen in Endothelzellen beeinflusst, hemmten wir die Glykolyse durch 2-Deoxy-Glucose (2DG). Die Zellen wurden anschließend mit TNF-α stimuliert und die Expression von inflammatorischen Adhäsionsmolekülen wurde quantifiziert. Die mRNA-Expression von vaskulärem Adhäsionsmolekül 1 (VCAM1) und E-Selectin waren nach der Stimulierung mit TNF-α erhöht, während die Hemmung der Glykolyse durch vor Stimulierung mit TNF-α zu einer signifikanten dosisabhängigen Abnahme der Expression der beiden Adhäsionsmoleküle führte. Diese Ergebnisse deuteten darauf hin, dass eine geringe glykolytischen Aktivität Endothelzellen vor einer TNF-α abhängiger Induktion einer Entzündungsreaktion schützt. Die Daten zeigen außerdem, dass PFKFB3 nicht in der Inhibition von inflammatorisch induzierter Glykolyseinhibition durch KLF2 involviert ist. Eventuell spielen hier andere durch KLF2 regulierte Enzyme wie HK2 oder PFK1 eine Rolle.

Zusammenfassend konnte in dieser Studie gezeigt werden, dass der durch laminare Schubspannung induzierte Transkriptionsfaktor KLF2 den Metabolismus von Endothelzellen durch die Hemmung von glykolytischem und respiratorischem Metabolismus moduliert. KLF2 sorgte für eine geringere Aufnahme von Glukose und Sauerstoff durch Endothelzellen und könnte so einen besseren Transport der beiden Stoffe in darunter liegendes Gewebe ermöglichen. Es konnte gezeigt werden, dass laminare Schubspannung die Glykolyse in Endothelzellen durch eine KLF2-vermittelte Repression der Transkription von PFKFB3, ein Enzym welches kritisch die Umsatzrate der Glykolyse reguliert, reduziert. KLF2 könnte daher auf Grund seines inhibitorischen Effektes auf die von PFKFB3 abhängige Glykolyse, ein attraktives Ziel für anti-angiogenetische Therapien darstellen. Die hier vorgelegten Daten deuten außerdem darauf hin, dass die Inhibition der Glykolyse durch KLF2 durch die Reduktion der inflammatorischen Aktivierung von Endothelzellen zu einem atheroprotektiven und quieszenten Endothelium führt. Dieser Effekt könnte in der Therapie von Entzündungsreaktionen während der Entstehung von Atherosklerose und anderen

entzündlichen Erkrankungen des Endotheliums nützlich sein. Diese Studie trägt zum Verständnis der Regulation des metabolischen Zustandes von Endothelzellen in Abhängigkeit von laminarer Schubspannung und der Änderung des metabolischen Zustandes von einem angiogenetisch aktiven zu einem quieszenten Zustand bei. Des Weiteren wurde hier eine neue Ebene in der Beziehung zwischen Hämodynamik und zellulärer Quieszenz, welche die metabolische Regulation von Endothelzellen miteinbezieht, aufgedeckt.

8. BIBLIOGRAPHY

1. Jain, R. K. Molecular regulation of vessel maturation. *Nat. Med.* **9,** 685–93 (2003).

2. Swift, M. R. & Weinstein, B. M. Arterial-venous specification during development. *Circ. Res.* **104,** 576–588 (2009).

3. Carmeliet, P. Manipulating angiogenesis in medicine. *J. Intern. Med.* **255,** 538–561 (2004).

4. Meisner, J. K. & Price, R. J. Spatial and Temporal Coordination of Bone Marrow-Derived Cell Activity during Arteriogenesis: Regulation of the Endogenous Response and Therapeutic Implications. *Microcirculation* **17,** 583–599 (2010).

5. Makanya, A. N., Hlushchuk, R. & Djonov, V. G. Intussusceptive angiogenesis and its role in vascular morphogenesis, patterning, and remodeling. *Angiogenesis* **12,** 113–123 (2009).

6. Folkman, J. & Shing, Y. Angiogenesis. *J. Biol. Chem.* **267,** 10931–4 (1992).

7. Geudens, I. & Gerhardt, H. Coordinating cell behaviour during blood vessel formation. *Development* **138,** 4569–83 (2011).

8. Potente, M., Gerhardt, H. & Carmeliet, P. Basic and therapeutic aspects of angiogenesis. *Cell* **146,** 873–87 (2011).

9. Mazzone, M. *et al.* Heterozygous Deficiency of PHD2 Restores Tumor Oxygenation and Inhibits Metastasis via Endothelial Normalization. *Cell* **136,** 839–851 (2009).

10. Ferrara, N. *et al.* Heterozygous embryonic lethality induced by targeted inactivation of the VEGF gene. *Nature* **380,** 439–442 (1996).

11. Carmeliet, P. *et al.* Abnormal blood vessel development and lethality in embryos lacking a single VEGF allele. *Nature* **380,** 435–439 (1996).

12. Phng, L.-K. & Gerhardt, H. Angiogenesis: a team effort coordinated by notch. *Dev. Cell* **16,** 196–208 (2009).

13. Roca, C. & Adams, R. H. Regulation of vascular morphogenesis by Notch signaling. *Genes Dev.* **21,** 2511–24 (2007).

14. Hellström, M. *et al.* Dll4 signalling through Notch1 regulates formation of tip cells during angiogenesis. *Nature* **445,** 776–780 (2007).

15. Siekmann, A. F. & Lawson, N. D. Notch signalling limits angiogenic cell behaviour in developing zebrafish arteries. *Nature* **445,** 781–784 (2007).

16. Dejana, E. The role of wnt signaling in physiological and pathological angiogenesis. *Circ. Res.* **107,** 943–952 (2010).

17. Phng, L.-K. *et al.* Nrarp coordinates endothelial Notch and Wnt signaling to control vessel density in angiogenesis. *Dev. Cell* **16,** 70–82 (2009).

18. Corada, M. *et al.* The Wnt/β-catenin pathway modulates vascular remodeling and specification by upregulating Dll4/notch signaling. *Dev. Cell* **18,** 938–949 (2010).

19. Corada, M. *et al.* The Wnt/β-catenin pathway modulates vascular remodeling and specification by upregulating Dll4/notch signaling. *Dev. Cell* **18,** 938–949 (2010).

20. Duarte, A. *et al.* Dosage-sensitive requirement for mouse Dll4 in artery development. *Genes Dev.* **18,** 2474–2478 (2004).

21. Saharinen, P. *et al.* Angiopoietins assemble distinct Tie2 signalling complexes in endothelial cell-cell and cell-matrix contacts. *Nat. Cell Biol.* **10,** 527–537 (2008).

22. Augustin, H. G., Koh, G. Y., Thurston, G. & Alitalo, K. Control of vascular morphogenesis and homeostasis through the angiopoietin-Tie system. *Nat. Rev. Mol. Cell Biol.* **10,** 165–77 (2009).

23. Majmundar, A. J., Wong, W. J. & Simon, M. C. Review Hypoxia-Inducible Factors and the Response to Hypoxic Stress. *Mol. Cell* **40,** 294–309 (2010).

24. Fraisl, P., Mazzone, M., Schmidt, T. & Carmeliet, P. Regulation of angiogenesis by oxygen and metabolism. *Dev. Cell* **16,** 167–79 (2009).

25. Forsythe, J. a *et al.* Activation of vascular endothelial growth factor gene transcription by hypoxia-inducible factor 1. *Mol. Cell. Biol.* **16,** 4604–4613 (1996).

26. Carmeliet, P. & Jain, R. K. Molecular mechanisms and clinical applications of angiogenesis. *Nature* **473,** 298–307 (2011).

27. Nigro, P., Abe, J.-I. & Berk, B. C. Flow shear stress and atherosclerosis: a matter of site specificity. *Antioxid. Redox Signal.* **15,** 1405–14 (2011).

28. Malek, A. M., Alper, S. L. & Izumo, S. Hemodynamic shear stress and its role in atherosclerosis. *JAMA* **282,** 2035–2042 (1999).

29. Li, Y.-S. J., Haga, J. H. & Chien, S. Molecular basis of the effects of shear stress on vascular endothelial cells. *J. Biomech.* **38,** 1949–1971 (2005).

30. Hahn, C. & Schwartz, M. a. Mechanotransduction in vascular physiology and atherogenesis. *Nat. Rev. Mol. Cell Biol.* **10,** 53–62 (2009).

31. Davies, P. F. *et al.* Spatial relationships in early signaling events of flow-mediated endothelial mechanotransduction. *Annu. Rev. Physiol.* **59,** 527–549 (1997).

32. Davies, P. F. Flow-mediated endothelial mechanotransduction. *Physiol. Rev.* **75,** 519–560 (1995).

33. Kim, D. W., Langille, B. L., Wong, M. K. & Gotlieb, a I. Patterns of endothelial microfilament distribution in the rabbit aorta in situ. *Circ. Res.* **64,** 21–31 (1989).

34. Zarins, C. K. *et al.* Carotid bifurcation atherosclerosis. Quantitative correlation of plaque localization with flow velocity profiles and wall shear stress. *Circ. Res.* **53,** 502–514 (1983).

35. Chatzizisis, Y. S. *et al.* Role of endothelial shear stress in the natural history of coronary atherosclerosis and vascular remodeling: molecular, cellular, and vascular behavior. *J. Am. Coll. Cardiol.* **49,** 2379–93 (2007).

36. Wang, J. C. & Bennett, M. Aging and atherosclerosis: Mechanisms, functional consequences, and potential therapeutics for cellular senescence. *Circ. Res.* **111,** 245–259 (2012).

37. Libby, P., Ridker, P. M. & Hansson, G. K. Progress and challenges in translating the biology of atherosclerosis. *Nature* **473,** 317–325 (2011).

38. Paszkowiak, J. J. & Dardik, a. Arterial Wall Shear Stress: Observations from the Bench to the Bedside. *Vasc. Endovascular Surg.* **37,** 47–57 (2003).

39. Hayden, M. S. & Ghosh, S. Signaling to NF-kB. *Genes Dev* **18,** 2195–2224 (2004).

40. Mohan, S., Mohan, N. & Sprague, E. a. Differential endothelial activation of NF-KB in human aortic cells conditioned to specific flow environments. *Am. J. Physiol. Cell Physiol.* **273,** C572–8 (1997).

41. Partridge, J. *et al.* Laminar shear stress acts as a switch to regulate divergent functions of NF-kappaB in endothelial cells. *FASEB J.* **21,** 3553–3561 (2007).

42. Read, M. a *et al.* Tumor necrosis factor alpha-induced E-selectin expression is activated by the nuclear factor-kappaB and c-JUN N-terminal kinase/p38 mitogen-activated protein kinase pathways. *J. Biol. Chem.* **272,** 2753–2761 (1997).

43. Pan, S. Molecular mechanisms responsible for the atheroprotective effects of laminar shear stress. *Antioxid. Redox Signal.* **11,** 1669–1682 (2009).

44. Surapisitchat, J. *et al.* Fluid shear stress inhibits TNF-alpha activation of JNK but not ERK1/2 or p38 in human umbilical vein endothelial cells: Inhibitory crosstalk among MAPK family members. *Proc. Natl. Acad. Sci. U. S. A.* **98,** 6476–6481 (2001).

45. Yamawaki, H., Lehoux, S. & Berk, B. C. Chronic physiological shear stress inhibits tumor necrosis factor-induced proinflammatory responses in rabbit aorta perfused ex vivo. *Circulation* **108,** 1619–1625 (2003).

46. Liu, Y., Yin, G., Surapisitchat, J., Berk, B. C. & Min, W. Laminar flow inhibits TNF-induced ASK1 activation by preventing dissociation of ASK1 from its inhibitor 14-3-3. *J. Clin. Invest.* **107,** 917–923 (2001).

47. Zakkar, M. *et al.* Increased endothelial mitogen-activated protein kinase phosphatase-1 expression suppresses proinflammatory activation at sites that are resistant to atherosclerosis. *Circ. Res.* **103,** 726–732 (2008).

48. Akimoto, S., Mitsumata, M., Sasaguri, T. & Yoshida, Y. Laminar shear stress inhibits vascular endothelial cell proliferation by inducing cyclin-dependent kinase inhibitor p21(Sdi1/Cip1/Waf1). *Circ. Res.* **86,** 185–190 (2000).

49. Lin, K. *et al.* Molecular mechanism of endothelial growth arrest by laminar shear stress. *Proc. Natl. Acad. Sci. U. S. A.* **97,** 9385–9389 (2000).

50. Malek, a M., Jackman, R., Rosenberg, R. D. & Izumo, S. Endothelial expression of thrombomodulin is reversibly regulated by fluid shear stress. *Circ. Res.* **74,** 852–860 (1994).

51. SenBanerjee, S. *et al.* KLF2 Is a novel transcriptional regulator of endothelial proinflammatory activation. *J. Exp. Med.* **199,** 1305–1315 (2004).

52. Sharefkin, J. B., Diamond, S. L., Eskin, S. G., McIntire, L. V. & Dieffenbach, C. W. Fluid flow decreases preproendothelin mRNA levels and suppresses endothelin-1 peptide release in cultured human endothelial cells. *J. Vasc. Surg.* **14,** 1–9 (1991).

53. Shinoki, N. *et al.* Shear stress down-regulates gene transcription and production of adrenomedullin in human aortic endothelial cells. *J. Cell. Biochem.* **71,** 109–115 (1998).

54. Rieder, M. J., Carmona, R., Krieger, J. E., Pritchard, K. A. & Greene, A. S. Suppression of Angiotensin-Converting Enzyme Expression and Activity by Shear Stress. *Circ. Res.* **80,** 312–319 (1997).

55. Dimmeler, S., Haendeler, J., Rippmann, V., Nehls, M. & Zeiher, a M. Shear stress inhibits apoptosis of human endothelial cells. *FEBS Lett.* **399,** 71–74 (1996).

56. Dimmeler, S., Hermann, C., Galle, J. & Zeiher, a M. Upregulation of superoxide dismutase and nitric oxide synthase mediates the apoptosis-suppressive effects of shear stress on endothelial cells. *Arterioscler. Thromb. Vasc. Biol.* **19,** 656–664 (1999).

57. Dimmeler, S., Assmus, B., Hermann, C., Haendeler, J. & Zeiher, A. M. Fluid Shear Stress Stimulates Phosphorylation of Akt in Human Endothelial Cells. Involvement in Suppression of Apoptosis. *Circ. Res.* 334–341 (1998).

58. Datta, S. R. *et al.* Akt phosphorylation of BAD couples survival signals to the cell-intrinsic death machinery. *Cell* **91,** 231–241 (1997).

59. Mattiussi, S. *et al.* p21Waf1/Cip1/Sdi1 mediates shear stress-dependent antiapoptotic function. *Cardiovasc. Res.* **61,** 693–704 (2004).

60. Conway, D. E. & Schwartz, M. a. Flow-dependent cellular mechanotransduction in atherosclerosis. *J. Cell Sci.* **126,** 5101–9 (2013).

61. Dai, G. *et al.* Biomechanical forces in atherosclerosis-resistant vascular regions regulate endothelial redox balance via phosphoinositol 3-kinase/Akt-dependent activation of Nrf2. *Circ. Res.* **101,** 723–733 (2007).

62. Dekker, R. J. *et al.* Endothelial KLF2 links local arterial shear stress levels to the expression of vascular tone-regulating genes. *Am. J. Pathol.* **167,** 609–618 (2005).

63. Chen, X. L. *et al.* Laminar flow induction of antioxidant response element-mediated genes in endothelial cells: A novel anti-inflammatory mechanism. *J. Biol. Chem.* **278,** 703–711 (2003).

64. Kensler, T. W., Wakabayashi, N. & Biswal, S. Cell survival responses to environmental stresses via the Keap1-Nrf2-ARE pathway. *Annu. Rev. Pharmacol. Toxicol.* **47,** 89–116 (2007).

65. Ishikawa, K. *et al.* Heme oxygenase-1 inhibits atherosclerotic lesion formation in ldl-receptor knockout mice. *Circ. Res.* **88,** 506–512 (2001).

66. Nakamura, S. I. *et al.* Polymorphism in glutamate-cysteine ligase modifier subunit gene is associated with impairment of nitric oxide-mediated coronary vasomotor function. *Circulation* **108,** 1425–1427 (2003).

67. Nakamura, S. -i. Polymorphism in the 5'-Flanking Region of Human Glutamate-Cysteine Ligase Modifier Subunit Gene Is Associated With Myocardial Infarction. *Circulation* **105,** 2968–2973 (2002).

68. Fledderus, J. O. *et al.* KLF2 primes the antioxidant transcription factor Nrf2 for activation in endothelial cells. *Arterioscler. Thromb. Vasc. Biol.* **28,** 1339–1346 (2008).

69. Boon, R. a & Horrevoets, a J. G. Key transcriptional regulators of the vasoprotective effects of shear stress Shear stress. *Mol. Cell* 39–43 (2009).

70. Preiss, A., Rosenberg, U. B., Kienlin, A., Seifert, E. & Jäckle, H. Molecular genetics of Krüppel, a gene required for segmentation of the Drosophila embryo. *Nature* **313,** 27–32

71. Dang, D. T., Pevsner, J. & Yang, V. W. The biology of the mammalian Krüppel-like family of transcription factors. *Int. J. Biochem. Cell Biol.* **32,** 1103–1121 (2000).

72. Atkins, G. B. & Jain, M. K. Role of Krüppel-like transcription factors in endothelial biology. *Circ. Res.* **100,** 1686–95 (2007).

73. Anderson, K. P., Kern, C. B., Crable, S. C. & Lingrel, J. B. Isolation of a gene encoding a functional zinc finger protein homologous to erythroid Krüppel-like factor: identification of a new multigene family. *Mol. Cell. Biol.* **15,** 5957–5965 (1995).

74. Wani, M. a, Wert, S. E. & Lingrel, J. B. Lung Kruppel-like factor, a zinc finger transcription factor, is essential for normal lung development. *J. Biol. Chem.* **274,** 21180–21185 (1999).

75. Wu, J., Bohanan, C. S., Neumann, J. C. & Lingrel, J. B. KLF2 transcription factor modulates blood vessel maturation through smooth muscle cell migration. *J. Biol. Chem.* **283,** 3942–50 (2008).

76. Lee, J. S. *et al.* Klf2 Is an Essential Regulator of Vascular Hemodynamic Forces In Vivo. *Dev. Cell* **11,** 845–857 (2006).

77. Wani, M. a., Means, R. T. & Lingrel, J. B. Loss of LKLF function results in embryonic lethality in mice. *Transgenic Res.* **7,** 229–238 (1998).

78. Kuo, C. T. *et al.* The LKLF transcription factor is required for normal tunica media formation and blood vessel stabilization during murine embryogenesis. *Genes Dev.* **11,** 2996–3006 (1997).

79. Atkins, G. B. *et al.* Hemizygous deficiency of kr??ppel-like factor 2 augments experimental atherosclerosis. *Circ. Res.* **103,** 690–693 (2008).

80. Dekker, R. J. *et al.* Prolonged fluid shear stress induces a distinct set of endothelial cell genes, most specifically lung Kr??ppel-like factor (KLF2). *Blood* **100,** 1689–1698 (2002).

81. Huddleson, J. P., Ahmad, N., Srinivasan, S. & Lingrel, J. B. Induction of KLF2 by fluid shear stress requires a novel promoter element activated by a phosphatidylinositol 3-kinase-dependent chromatin-remodeling pathway. *J. Biol. Chem.* **280,** 23371–23379 (2005).

82. Parmar, K. M. *et al.* Integration of flow-dependent endothelial phenotypes by Kruppel-like factor 2. *J. Clin. Invest.* **116,** 49–58 (2006).

83. Wang, X. *et al.* Targeted Deletion of mek5 Causes Early Embryonic Death and Defects in the Extracellular Signal-Regulated Kinase 5 / Myocyte Enhancer Factor 2 Cell Survival Pathway. **25,** 336–345 (2005).

84. Regan, C. P. *et al.* Erk5 null mice display multiple extraembryonic vascular and embryonic cardiovascular defects. *Proc. Natl. Acad. Sci. U. S. A.* **99,** 9248–9253 (2002).

85. Hayashi, M. *et al.* Targeted deletion of BMK1/ERK5 in adult mice perturbs vascular integrity and leads to endothelial failure. *J. Clin. Invest.* **113,** 1138–1148 (2004).

86. Lin, Q. *et al.* Requirement of the MADS-box transcription factor MEF2C for vascular development. *Development* **125,** 4565–4574 (1998).

87. Wang, L., Fan, C., Topol, S. E., Topol, E. J. & Wang, Q. Mutation of MEF2A in an inherited disorder with features of coronary artery disease. *Science* **302,** 1578–1581 (2003).

88. Schiltz, R. L. *et al.* Overlapping but distinct patterns of histone acetylation by the human coactivators p300 and PCAF within nucleosomal substrates. *J. Biol. Chem.* **274,** 1189–1192 (1999).

89. Huddleson, J. P., Ahmad, N. & Lingrel, J. B. Up-regulation of the KLF2 transcription factor by fluid shear stress requires nucleolin. *J. Biol. Chem.* **281,** 15121–15128 (2006).

90. Lin, Z. *et al.* Kruppel-like factor 2 (KLF2) regulates endothelial thrombotic function. *Circ. Res.* **96,** e48–e57 (2005).

91. Dekker, R. J. *et al.* KLF2 provokes a gene expression pattern that establishes functional quiescent differentiation of the endothelium. *Blood* **107,** 4354–63 (2006).

92. Lin, Z., Hamik, A., Jain, R., Kumar, A. & Jain, M. K. Kruppel-like factor 2 inhibits protease activated receptor-1 expression and thrombin-mediated endothelial activation. *Arterioscler. Thromb. Vasc. Biol.* **26,** 1185–1189 (2006).

93. Fledderus, J. O. *et al.* Prolonged shear stress and KLF2 suppress constitutive proinflammatory transcription through inhibition of ATF2. *Blood* **109,** 4249–4257 (2007).

94. Boon, R. a. *et al.* KLF2 suppresses TGF-beta signaling in endothelium through induction of Smad7 and inhibition of AP-1. *Arterioscler. Thromb. Vasc. Biol.* **27,** 532–539 (2007).

95. Kumar, A., Lin, Z., Senbanerjee, S. & Jain, M. K. Tumor Necrosis Factor Alpha-Mediated Reduction of KLF2 Is Due to Inhibition of MEF2 by NF- κ B and Histone Deacetylases. *Mol. Cell. Biol.* **25,** 5893–5903 (2005).

96. Boon, R. a *et al.* KLF2-induced actin shear fibers control both alignment to flow and JNK signaling in vascular endothelium KLF2-induced actin shear fibers control both alignment to flow and JNK signaling in vascular endothelium. **115,** 2533–2542 (2011).

97. Bhattacharya, R. *et al.* Inhibition of vascular permeability factor/vascular endothelial growth factor-mediated angiogenesis by the Kruppel-like factor KLF2. *J. Biol. Chem.* **280,** 28848–28851 (2005).

98. Kawanami, D. *et al.* Kruppel-like factor 2 inhibits hypoxia-inducible factor 1alpha expression and function in the endothelium. *J. Biol. Chem.* **284,** 20522–30 (2009).

99. Jain, M. K. & Ridker, P. M. Anti-inflammatory effects of statins: clinical evidence and basic mechanisms. *Nat. Rev. Drug Discov.* **4,** 977–987 (2005).

100. Sen-Banerjee, S. *et al.* Kruppel-like factor 2 as a novel mediator of statin effects in endothelial cells. *Circulation* **112,** 720–6 (2005).

101. Parmar, K. M. *et al.* Statins exert endothelial atheroprotective effects via the KLF2 transcription factor. *J. Biol. Chem.* **280,** 26714–26719 (2005).

102. Dichtl, W. *et al.* HMG-CoA reductase inhibitors regulate inflammatory transcription factors in human endothelial and vascular smooth muscle cells. *Arterioscler. Thromb. Vasc. Biol.* **23,** 58–63 (2003).

103. Van Thienen, J. V. *et al.* Shear stress sustains atheroprotective endothelial KLF2 expression more potently than statins through mRNA stabilization. *Cardiovasc. Res.* **72,** 231–240 (2006).

104. Bu, D. *et al.* Statin-induced Kruppel-like factor 2 expression in human and mouse T cells reduces inflammatory and pathogenic responses. **120,** 1961–1970 (2010).

105. Tuomisto, T. T. *et al.* Simvastatin has an anti-inflammatory effect on macrophages via upregulation of an atheroprotective transcription factor, Kruppel-like factor 2. *Cardiovasc. Res.* **78,** 175–84 (2008).

106. Ouchi, N., Shibata, R. & Walsh, K. AMP-activated protein kinase signaling stimulates VEGF expression and angiogenesis in skeletal muscle. *Circ. Res.* **96,** 838–46 (2005).

107. Arany, Z. *et al.* HIF-independent regulation of VEGF and angiogenesis by the transcriptional coactivator PGC-1alpha. *Nature* **451,** 1008–1012 (2008).

108. Potente, M. *et al.* Involvement of Foxo transcription factors in angiogenesis and postnatal neovascularization. *J. Clin. Invest.* **115,** 2382–2392 (2005).

109. Schoors, S. *et al.* Partial and transient reduction of glycolysis by PFKFB3 blockade reduces pathological angiogenesis. *Cell Metab.* **19,** 37–48 (2014).

110. Schoors, S. *et al.* Fatty acid carbon is essential for dNTP synthesis in endothelial cells. *Nature* **520,** 192 (2015).

111. De Bock, K. *et al.* Role of PFKFB3-driven glycolysis in vessel sprouting. *Cell* **154,** 651–63 (2013).

112. Culic, O., Gruwel, M. L. & Schrader, J. Energy turnover of vascular endothelial cells. *Am. J. Physiol.* **273,** C205–C213 (1997).

113. Mertens, S., Noll, T., Spahr, R., Krutzfeldt, A. & Piper, H. M. Energetic response of coronary endothelial cells to hypoxia. (1990).

114. Vander Heiden, M. G., Cantley, L. C. & Thompson, C. B. Understanding the Warburg effect: the metabolic requirements of cell proliferation. *Science* **324,** 1029–33 (2009).

115. Groschner, L. N., Waldeck-Weiermair, M., Malli, R. & Graier, W. F. Endothelial mitochondria-less respiration, more integration. *Pflugers Arch. Eur. J. Physiol.* **464,** 63–76 (2012).

116. Quintero, M., Colombo, S. L., Godfrey, A. & Moncada, S. Mitochondria as signaling organelles in the vascular endothelium. *Proc. Natl. Acad. Sci. U. S. A.* **103,** 5379–5384 (2006).

117. Stapor, P., Wang, X., Goveia, J., Moens, S. & Carmeliet, P. Angiogenesis revisited - role and therapeutic potential of targeting endothelial metabolism. *J. Cell Sci.* **127,** 4331–41 (2014).

118. Zecchin, A., Borgers, G. & Carmeliet, P. Endothelial cells and cancer cells: metabolic partners in crime? *Curr. Opin. Hematol.* (2015). doi:10.1007/3-540-36028-X-10

119. De Bock, K., Georgiadou, M. & Carmeliet, P. Role of endothelial cell metabolism in vessel sprouting. *Cell Metab.* **18,** 634–47 (2013).

120. Merchan, J. R. *et al.* Antiangiogenic activity of 2-deoxy-D-glucose. *PLoS One* **5,** (2010).

121. Benedito, R. *et al.* The notch ligands Dll4 and Jagged1 have opposing effects on angiogenesis. *Cell* **137,** 1124–35 (2009).

122. Vaisman, N., Gospodarowicz, D. & Neufeld, G. Characterization of the receptors for vascular endothelial growth factor. *J. Biol. Chem.* **265,** 19461–19466 (1990).

123. Vizán, P. *et al.* Characterization of the metabolic changes underlying growth factor angiogenic activation: Identification of new potential therapeutic targets. *Carcinogenesis* **30,** 946–952 (2009).

124. Leopold, J. a *et al.* Glucose-6-phosphate dehydrogenase modulates vascular endothelial growth factor-mediated angiogenesis. *J. Biol. Chem.* **278,** 32100–32106 (2003).

125. Krützfeldt, A., Spahr, R., Mertens, S., Siegmund, B. & Piper, H. M. Metabolism of exogenous substrates by coronary endothelial cells in culture. *J. Mol. Cell. Cardiol.* **22,** 1393–404 (1990).

126. Patella, F. *et al.* Proteomics-based metabolic modelling reveals that fatty acid oxidation controls endothelial cell permeability. *Mol. Cell. Proteomics* **44,** (2015).

127. Elmasri, H. *et al.* Fatty acid binding protein 4 is a target of VEGF and a regulator of cell proliferation in endothelial cells. *FASEB J.* **23,** 3865–3873 (2009).

128. Ghelfi, E. *et al.* Fatty acid binding protein 4 regulates VEGF-induced airway angiogenesis and inflammation in a transgenic mouse model: Implications for asthma. *Am. J. Pathol.* **182,** 1425–1433 (2013).

129. Wu, G., Haynes, T. E., Li, H. & Meininger, C. J. Glutamine metabolism in endothelial cells: ornithine synthesis from glutamine via pyrroline-5-carboxylate synthase. *Comp. Biochem. Physiol. A. Mol. Integr. Physiol.* **126,** 115–123 (2000).

130. Lohmann, R., Souba, W. W. & Bode, B. P. Rat liver endothelial cell glutamine transporter and glutaminase expression contrast with parenchymal cells. *Am. J. Physiol.* **276,** G743–G750 (1999).

131. Leighton, B., Curi, R., Hussein, a & Newsholme, E. a. Maximum activities of some key enzymes of glycolysis, glutaminolysis, Krebs cycle and fatty acid utilization in bovine pulmonary endothelial cells. *FEBS Lett.* **225,** 93–96 (1987).

132. Wu, G., Haynes, T. E., Yan, W. & Meininger, C. J. Presence of glutamine:fructose-6-phosphate amidotransferase for glucosamine-6-phosphate synthesis in endothelial cells: Effects of hyperglycaemia and glutamine. *Diabetologia* **44,** 196–202 (2001).

133. Unterluggauer, H. *et al.* Premature senescence of human endothelial cells induced by inhibition of glutaminase. *Biogerontology* **9,** 247–259 (2008).

134. DeBerardinis, R. J. & Cheng, T. Q's next: the diverse functions of glutamine in metabolism, cell biology and cancer. *Oncogene* **29,** 313–324 (2010).

135. Hinshaw, D. B. & Burger, J. M. Protective effect of glutamine on endothelial cell ATP in oxidant injury. *J. Surg. Res.* **49,** 222–227 (1990).

136. Fleming, I., Bauersachs, J., Fisslthaler, B. & Busse, R. Ca2+-independent activation of the endothelial nitric oxide synthase in response to tyrosine phosphatase inhibitors and fluid shear stress. *Circ. Res.* **82,** 686–695 (1998).

137. Boon, R. a. *et al.* Krüppel-like factor 2 improves neovascularization capacity of aged proangiogenic cells. *Eur. Heart J.* **32,** 371–377 (2011).

138. Michalik, K. M. *et al.* The long noncoding RNA malat1 regulates endothelial cell function and vessel growth. *Circ. Res.* (2014).

139. Ovcharenko, I., Nobrega, M. a., Loots, G. G. & Stubbs, L. ECR Browser: A tool for visualizing and accessing data from comparisons of multiple vertebrate genomes. *Nucleic Acids Res.* **32,** 280–286 (2004).

140. Loots, G. G. & Ovcharenko, I. rVISTA 2.0: Evolutionary analysis of transcription factor binding sites. *Nucleic Acids Res.* **32,** 217–221 (2004).

141. Hergenreider, E. *et al.* Atheroprotective communication between endothelial cells and smooth muscle cells through miRNAs. *Nat. Cell Biol.* **14,** 249–56 (2012).

142. Korff, T. & Augustin, H. G. Integration of Endothelial Cells in Multicellular Spheroids Prevents Apoptosis and Induces Differentiation. *J. Cell Biol.* **143,** 1341–1352 (1998).

143. Pitulescu, M. E., Schmidt, I., Benedito, R. & Adams, R. H. Inducible gene targeting in the neonatal vasculature and analysis of retinal angiogenesis in mice. *Nat. Protoc.* **5,** 1518–34 (2010).

144. Boon, R. a *et al.* MicroRNA-34a regulates cardiac ageing and function. *Nature* **495,** 107–10 (2013).

145. Baker, M. *et al.* Use of the mouse aortic ring assay to study angiogenesis. *Nat. Protoc.* **7,** 89–104 (2012).

146. Shyy, J. Y. J. & Chien, S. Role of integrins in endothelial mechanosensing of shear stress. *Circ. Res.* **91,** 769–775 (2002).

147. Boon, R. a *et al.* KLF2-induced actin shear fibers control both alignment to flow and JNK signaling in vascular endothelium. *Blood* **115,** 2533–42 (2010).

148. Warburg, O. Injuring of Respiration the Origin of Cancer Cells. *Science (80-.).* **123,** 309–14 (1956).

149. Folmes, C. D. L. *et al.* Somatic oxidative bioenergetics transitions into pluripotency-dependent glycolysis to facilitate nuclear reprogramming. *Cell Metab.* **14,** 264–271 (2011).

150. Houtkooper, R. H. & Auwerx, J. Exploring the therapeutic space around NAD+. *J. Cell Biol.* **199,** 205–209 (2012).

151. Ni, C.-W., Hsieh, H.-J., Chao, Y.-J. & Wang, D. L. Shear flow attenuates serum-induced STAT3 activation in endothelial cells. *J. Biol. Chem.* **278,** 19702–19708 (2003).

152. Arqueol, A., Arqueol, A., Rupestres, E. & Rupestres, E. This information is current as of February 2008. *Group* (2008). doi:10.4049/jimmunol.1301769

153. Das, M. *et al.* Kruppel-Like Factor 2 (KLF2) Regulates Monocyte Differentiation and Functions in mBSA and IL-1β-Induced Arthritis. *Curr. Mol. Med.* **12,** 113–125 (2012).

154. Young, A. *et al.* Flow activation of AMP-activated protein kinase in vascular endothelium leads to Krüppel-like factor 2 expression. *Arterioscler. Thromb. Vasc. Biol.* **29,** 1902–8 (2009).

155. Cleeter, M. W., Cooper, J. M., Darley-Usmar, V. M., Moncada, S. & Schapira, a H. Reversible inhibition of cytochrome c oxidase, the terminal enzyme of the mitochondrial respiratory chain, by nitric oxide. Implications for neurodegenerative diseases. *FEBS Lett.* **345,** 50–54 (1994).

156. Brown, G. C. Nanomolar concentrations of nitric oxide reversibly inhibit synaptosomal respiration by competing with oxygen at cytochrome oxidase. *FEBS Lett.* **356,** 295–298 (1994).

157. J. Bereta, M. B. Stimulation of Glyceraldehyde-3-Phosphate Dehydrogenase mRNA Levels by Endogenous Nitric Oxide in Cytokine-Activated Endothelium. *Biochem. Biophys. Res. Commun.* **217,** 363–369 (1995).

158. Obach, M. *et al.* 6-Phosphofructo-2-kinase (pfkfb3) gene promoter contains hypoxia-inducible factor-1 binding sites necessary for transactivation in response to hypoxia. *J. Biol. Chem.* **279,** 53562–53570 (2004).

159. Liu, J. *et al.* Aldolase B knockdown prevents high glucose-induced methylglyoxal overproduction and cellular dysfunction in endothelial cells. *PLoS One* **7,** (2012).

160. Noria, S. *et al.* Assembly and reorientation of stress fibers drives morphological changes to endothelial cells exposed to shear stress. *Am. J. Pathol.* **164,** 1211–1223 (2004).

161. Girard, P. R. & Nerem, R. M. Shear stress modulates endothelial cell morphology and F-actin organization through the regulation of focal adhesion-associated proteins. *J. Cell. Physiol.* **163,** 179–193 (1995).

162. Davies, P. & Barbee, K. Endothelial Cell Surface Imaging: Insights Into Hemodynamic Force Transduction. *Physiology* **9,** 153–157 (1994).

163. Davies, P. F. Endothelial transcriptome profiles in vivo in complex arterial flow fields. *Ann. Biomed. Eng.* **36,** 563–570 (2008).

164. Desai, S. Y. *et al.* Mechanisms of endothelial survival under shear stress. *Endothelium* **9,** 89–102 (2002).

165. Suárez, J. & Rubio, R. Regulation of glycolytic flux by coronary flow in guinea pig heart. Role of vascular endothelial cell glycocalyx. *Am. J. Physiol.* **261,** H1994–H2000 (1991).

166. Curry, F. E. & Adamson, R. H. Endothelial glycocalyx: Permeability barrier and mechanosensor. *Ann. Biomed. Eng.* **40,** 828–839 (2012).

167. Kluge, M. a., Fetterman, J. L. & Vita, J. a. Mitochondria and endothelial function. *Circ. Res.* **112,** 1171–1188 (2013).

168. Chen, Z. *et al.* Shear stress, SIRT1, and vascular homeostasis. *Proc. Natl. Acad. Sci. U. S. A.* **107,** 10268–10273 (2010).

169. Kilburn, D. G., Lilly, M. D. & Webb, F. C. The energetics of mammalian cell growth. *J. Cell Sci.* **4,** 645–654 (1969).

170. Borutaite, V., Jekabsone, A., Morkuniene, R. & Brown, G. C. Inhibition of mitochondrial permeability transition prevents mitochondrial dysfunction, cytochrome c release and apoptosis induced by heart ischemia. *J. Mol. Cell. Cardiol.* **35,** 357–366 (2003).

171. Wei, Z. *et al.* Simulated ischemia in flow-adapted endothelial cells leads to generation of reactive oxygen species and cell signaling. *Circ. Res.* **85,** 682–689 (1999).

172. Davies, P. F., Remuzzi, A., Gordon, E. J., Dewey, C. F. & Gimbrone, M. a. Turbulent fluid shear stress induces vascular endothelial cell turnover in vitro. *Proc. Natl. Acad. Sci.* **83,** 2114–2117 (1986).

173. Atkins, G. B. & Jain, M. K. Role of Krueppel-like transcription factors in endothelial biology. *Circ. Res.* **100,** 1686–1695 (2007).

174. Desai, S. Y. *et al.* Mechanisms of endothelial survival under shear stress. *Endothelium* **9,** 89–102 (2002).

175. Chen, Z. P. *et al.* AMP-activated protein kinase phosphorylation of endothelial NO synthase. *FEBS Lett.* **443,** 285–9 (1999).

176. Morrow, V. a *et al.* Direct activation of AMP-activated protein kinase stimulates nitric-oxide synthesis in human aortic endothelial cells. *J. Biol. Chem.* **278,** 31629–31639 (2003).

177. Zhang, Y. *et al.* AMP-activated protein kinase is involved in endothelial NO synthase activation in response to shear stress. *Arterioscler. Thromb. Vasc. Biol.* **26,** 1281–1287 (2006).

178. Nagata, D., Mogi, M. & Walsh, K. AMP-activated protein kinase (AMPK) signaling in endothelial cells is essential for angiogenesis in response to hypoxic stress. *J. Biol. Chem.* **278,** 31000–31006 (2003).

179. Mathupala, S. P., Ko, Y. H. & Pedersen, P. L. Hexokinase II: cancer's double-edged sword acting as both facilitator and gatekeeper of malignancy when bound to mitochondria. *Oncogene* **25,** 4777–4786 (2006).

180. Yalcin, A., Telang, S., Clem, B. & Chesney, J. Regulation of glucose metabolism by 6-phosphofructo-2-kinase/fructose-2,6-bisphosphatases in cancer. *Exp. Mol. Pathol.* **86,** 174–179 (2009).

181. Moreno-Sánchez, R., Rodríguez-Enríquez, S., Marín-Hernández, A. & Saavedra, E. Energy metabolism in tumor cells. *FEBS J.* **274,** 1393–1418 (2007).

182. Chesney, J. *et al.* An inducible gene product for 6-phosphofructo-2-kinase with an AU-rich instability element: role in tumor cell glycolysis and the Warburg effect. *Proc. Natl. Acad. Sci. U. S. A.* **96,** 3047–3052 (1999).

183. Clem, B. *et al.* Small-molecule inhibition of 6-phosphofructo-2-kinase activity suppresses glycolytic flux and tumor growth. *Mol. Cancer Ther.* **7,** 110–20 (2008).

184. Hara, T., Mizuguchi, M., Fujii, M. & Nakamura, M. Krüppel-like Factor 2 Represses Transcription of the Telomerase Catalytic Subunit Human Telomerase Reverse Transcriptase (hTERT) in Human T Cells. *J. Biol. Chem.* **290,** 8758–8763 (2015).

185. Sebzda, E., Zou, Z., Lee, J. S., Wang, T. & Kahn, M. L. Transcription factor KLF2 regulates the migration of naive T cells by restricting chemokine receptor expression patterns. *Nat. Immunol.* **9,** 292–300 (2008).

186. Wang, F. *et al.* Transcriptional repression of WEE1 by Kruppel-like factor 2 is involved in DNA damage-induced apoptosis. *Oncogene* **24,** 3875–3885 (2005).

187. Schoors, S. *et al.* Incomplete and transitory decrease of glycolysis: A new paradigm for anti-angiogenic therapy? *Cell Cycle* **13,** 16–22 (2014).

188. Zhou, W. *et al.* HIF1α induced switch from bivalent to exclusively glycolytic metabolism during ESC-to-EpiSC/hESC transition. *EMBO J.* **31,** 2103–2116 (2012).

189. Cao, Z., Sun, X., Icli, B., Wara, A. K. & Feinberg, M. W. Role of Kruppel-like factors in leukocyte development, function, and disease. *Blood* **116,** 4404–4414 (2010).

190. Lingrel, J. B. *et al.* Myeloid-specific krüppel-like factor 2 inactivation increases macrophage and neutrophil adhesion and promotes atherosclerosis. *Circ. Res.* **110,** 1294–1302 (2012).

191. Vaughan, R. a. *et al.* Tumor necrosis factor alpha induces Warburg-like metabolism and is reversed by anti-inflammatory curcumin in breast epithelial cells. *Int. J. Cancer* **133,** 2504–2510 (2013).

192. Straus, D. S. TNFα and IL-17 cooperatively stimulate glucose metabolism and growth factor production in human colorectal cancer cells. *Mol. Cancer* **12,** 78 (2013).

193. Remels, A. H. V, Gosker, H. R., Verhees, K. J. P., Langen, R. C. J. & Schols, A. M. W. J. TNF-α-Induced NF-κB Activation Stimulates Skeletal Muscle Glycolytic Metabolism Through Activation of HIF-1α. *Endocrinology* **156,** 1770–81 (2015).

194. Chang, C.-H. *et al.* Posttranscriptional control of T cell effector function by aerobic glycolysis. *Cell* **153,** 1239–51 (2013).

195. Cortese, M., Sinclair, C. & Pulendran, B. Translating glycolytic metabolism to innate immunity in dendritic cells. *Cell Metab.* **19,** 737–739 (2014).

196. Cybulsky, M. I. *et al.* A major role for VCAM-1, but not ICAM-1, in early atherosclerosis. *J. Clin. Invest.* **107,** 1255–1262 (2001).

197. Rao, R. M., Yang, L., Garcia-Cardena, G. & Luscinskas, F. W. Endothelial-dependent mechanisms of leukocyte recruitment to the vascular wall. *Circ. Res.* **101,** 234–247 (2007).

198. Chiu, J. J. *et al.* Shear Stress Increases ICAM-1 and Decreases VCAM-1 and E-selectin Expressions Induced by Tumor Necrosis Factor-α in Endothelial Cells. *Arterioscler. Thromb. Vasc. Biol.* **24,** 73–79 (2004).

199. Tawakol, A. *et al.* HIF-1α and PFKFB3 Mediate a Tight Relationship Between Proinflammatory Activation and Anerobic Metabolism in Atherosclerotic Macrophages. *Arterioscler. Thromb. Vasc. Biol.* **35,** 1463–1471 (2015).

9. ABBREVIATIONS

2D	2 dimensional
2-DG	2-deoxyglucose
2-NBDG	2-(N-(7-Nitrobenz-2-oxa-1,3-diazol-4-yl)Amino)-2-Deoxyglucose
3D	3 dimensional
3-PO	3-(3-pyridinyl)-1-(4-pyridinyl)-2-propen-1-one
7-AAD	7 aminoactinomycin D
ACE	Angiotensin converting enzyme
AF-488	Alexa Fluor 488
Alk1	Activin receptor like kinase 1
AMPK	Adenosine mono phosphate activated protein kinase
ANG2	Angiopoietin 2
ANOVA	Analysis of variance
AP-1	Activator protein 1
APC	Allophycocyanin
ApoE	Apolipoprotein E
APS	Ammonium per sulphate
ARE	Antioxidant response element
ASK1	Apoptosis signal regulating kinase 1
ATP	Adenosine triphosphate
Bad	Bcl-2 associated death promotor
BAEC	Bovine aortic endothelial cells
BDM	2,3-Butanedione monoxime
BM	Basement membrane
bp	Base pairs
BrdU	Bromodeoxyuridine
BSA	Bovine Serum Albumin
$CaCl_2$	Calcium chloride
Cdh5	Cadherin 5
Cdk	Cyclin dependent kinase
cDNA	Complementary deoxyribonucleic acid
ChIP	Chromatin immunoprecipitation
CMV	cytomegalovirus
CO_2	Carbon dioxide
Con	Control
CPT1	Carnitine palmitoyltransferase 1
Ct	Threshold cycle
Cu/Zn SOD	Copper/Zinc superoxide dismutase
DAPI	4', 6- diamidin-2-phenylindol
DFO	Desferrioxamine
DLL4	Delta like 4
DMEM	Dulbecco's modified Eagle's medium
DMSO	Dimethyl sulfoxide
DNA	Deoxyribonucleic acid
DTT	Dithiothretol
EBM	Endothelial growth basal medium
EC	Endothelial cell
ECAR	Extra cellular acidification rate
ECM	Extracellular matrix
Edg1	Endothelial differentiation gene 1

EDTA	Ethylene diamine tetra acetic acid
EEL	External elastic lamina
EGM	Endothelial cell growth medium
EGR1	Early growth response protein 1
Em	Emission maxima
eNOS	Endothelial nitric oxide synthase
EpiSc	Epiblast stem cells
ERK5	Extracellular signal regulated kinase 5
ERRα	Estrogen related receptor alpha
ERT2	Estrogen receptor 2
EtOH	Ethanol
Ex	Excitation maxima
F1,6BP	Fructose-1,6-bisphosphate
F2,6BP	Fructose-2,6-bisphosphate
F2R	Coagulation factor receptor 2
F6P	Fructose-6-phosphate
FABP4	Fatty acid binding protein 4
FACS	Fluorescence activated cell sorting
FAK	Focal adhesion kinase
FAO	Fatty acid oxidation
FBS	Fetal bovine serum
FCCP	Carbonilcyanide p-triflouromethoxyphenylhydrazone
FGF	Fibroblast growth factor
FITC	Fluorescein isothiocyanate
fl/fl	Flox/flox
FOXO	Forkhead box O
FTH	Ferritin, heavy polypeptide
G6P	Glucose 6 phosphate
GADD45	Growth arrest and DNA damage inducible 45
GAPDH	Glyceraldehyde 3-phosphate dehydrogenase
GCLM	Glutamate cysteine ligase, modifier subunit
GEO	Gene expression omnibus
GGPP	Geranyl-geranyl-pyro phosphate
GLUT	Glucose transporter
GTPase	Guanosine triphosphatase
h or hr	Hour
HBP	Hexoamine biosynthesis pathway
HBSS	Hank's balanced salt solution
HCl	Hydrogen chloride
HDAC	Histone deacetylase
HEK	Human embryonic kidney
HEPES	4-(2-hydroxyethyl)-1-piperazineethanesulfonic acid
HF	High fidelity
HIF	Hypoxia inducing factor
HK2	Hexokinase 2
HLI	Hind limb ischemia
HMG-CoA	3- hydroxy-3-methylglutaryl coenzyme A
hnRNP	Heterogeneous nuclear ribonucleoprotein
HO1	Heme oxygenase 1
HRP	Horse radish peroxidase
HSP60	Heat shock protein 60
hTERT	Human telomerase reverse transcriptase

HUVEC	Human umbilical vein endothelial cells
ICAM1	Intracellular adhesion molecule 1
IEL	Internal elastic lamina
IL-1β	Interleukin 1 beta
IL-8	Interleukin 8
JAG1	Jagged 1
JC-1	5,5′,6,6′-tetrachloro-1,1′,3,3′-tetraethylbenzimidazolylcarbocyanine iodide
JNK	c-Jun N-terminal kinase
KCl	Potassium chloride
Keap1	Kelch-like ECH-associated protein 1
KH_2PO_4	Potassium dihydrogen phosphate
$KHCO_3$	Potassium bicarbonate
KLF2	Krüppel like factor 2
KO	Knockout
LDHA	Lactate dehydrogenase A
LDL	Low density lipoprotein
LEF1	Lymphoid enhancer binding factor 1
L-NAME	Nω-nitro-L-arginine methyl ester hydrochloride
LSS	Laminar shear stress
Luc2	Firefly luciferase 2
MAPK	Mitogen activated protein kinase
MCP1	Monocyte chemoattractant protein 1
MEF2	Myocyte enhancer binding factor 2
MEK5	MAPK/Erk kinase 5
$MgCl_2$	Magnesium dichloride
$MgSO_4$	Magnesium sulphate
min	Minute
MKP1	Mitogen activated protein phosphatase 1
MMP	Matric metallopoteinase
$MnCl_2$	Manganese dichloride
mtND1	Mitochondrially encoded NADH dehydrogenase 1
mTOR	Mechanistic target of rapamycin
MTT	Diphenyltetrazolium Bromide
MuLV	Murine leukemia virus
Mut	Mutant
Na_2HPO_4	Disodium phosphate
NaCl	Sodium chloride
NAD	Nicotinamide adenine dinucleotide
NADPH	Nicotinamide adenine dinucleotide phosphate
$NaHCO_3$	Sodium bicarbonate
NaOH	Sodium hydroxide
NCBI	National center for biotechnology information
NFκB	Nuclear factor kappa B
NICD	Notch intra cellular domain
NIH	National Institutes of Health
NO	Nitric oxide
NQO1	NAD(P)H dehydrogenase (quinone 1)
NRARP	Notch-regulated ankyrin repeat protein
Nrf2	Nuclear factor erythroid 2- related factor 2
OCR	Oxygen consumption rate
OD	Optical density
OXPHOS	Oxidative phosphorylation

PAGE	Polyacrylamide gel electrophoresis
PAK	p-21 activated kinase
PAR1	Proteinase activated receptor 1
PBS	Phosphate buffer saline
PC	Pericyte
PCAF	P300/CREB binding protein associated factor
PCR	Polymerase chain reaction
PDGF	Platelet derived growth factor
pDNA	Plasmid DNA
PE	R-phycoerythrin
PECAM1	Platelet endothelial cell adhesion molecule 1
PET	Polyethylene terephthalate
PFA	Paraformaldehyde
PFK1	Phosphofructokinase 1
PFKFB3	6-phosphofructose-2-kinase/fructose-2,6-biphosphatase 3
PFKP	Phosphofructokinase (platelet)
PGC1α	Peroxisome proliferator-activated receptor gamma, coactivator 1 alpha
PGK	Phosphoglycerate kinase
PHD	Prolyl hydroxylase domain
PI3K	Phosphoinositide 3-kinase
PPP	Pentose phosphate pathway
PVDF	Polyvinylidene difluoride
qPCR	Quantitative polymerase chain reaction
Rb	Retinoblastoma
RFU	Relative fluorescence unit
RIPA	Radio immune precipitation assay
Rluc	Renilla luciferase
RNA pol II	Ribonucleic acid polymerase II
ROS	Reactive oxygen species
RPLP0	Ribosomal protein large, P0
rpm	Rotation per minute
RT	Room temperature
S1P	Sphingosine 1 phosphate
SDS	Sodium dodecyl sulphate
sec	Second
Sema3F	Semaphorin 3 F
shRNA	Short hairpin ribonucleic acid
siRNA	Short interfering ribonucleic acid
SIRT1	Sirtuin 1
SMC	Smooth muscle cell
SOC	Super optimal broth with catabolite repression
Sp1	Specificity protein 1
STAT3	Signal transducer and activator of transcription 3
TBS-T	Tris buffered saline with Tween 20
TCA	Tricarboxylic acid
TEMED	Tetra methyl ethylene diamine
TGF-β	Transforming growth factor beta
TM	Thrombomodulin
TMR	Tetra methyl rhodamine
TMRM	tetramethylrhodamine, methyl ester
TNF-α	Tumor necrosis factor alpha
tPA	Tissue plasminogen activator

UDPGlcNAc	UDP-N-acetyl-Glucosamine
VCAM1	Vascular cell adhesion molecule 1
VE-cadherin	Vascular endothelial cadherin
VEGF	Vascular endothelial growth factor
VEGFR1	Vascular endothelial growth factor receptor 1
VEGFR2	Vascular endothelial growth factor receptor 2
VSMC	Vascular smooth muscle cell
WNK1	With no lysine (K)
WT	Wild type
$\Delta\Psi_m$	Mitochondrial membrane potential

10. EIDESSTATTLICHE ERKLÄUNG

Hiermit versichere ich, dass ich die vorliegende Dissertation selbständig und nur unter zu Hilfe-nahme der hier angegebenen Quellen und Hilfsmitteln verfasst habe.

Die Dissertation wurde bisher keiner anderen Fakultät vorgelegt. Ich erkläre, dass ich bisher kein Promotionsverfahren erfolglos beendet habe und dass keine Aberkennung eines bereits erworbenen Doktorgrades vorliegt.

Frankfurt, den 08.06.2015

Anuradha Doddaballapur